SINTERING OF HETEROGENEOUS GLASS POWDER COMPACTS

by

Katherine Ann Blackmore

A Thesis Submitted to the Faculty of the

DEPARTMENT OF MATERIALS SCIENCE
AND ENGINEERING

In Partial Fulfillment of the Requirements
For the Degree of

MASTER OF SCIENCE

In the Graduate College

THE UNIVERSITY OF ARIZONA

1995

Statement by Author

This thesis has been submitted in partial fulfillment of requirements for an advanced degree at The University of Arizona and is deposited in the University Library to be made available to borrowers under the rules of the Library.

Brief quotations from this thesis are allowable without special permission, provided that accurate acknowledgement of source is made. Requests for permission for extended quotation from or reproduction of this manuscript in whole or in part may be granted by the copyright holder.

SIGNED: Katherine A. Blackmore

APPROVAL BY THESIS DIRECTOR

This thesis has been approved on the date shown below:

Brian J. Zelinski — 5/9/95

Brian J.J. Zelinski — Date

Professor of Materials Science and Engineering

TABLE OF CONTENTS

TABLE OF CONTENTS - Continued

LIST OF FIGURES

LIST OF FIGURES - Continued

LIST OF FIGURES - Continued

LIST OF FIGURES - Continued

LIST OF FIGURES - Continued

LIST OF TABLES

ABSTRACT

A modification of Scherer's Self-Consistent model and a new model, the Interlocking Cell model, have been developed to characterize the sintering behavior of mixtures of two glass powders. The theoretical sintering curves predicted by both these models are compared to each other and to experimental densification behaviors. Viscosities extrapolated from homogeneous sintering curves of sol-gel derived powders are transient and cannot be predicted based on composition alone. These transient viscosities have a significant effect on the sintering kinetics. The Self-Consistent and Interlocking Cell models assume very different microstructural changes during sintering. However, differences between the two models can just be distinguished using experimental densification curves of sol-gel cordierite based glass mixtures.

CHAPTER 1

INTRODUCTION

Sintering is defined as the coalescence of multiple particles into a single mass. The primary driving force for sintering is the overall reduction in surface area. Industrial applications of powders with high surface areas are fairly wide-spread and include all types of materials: ceramics, glasses, metals, and composites. Sintering is part of the manufacturing process when the initial materials are in powder form and the final product is a dense sample.

One application where powder processing is very useful is in the formation of complex shapes. By placing a powder and some binder in a mold and sintering it, samples can be made with geometries very similar to the final product, reducing the amount of machining required. Electronic packages often utilize a screening technique in which a powder is deposited in the desired pattern and then heated until it is fully dense.

Glass or ceramic pieces often are produced via powder processing techniques because other methods require higher processing temperatures. Metals with low melting points are often cast by pouring the molten metal into a plastic or metal

mold. However, most finished glass products are not made by this method. Ceramic and glass castings are generally made by placing some powder and binder in the mold and heating the mixture until it sinters. The sintering temperature is much lower than the melting point; therefore, it is also often considered more energy efficient.

Powder processing also lends itself to the manufacturing of composites. It is possible to cast one component around the another (such as steel reinforced concretes). However, when the alignment of the embedded material is not critical, it is much easier to cast and sinter both components at the same time. When the alignment of fibers in a matrix is important, it is sometimes possible to align one component with an electric or magnetic field allowing both components to be cast simultaneously.

Some applications require very careful monitoring of the sintering behavior during manufacturing. For example, the core and cladding of some optical waveguides can be made simultaneously by varying the radial composition as the glass is deposited. Sometimes problems develop when trying to sinter the fiber, because the core and cladding materials sinter at different rates.[1,2] Other applications which use powder processing to end up with a product with specific dimensions require very tight tolerance on the amount of shrinkage due to heating. Some applications require a final product which is fully dense or it will "fail" in use,

i.e.: pores within optical waveguides scatter light, cracks in printed electrical paths cause opens, and voids in composites decrease their strength.

Sawhill[3] mentions using mixtures of two glass powders in order to produce dielectric substrates. Often sintering mixtures of two glasses and allowing one to crystallize produces fairly dense samples. However, the samples must reach full or near full density before crystallization halts densification. In order to produce high quality substrates, the compositions of the glasses can be tailored to promote sintering before the desired phases begin crystallizing.

All of these applications involve inhomogeneous or heterogeneous sintering, which for this document is defined as the densification of a sample containing two or more components with different properties. Chemical variations within the sample, whether intentional or not, affect the densification behavior. It is not possible to accurately determine the sintering behavior of samples with more than one component by simply averaging the sintering times of each of the components. Models which predict the sintering behavior of heterogeneous samples should be developed. By using heterogeneous sintering models, it can be determined how changes in the properties of the individual components or the heat treatment procedures will impact the properties of the final product.

1.1 Objectives

The objective of this work was to characterize and model heterogeneous sintering. Several models exist for predicting the sintering behavior of heterogeneous crystalline samples,[4,5] but only one that this author is aware of describes the behavior of inhomogeneous viscous glasses.[6] Even Scherer's Self-Consistent model[6] has only been explored for rigid inclusions in a glassy matrix[7] and bimodal pore size distributions.[6] Very little experimental work has been published on the sintering of either heterogeneous glass or ceramic powders.

Results of sintering studies on homogeneous glass powders in the MgO-Al_2O_3-SiO_2 system near the cordierite composition will be presented. These glass powders were produced via a sol-gel route described by Aruchamy et al. which produces homogeneous powders.[8] The sintering behavior of three different compositions will be characterized and compared.

The effect of heterogeneities on experimental sintering behavior will also be studied. A heterogeneous sample with the same bulk composition as stoichiometric cordierite was produced by mixing two different powders. The sintering behavior of this mixed sample will be compared to the sintering behavior of a homogeneous powder with the same composition.

Two heterogeneous sintering models will be presented and compared to the experimental densification behavior of the mixed sample. One of these models, the

Interlocking Cell model, has been developed for this study and is an extension of Scherer's model for homogeneous sintering.[9] A modification of Scherer's Self-Consistent model which can be applied to mixtures of powders with different viscosities[6] will also be presented. These two models assume different microstructures develop due to sintering, suggesting that only one of these models can correctly model the sintering behavior of a heterogeneous sample at any given time. It is hoped that the experimental sintering results will allow a determination of which model is more suitable for this system of glass powders.

CHAPTER 2

LITERATURE REVIEW

In this chapter the pertinent models which have been developed to describe sintering behavior under a variety of conditions will be presented. The first section will describe the basic Frenkel[10] and Mackenzie-Shuttleworth[11] models for homogeneous sintering. A more detailed description of the Scherer homogeneous sintering model[9] will be presented because several of the models in this chapter and in the rest of this document are based on the Scherer unit cell geometry. The following section of this chapter will contain a brief description of the approaches used to model pore size distributions, including the Self-Consistent model.[6] Several different heterogeneous sintering models which can be applied to rigid inclusions will be presented and compared. Since the experimental work for this study has been conducted using powders in the MgO-Al_2O_3-SiO_2 system, some background information on similar compositions is given in the last section.

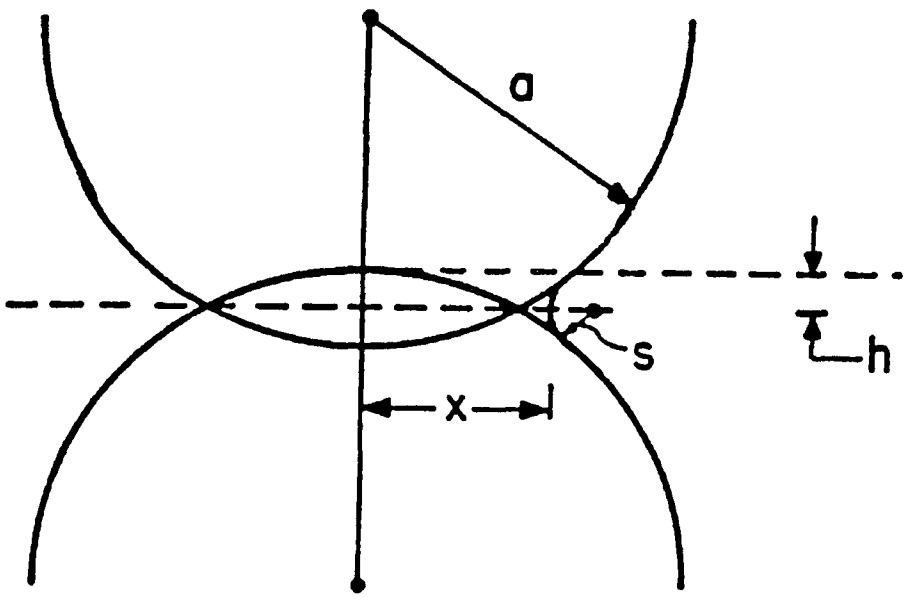

Figure 2.1: Center-to-center approach of two spherical particles. Geometry assumed by Frenkel.[10]

2.1 Homogeneous Sintering

A variety of models have been developed for describing the sintering behavior of homogeneous glass powders. The major differences between the models are the assumed microstructures of the powder compacts. The assumed geometries affect the range of relative densities over which the models should apply.

Frenkel developed the first model which described the sintering behavior of powders.[10] In the initial stages of sintering, the densification rate is related to the center-to-center approach of two spherical particles as shown in Figure 2.1. Frenkel was the first to assume that the rate of energy dissipation through viscous flow into the neck region between the particles is balanced by the rate of energy gained due to a reduction in surface area. The relative change in length of a sintering sample, $\Delta L/L_o$, can be expressed as[12]

$$\frac{\Delta L}{L_o} = \frac{3\gamma}{8\eta a} t \qquad (2.1)$$

where γ is the surface energy, η is the viscosity, a is the particle size, and t is time. This equation has been found to satisfactorily fit experimental data during the initial 4 to 10% of sintering.[12]

At the other extreme, Mackenzie and Shuttleworth developed a viscous sintering model for the final stages of sintering.[11] The energy rate balance developed

by Frenkel was applied to an isolated pore surrounded by a shell of material. The rate at which a single pore closes is

$$\frac{dr}{dt} = -\frac{\gamma}{2\eta}\frac{1}{\rho_r} \tag{2.2}$$

where ρ_r is the relative density of the bulk sample. The relative density can be calculated as a function of time, t, by

$$K'(t-t_o) = \frac{2}{3}\left(\frac{3}{4\pi}\right)^{1/3}\int_0^{\rho_r}\frac{d\rho_r}{(1-\rho_r)^{2/3}\rho_r^{1/3}} \tag{2.3}$$

where

$$K' = \frac{\gamma n^{1/3}}{\eta} \tag{2.4}$$

and n is the number of pores per unit volume.

Scherer[9] used the same energy balance as Frenkel[10] and Mackenzie and Shuttleworth[11] to develop a model for the intermediate stages of sintering. The geometries assumed by Frenkel and Mackenzie and Shuttleworth do not adequately describe a glass powder compact with a network of open pores. Scherer's model was

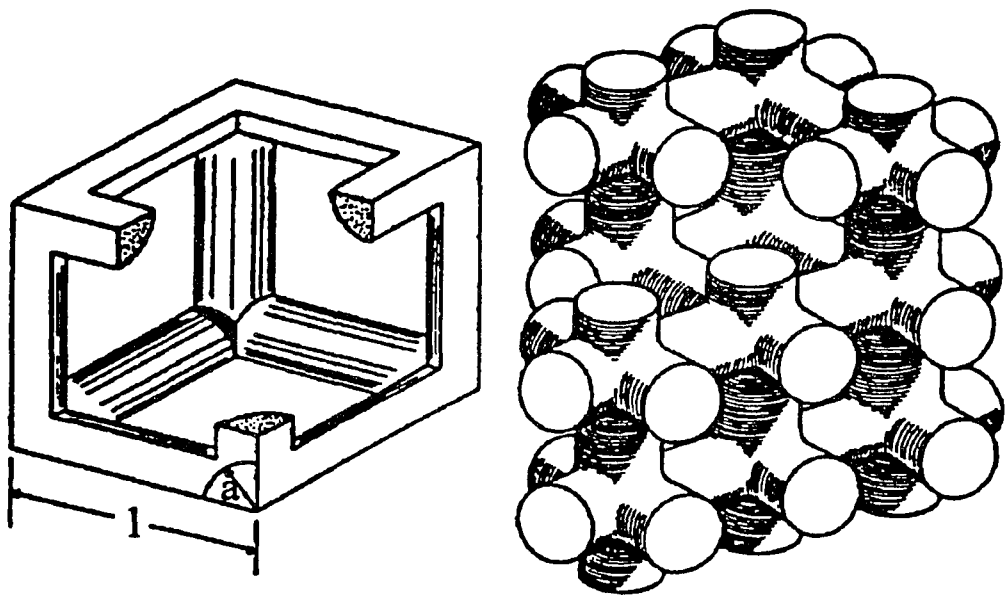

Figure 2.2: Cubic array of right circular cylinders. Geometry assumed by Scherer.[9]

designed to describe the sintering behavior of glasses produced by flame hydrolysis or gelation.

The geometry assumed by Scherer[9] is depicted in Figure 2.2. The Scherer unit cell consists of a cubic array of right circular cylinders. The cylinders have a length, l, and a radius, a, and represent a row of individual particles with the same radius.

By using this geometry, the sample geometry and microstructure can be represented by the unit cell dimensions. The relative density of a sample can be calculated as the ratio of the volume of the cylinders to the volume of the unit cell, or

$$\rho_r = \frac{3\pi a^2 l - 8\sqrt{2}a^3}{l^3} \qquad (2.5)$$

where the second term in the numerator represents the material in the corners of the unit cell. The hole in the side of the unit cell is

$$d_o = \frac{\sqrt{\pi}}{2}(l-2a) \qquad (2.6)$$

which represents the pore size measured by a technique such as mercury porosimetry. Therefore, the bulk properties of relative density and average pore size can define all of the unit cell dimensions.

The relative density of the unit cell can be re-expressed in terms of x as

$$\rho_r = 3\pi x^2 - 8\sqrt{2}x^3 \tag{2.7}$$

where x is a unitless parameter and x=a/l. The length of the unit cell, l, can also be expressed in terms of $\dot{x}$,

$$l = \frac{l_o \rho_{r_o}}{(3\pi x^2 - 8\sqrt{2}x^3)^{1/3}} \tag{2.8}$$

where l_o is the initial length of the unit cell, and ρ_{ro} is the initial relative density.

Since the flow fields of the array of intersecting cylinders is fairly complex, a simpler system of three cylinders was used for the energy balance. The total volume of these three equivalent cylinders is the same as the volume of the cylinders in the unit cell. The rate of energy dissipated by one of these equivalent cylinders by viscous flow is

$$\dot{E}_v = \frac{3\pi\eta a^2}{h}\left(\frac{dh}{dt}\right)^2 \tag{2.9}$$

where h is the height of the equivalent cylinder, h = 1-8$\sqrt{2}$a/3π. This rate of energy dissipation must be equal to the rate of energy change due to a reduction in surface area,

$$\dot{E}_s = \gamma \frac{dS}{dt} = \gamma \frac{d}{dt}(2\pi ah - \frac{8\sqrt{2}}{3\pi}a^3) \qquad (2.10)$$

After combining Equations 2.9 and 2.10 and doing some manipulation, changes in the sample due to sintering can be represented by

$$\frac{dx}{dt} = \frac{\gamma}{2\eta}\frac{1}{l} \qquad (2.11)$$

and

$$\frac{d\rho_r}{dt} = (6\pi x - 24\sqrt{2}x^2)\frac{dx}{dt} \qquad (2.12)$$

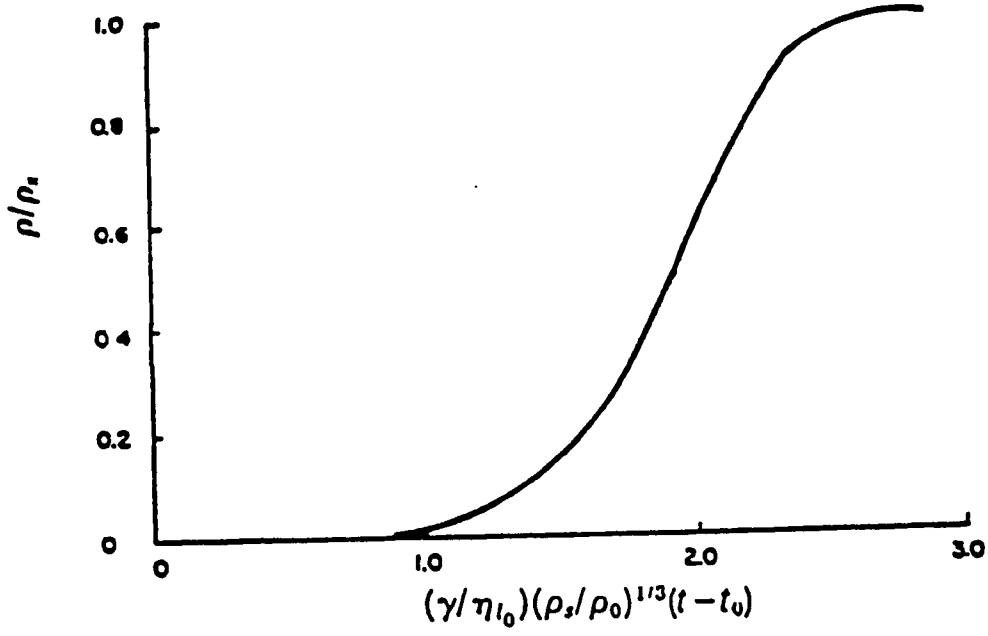

Figure 2.3: Predicted densification behavior for a cubic array of right circular cylinders.[9]

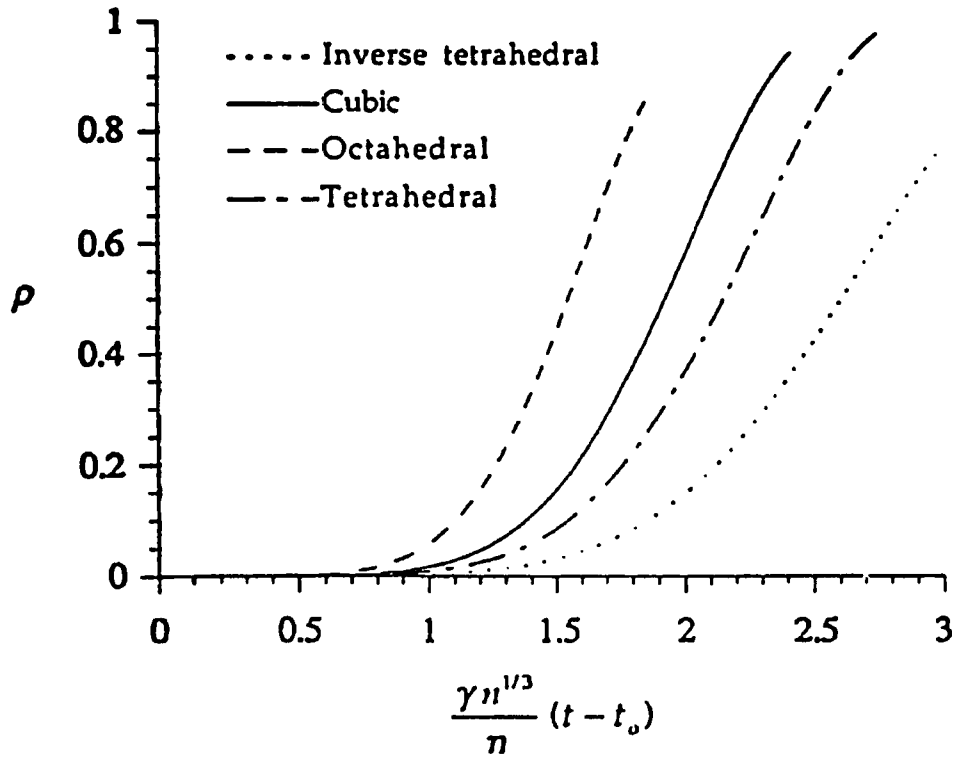

Figure 2.4: Predicted densification behavior for a variety of different arrangements of right circular cylinders.[13]

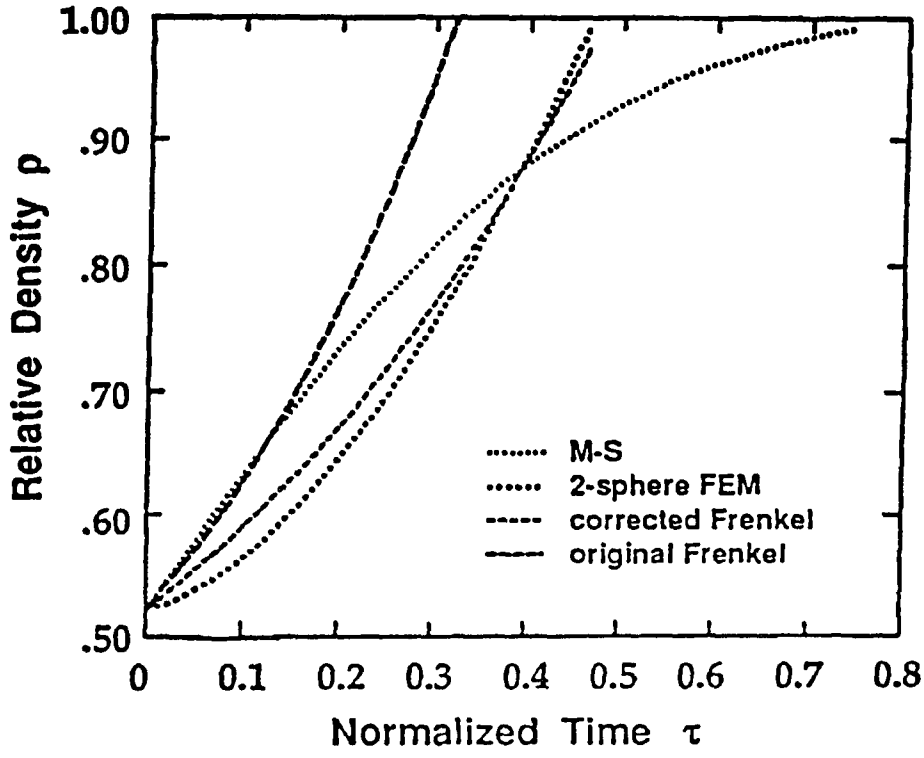

Figure 2.5: Predicted densification behavior for Frenkel's model (both corrected[10] and uncorrected[44]), Mackenzie-Shuttleworth (MS) model,[11] and finite element analysis for two spheres.[14] (From Scherer[44]).

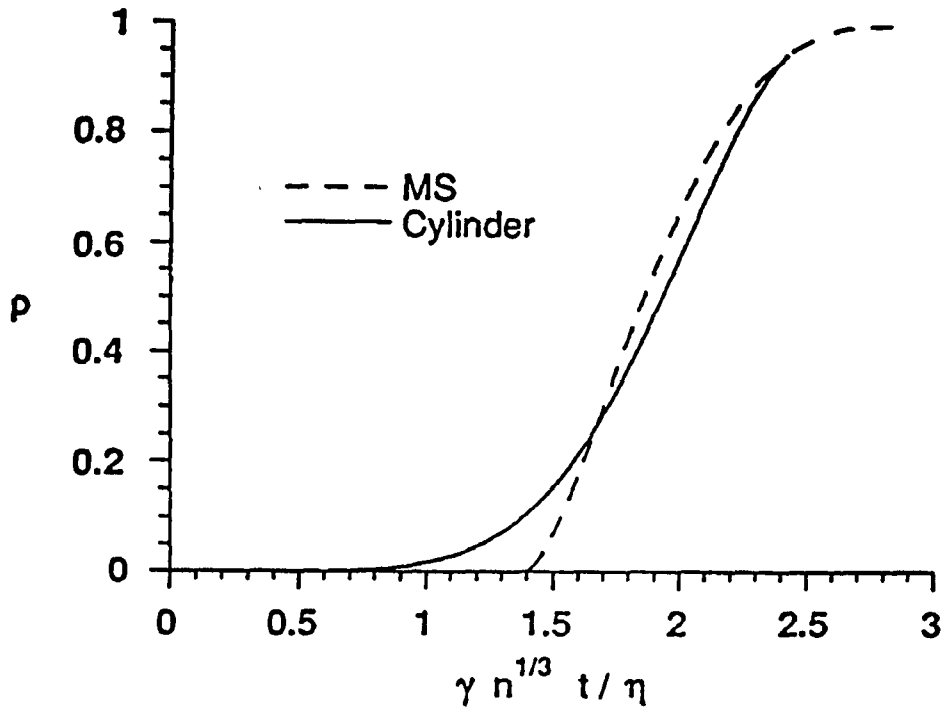

Figure 2.6: Comparisons of the densification behavior according to Scherer's (Cylinder) model,[9] and Mackenzie-Shuttleworth (MS).[11] (From Scherer[9]).

However, it is not possible to explicitly solve for the relative density as a function of time, which is shown graphically in Figure 2.3 as a function of normalized time, $K(t-t_o)$. Therefore, the solution to the Scherer sintering model is often expressed as

$$K(t-t_o) = \int_0^x \frac{2\,dx}{(3\pi - 8\sqrt{2})^{1/3} x^{2/3}} \tag{2.13}$$

where

$$K = \frac{\gamma}{\eta l_o \rho_{r_o}^{1/3}} \tag{2.14}$$

and t_o is the fictitious time where the relative density, and therefore x, are 0.

The derivation presented here has assumed a cubic array of right circular cylinders, but as shown in Figure 2.4 the same set of equations can be applied to several different geometries with similar results.[13] In fact, the results of different sintering models[9,10,11] are remarkably similar considering the very different assumed geometries. Comparisons between these three sintering models can be found in Figures 2.5 and 2.6.

Numerical simulations of the sintering of homogeneous powders correlates well with the three models presented in Figures 2.5 and 2.6. Jagota and Dawson[14] have conducted finite element analyses of two sintering particles which produced results very similar to Frenkel's model,[10] as shown in Figure 2.5.

All of these models have also been shown to accurately represent experimental sintering data.[12,15,16] Several groups have extrapolated viscosities from sintering curves and obtained values close to those measured by other techniques.[6,12,17,18] Some of the arguments presented to describe the observed differences between the experimental behavior and sintering models are rearrangement of the particles,[19] or anisotropic distributions of pores[20] or particles.[21] Since the experimental data from the literature appears to fit most of the models equally well, the Scherer geometry will be used in this document. This model was selected because the assumed geometry represents the microstructure of sol-gel glass powder compacts the best.

However, not all sintering compacts obey the assumptions on which all four of these models are based. The models assume that the unit cell or areas being examined are typical of the entire body. This implies that all the particles and pores must be the same size or at least have a fairly narrow distribution. Also, the materials properties are assumed to be the same everywhere; therefore, the sintering samples must have a uniform composition in order to apply these homogeneous sintering models. Since these two experimental conditions are not always met, in the next section several models will be presented which have been developed to describe heterogeneous sintering.

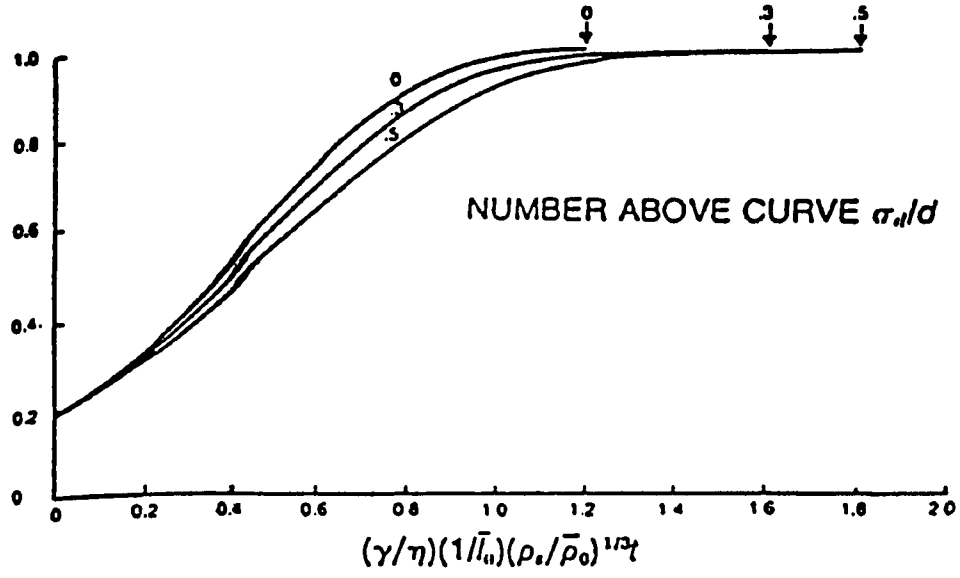

Figure 2.7: Effect of pore size distribution on sintering behavior.[22]

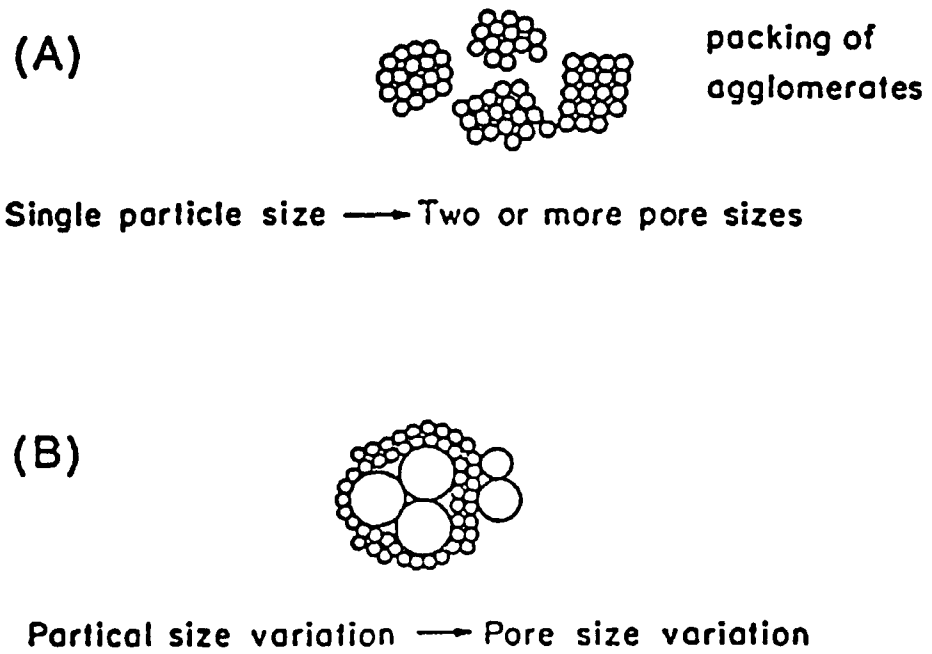

Figure 2.8: Two possible arrangements resulting in bimodal pore size distributions.[6]

2.2 Heterogeneous Sintering

2.2.1 Pore Size Distributions

In the last of the set of three original papers by Scherer[9,15,22] concerning the right circular cylinder model, he described the effect of assuming a distribution of pores on homogeneous sintering. Except when the distribution is fairly broad, only small differences are observed in the time to reach full density, as shown in Figure 2.7. Some of the difficulties encountered when attempting to remove large pores have been published,[23] and Scherer indicates that the pore size distribution approach[22] can be applied to hierarchical pore structures, such as the packing of agglomerates.[6]

The unit cells of Scherer's distribution model[22] have different dimensions, due to the distribution of pores, but sinter independently. This may be an acceptable approximation for fairly narrow or bimodal distributions of pores, as depicted in Figure 2.8A. However, as the small particles within agglomerates sinter and the agglomerates become smaller, in order to retain contact between the agglomerates the large pore in the center must also shrink. Therefore, even in an hierarchical structure, the sintering behaviors of the regions with different pore sizes are not independent.

A model which describes the shrinkage rate of one pore or region in terms of the rest of the sample should be used to describe powders with either of the

geometries shown in Figure 2.8. Scherer's Self-Consistent model[6] characterizes the sintering behavior of one region or pore in terms of the stresses applied by the surrounding matrix. For example, the smaller pores in a sample with a bimodal distribution sinter faster than the bulk sample or surrounding matrix. A resulting tensile stress on the material near the small pore slows its sintering rate. Similarly, a compressive stress around the large pore regions increases their sintering rate. By incorporating these stresses into a model, the densification rate of the matrix can be computed.

Selsing[24] calculated the hydrostatic stress in an inclusion, due to differences in thermal expansion between the rigid inclusion and its matrix, to be

$$\sigma_i = \frac{\epsilon_{f_m} - \epsilon_{f_i}}{[(1-2\nu_i)/E_i]+1/2[(1+\nu_m)/E_m]} \qquad (2.15)$$

The use of a constitutive equation such as[2]

$$\dot{\epsilon}_x = \dot{\epsilon}_f + (\frac{1}{E})[\sigma_x - \nu(\sigma_y+\sigma_z)] \qquad (2.16)$$

for viscous sintering was first postulated by Skorokhod.[25,26] The densification rate of each region can be calculated by applying the viscous analogy for a porous compact,[2]

$$\dot{\epsilon}_x = \dot{\epsilon}_f + (\frac{1}{F})[\sigma_x - N(\sigma_y + \sigma_z)] \tag{2.17}$$

where $F(\rho_r) \rightarrow 3\eta$ and $N(\rho_r) \rightarrow ½$ as the relative density approaches one. By using this analogy and Equation 2.15, the stresses in the different regions of a sample with a bimodal pore size distribution are

$$\sigma_s = \frac{\dot{\epsilon}_{f_m} - \dot{\epsilon}_{f_s}}{[(1-2N_s)/F_s] + 1/2[(1+N_m)/F_m]} \tag{2.18}$$

and

$$\sigma_l = \frac{\dot{\epsilon}_{f_m} - \dot{\epsilon}_{f_l}}{[(1-2N_l)/F_l] + 1/2[(1+N_m)/F_m]} \tag{2.19}$$

where the variables with the subscripts m, s, and l refer to the properties of the matrix, small pore regions, and large pore regions. Scherer used the average of the

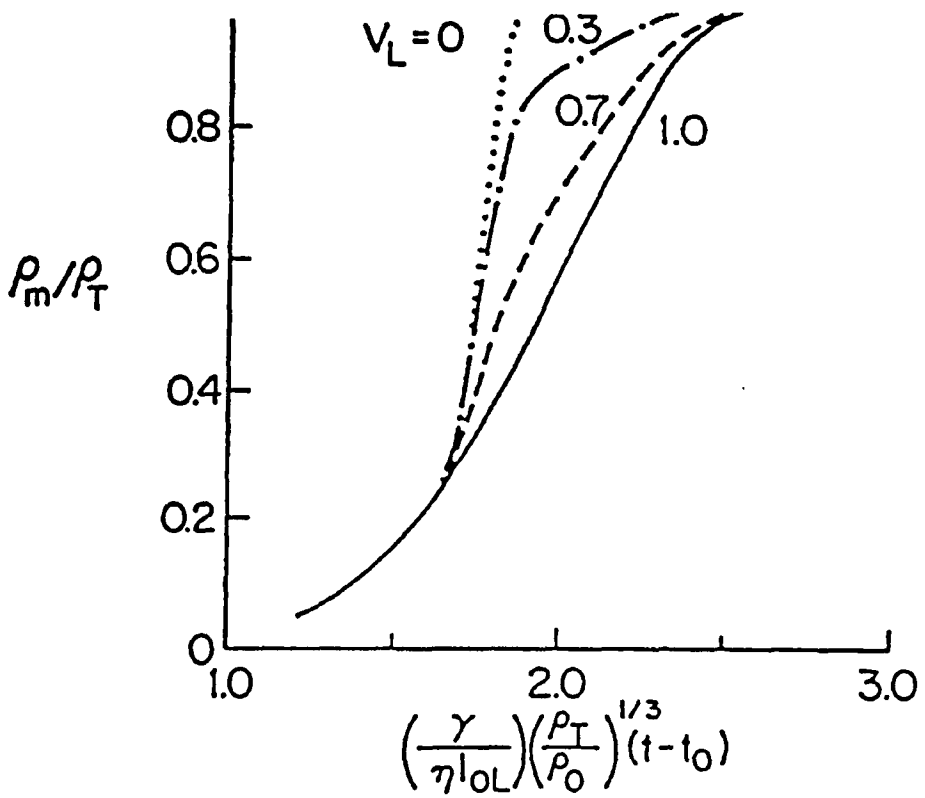

Figure 2.9: Densification behavior of samples with 0, 0.3, 0.7, and 1.0 volume fraction of large pore size material, with the remainder of sample containing smaller pores.[6]

upper and lower bounds of the Hashin-Shtrikman model[27] to compute the matrix properties. Since the strain rates are related to the densification rates by

$$\dot{\epsilon} = -\frac{1}{3}\frac{\dot{\rho}_r}{\rho_r} \tag{2.20}$$

the densification rates of the regions of the composite sample can be calculated using Equations 2.17, 2.18, 2.19, and 2.20. The densification rate of the matrix, as computed by Scherer,[6] is

$$\frac{\dot{\rho}_{r_m}}{\rho_{r_m}} = \frac{\rho_{r_l}}{\alpha\rho_{r_s}+\rho_{r_l}}\frac{\dot{\rho}_{r_s}}{\rho_{r_s}} + \frac{\alpha\rho_{r_s}}{\alpha\rho_{r_s}+\rho_{r_l}}\frac{\dot{\rho}_{r_l}}{\rho_{r_l}} \tag{2.21}$$

and is shown in Figure 2.9 for several different distributions of pores.

2.2.2 Chemical Distributions

The heterogeneities which exist in a sintering compact can be spatial, as described in the previous section for particle and pore size distributions, or chemical. The variations in materials properties due to chemical differences cause some regions in the sample to sinter faster than others. The incorporation of rigid particles in a

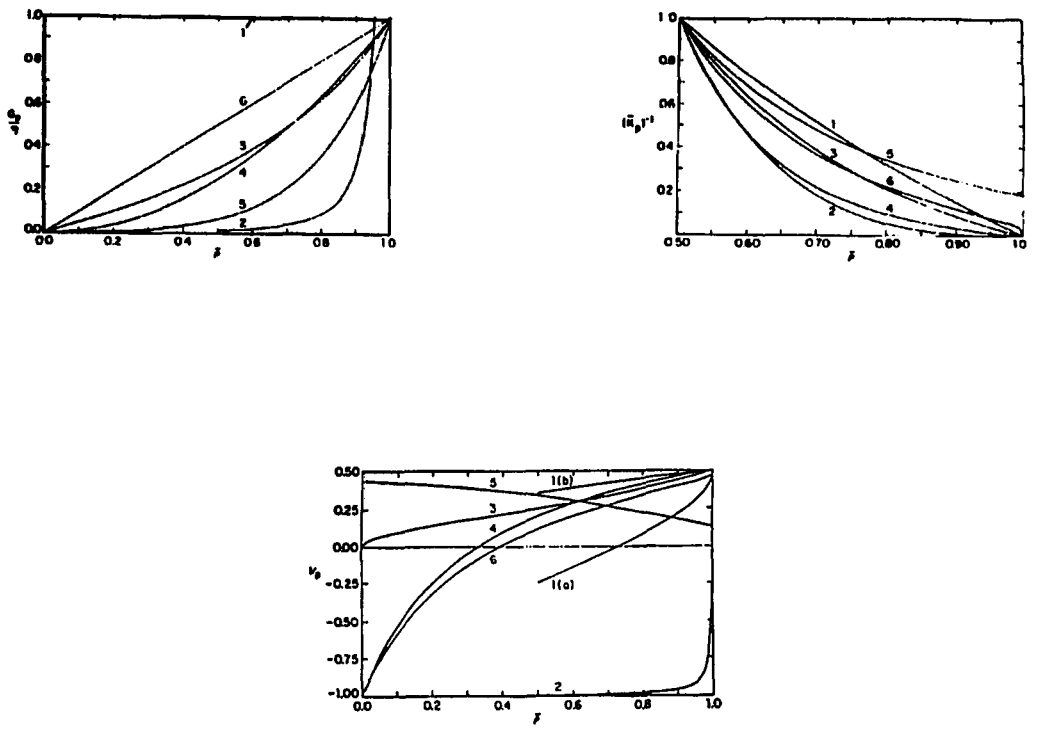

Figure 2.10: Calculated a) shear viscosity, b) bulk viscosity, and c) poisson's ratio for models proposed by 1) Raj and Bordia,[5] 2) Hsueh et al.,[4] 3) Scherer,[9] 4) Skorokhod,[25] 5) Rahaman et al.,[32] and 6) Venkatachari and Raj.[29] (From Bordia and Scherer[31]).

sintering matrix significantly slows the overall sintering rate. Samples of this type are often studied because they represent composites.

Several authors have proposed models for the sintering response of a material to an applied stress, caused either externally[28,29] or by heterogeneities in the sample.[2,4] Bordia and Scherer[30,31] compared several heterogeneous sintering models based on the computed values of bulk (K_p) and shear viscosities (G_p) and the values for poisson's ratio as a function of relative density (ν_p). All of the models discussed by Bordia and Scherer predicted acceptable values for the viscosities, but some resulted in negative values for poisson's ratio. The results of sinter-forging experiments suggest that when a large load is applied uniaxially on a sintering cylindrical pellet, the radius should shrink slower than without a load, implying positive values of poisson's ratio for all values of relative density.[29,32,33] In addition, the calculated values for poisson's ratio should approach ½ as the sample approaches full density.

Computed values of the shear viscosity, bulk viscosity, and poisson's ratio for several models are shown in Figure 2.10. Several of these models[31] were obtained by fitting experimental data to a function. Hsueh et al.[4] and Venkatachari and Raj[29] used experimental data for Al_2O_3 but obtained different relationships for the shear viscosity in terms of relative density. The expressions found by Hsueh et al.[4] have several problems due to the way in which the data, obtained by Coble and Kingery,[34] was interpreted; but both of these empirical relationships[4,29] result in negative values

for poisson's ratio at low relative densities.[31] The other empirical model described by Bordia and Scherer[31] and developed by Rahaman et al.[32] used sinter-forging data from several different compositions. The resulting values for the calculated poisson's ratios are positive for all values of relative density, but do not approach ½ as the sample reaches a relative density of 1.

Raj and Bordia[5] used a spring-dashpot approach to develop expressions for the shear and bulk viscosities for a sample sintering under shear. The developed equations depend on the dimensionless parameter, β, which represents the ratio of deformation rate constants in shear and in the bulk. If β is too small, the effective poisson's ratio is negative for low relative densities, but still approaches ½ as $\rho_r \rightarrow 1$.

The only model reviewed by Bordia and Scherer[31] which exhibits a relationship for poisson's ratio similar to what is observed experimentally[29,32,33] was the model developed by Scherer.[1] In this model the shear, G_p, and inverse bulk viscosities, $(K_p)^{-1}$, are computed geometrically

$$G_p = \frac{3\rho_r\eta}{6-4\rho_r+(3\rho_r-2\rho_r^2)^{1/2}} \qquad (2.22)$$

and

$$(K_p)^{-1} = \frac{3-2\rho_r-(3\rho_r-2\rho_r^2)^{1/2}}{2\rho_r} \qquad (2.23)$$

using a unit cell composed of right circular cylinders. This model predicts values for poisson's ratio between 0 and ½ for relative densities between 0 and 1. This is the only model analyzed by Bordia and Scherer[31] which gives the appropriate limits for poisson's ratio. This was also the only model presented which was developed for the sintering behavior of viscous instead of crystalline samples.

Lange[35] has also developed a model for the sintering of a heterogeneous sample with rigid inclusions. The inclusions are pinned to specific sites in a network, so the strain of the composite sample,

$$\epsilon_c = \epsilon_m(1-\frac{1}{\alpha}(\frac{f}{s})^{\frac{1}{3}}) \qquad (2.24)$$

depends on the free strain of the matrix, ϵ_m, the volume fraction of inclusions, f, the maximum volume fraction of inclusions, s, and a parameter which depends on the distribution of the inclusions, α. This model fits the sintering data of DeJonghe et al.[36] very well, but an effective poisson's ratio cannot be calculated and compared to some of the other models. One flaw in Lange's approach is that a simple

geometric model, such as this one, cannot explain the differences between crystalline and viscous sintering which is observed experimentally,[37] however, the effect of the sintering mechanism may be included in the free strain term, ϵ_m.

The current work has been limited to mixtures of glass powders. It has been shown experimentally[38] that Scherer's Self-Consistent model[6] can be applied to glass composites with a relatively low volume fraction of inclusions. If the matrix properties are measured instead of calculated using the Hashin-Shtrikman lower bound,[27] experimental data match the modelled behavior even though the percolation threshold of inclusions has been exceeded.[39] Chapter 3 of this document will describe how Scherer's Self-Consistent model has been modified to allow both glassy regions in a sample to sinter.

2.3 Background Information about Cordierite Composition

Several groups have studied the sintering behavior of glass powders of the cordierite composition.[8,12,40] Zelinski[12] and Aruchamy et al.[8] used cordierite glass powders to study the effect of processing on sintering and crystallization behaviors. Hardy and Rhine[40] monitored the densification behavior of composites using cordierite glass powders as the matrix material. This study will use glass powders having compositions near cordierite from which the effect of heterogeneities can be

studied. The effect of composition on the materials properties which affect sintering will be characterized.

Since cordierite glass powders densify by viscous sintering,[12,40] the porosity, initial relative density, theoretical density, viscosity, and surface energy must be characterized for each of the powders investigated. The porosity and initial relative density depend only on the processing conditions of the powder and the pressing conditions of the pellets. However, the other three are materials properties and vary with processing and composition.

The method for determining the theoretical densities of the glasses in this study is described in Chapter 4. However, it is worth noting here that by increasing the relative amount of spinel with respect to silica, the bulk density of the glass is expected to increase.[41] Cordierite glass, which has a composition along the silica/spinel tie-line, has a theoretical density of approximately 2.6 g/cc.[12,41]

The surface energy is not expected to vary significantly with composition. Ermolaeva[42] measured the surface tensions of a variety of glasses in this system, and found values between 240 and 364 ergs/cm^2. However, these measurements were made for melt glasses. Measurements of the surface energy of the solid compositions of interest have not been made. Therefore, for this document, a value of 300 ergs/cm^2 will be used for all of the powders.

The viscosity varies significantly with both composition and temperature. For most glasses along the SiO_2-$MgAl_2O_4$ tie line, as the amount of silica is increased so

does the viscosity.[43] This is supported by the data compiled by Mazurin et al.[41] However, the viscosity also depends on the processing conditions. Sintering studies have shown that the viscosities of sol-gel powders can be time-dependent.[12,28] Therefore, the viscosities for these powders will be measured and presented in Chapter 4.

CHAPTER 3

INHOMOGENEOUS SINTERING MODELS

Heterogeneities in sintering compacts may be caused by compositional variations resulting in differences in viscosity or surface energy, or may be due to particle/pore size distributions. Inhomogeneous sintering models should be able to predict the densification behavior for mixtures of powders. Chapter 2 reviewed several models which were developed to describe heterogeneous sintering. Most of these models apply if only one of the components is allowed to sinter, also called sintering with rigid inclusions.[7,37] A few models allow both of the components to sinter but have been explored primarily for inhomogeneities due to pore size distributions.[6] Only a few published models describe the sintering behavior of both components in a powder compact with compositional variations.[2]

In this chapter two different heterogeneous sintering models will be presented which can be applied to sintering compacts with either pore size or chemical distributions. One approach, the Self-Consistent Model, is an extension of Scherer's method for modelling powders with a bimodal pore size distribution.[6] The Interlocking Cell Model was developed for this work using interlocking Scherer unit

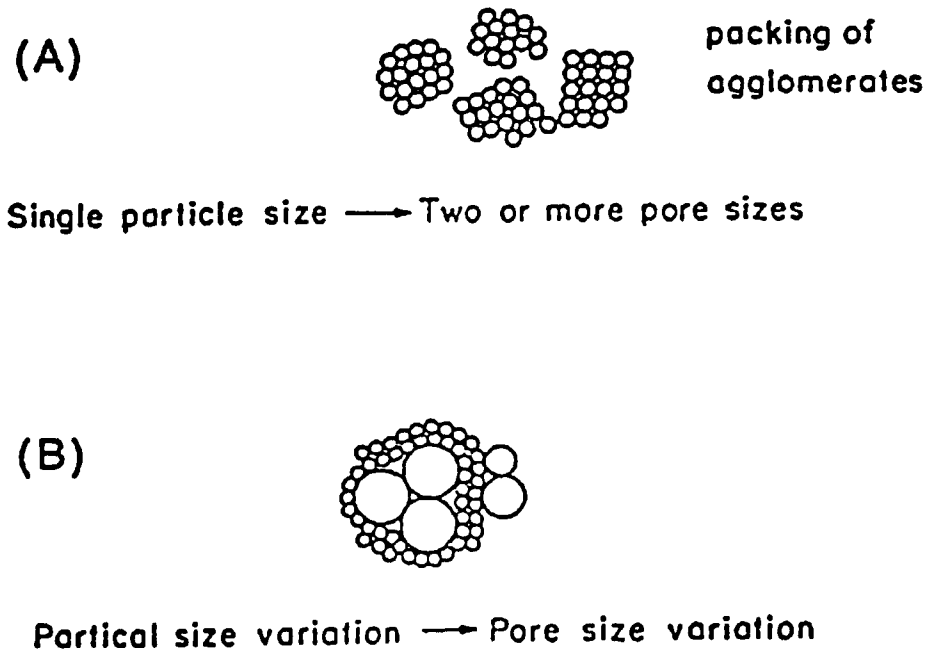

Figure 3.1: Two possible arrangements resulting in bimodal pore size distributions.[6] Figure A represents an hierarchical structure, while Figure B represents an anarchical structure.

cells[9] of various sizes which restrict the sintering of neighboring cells and of the overall sample. After the two models have been described, they will be compared and a description of the limitations of each model will be presented.

3.1 Self-Consistent Model

Scherer's version of the Self-Consistent model, referred to here as the SC model, was applied to bimodal distributions of pores.[6] When the pores are arranged in an anarchical manner as in Figure 3.1B, some regions of slowly sintering large pores are completely surrounded by faster sintering small pores, resulting in stresses in the sample. The same approach has been used to expand the SC model to describe the sintering of random distributions of particles with different viscosities. In a heterogeneous sample with two different viscosities, a tensile stress inhibiting sintering is applied to the low viscosity, faster sintering regions due to the sample's overall higher viscosity. Similarly, compressive stresses on the high viscosity regions result in faster sintering than if the same region were unconstrained.

In order to calculate the stresses due to heterogeneities in the sintering body, an analogy to thermal expansion models was made. Heating a mixture of two materials with different coefficients of thermal expansion results in internal stresses,

which affect the overall strain of the sample. Selsing calculated the stress, σ_i, due to the differences in thermal expansion in a sample with rigid inclusions to be:

$$\sigma_i = \frac{\epsilon_{fM} - \epsilon_{fi}}{[(1-2\nu_i)/E_i] + 1/2[(1+\nu_M)/E_M]} \tag{3.1}$$

where ϵ_f is the free strain, ν is poisson's ratio, E is the elastic modulus, and the subscripts i and M refer to the inclusion and matrix respectively.[24]

By using the viscous analogy and replacing the strains in Equation 3.1 with strain rates, expressions for the stress in an inhomogeneous sample which is sintering can be computed. Since the SC model allows both of the components (A and B) to sinter, the stresses surrounding both regions must be considered. The stresses, σ_A and σ_B, in a sintering compact due to the variations in sintering rates are:

$$\sigma_A = \frac{\dot{\epsilon}_{fM} - \dot{\epsilon}_{fA}}{[(1-2N_A)/F_A] + 1/2[(1+N_M)/F_M]} \tag{3.2}$$

and

$$\sigma_B = \frac{\dot{\epsilon}_{fM} - \dot{\epsilon}_{fB}}{[(1-2N_B)/F_B] + 1/2[(1+N_M)/F_M]} \tag{3.3}$$

where the subscripts A and B refer to the properties for each of the regions, and the subscript M refers to the overall matrix properties.[6] The variable $\dot{\epsilon}_f$ represents the

free strain rate, which is the rate at which a given region would normally sinter without an externally applied stress.

The variables F and N in Equations 3.2 and 3.3 represent the viscous analogies to the elastic modulus and poisson's ratio. In a sintering sample these properties are not constant and depend on materials parameters and the relative density. For a porous compact

$$F = \frac{3\eta\rho}{3\rho_t - 2\rho} \tag{3.4}$$

and

$$N = \left(\frac{2}{\pi}\right)^{3/2}\left(\frac{\rho}{3\rho_t - k\rho}\right)^{1/2} \tag{3.5}$$

where ρ_t is the theoretical density and $k = 3\text{-}1/2(4/\pi)^3 \approx 1.968$. As the density approaches the theoretical density ($\rho \rightarrow \rho_t$), then the variables F and N approach their steady-state values, $F(\rho) \rightarrow 3\eta$ and $N(\rho) \rightarrow ½$.[1]

Scherer[6] showed how the matrix properties, F_M and N_M, of a sintering material could be calculated from the bulk and shear viscosities using the Hashin-Shtrikman elastic limits.[27] Hashin and Shtrikman developed a set of equations to predict the upper and lower bounds of the viscosities for a mixture of materials.[27] This study follows Scherer's approach[6] and uses the average of the upper and lower limits to

predict the bulk and shear viscosities, from which the sintering properties, F_M and N_M, of the matrix can be calculated.

The matrix properties, F_M and N_M, can be used in Equations 3.2 and 3.3 to calculate the stresses in the different regions in the sample. By again applying the viscous analogy the strain rate of each region can be expressed as:

$$\dot{\epsilon}_A = \dot{\epsilon}_{fA} + (1-2N_A)\sigma_A/F_A \tag{3.6}$$

and

$$\dot{\epsilon}_B = \dot{\epsilon}_{fB} + (1-2N_B)\sigma_B/F_B \tag{3.7}$$

This assumes, however, that the stresses given in Equations 3.2 and 3.3 are applied hydrostatically.

The free strain rates, $\dot{\epsilon}_f$, for Equations 3.2, 3.3, 3.6, and 3.7 can be calculated from several different models. For this work the free strain rates of samples with relative densities less than 0.94 were found using Scherer's right circular cylinder model:[9]

$$\dot{\epsilon}_f = -\frac{(3\pi)^{1/3}}{6}\frac{\gamma}{\eta l_o}\left(\frac{\rho_t}{\rho_o}\right)^{1/3}\left[\frac{2-3cx}{x^{1/3}(1-cx)^{2/3}}\right] \tag{3.8}$$

Once the sample has reached closed pore stage, $\rho > 0.94\rho_t$, the Mackenzie-Shuttleworth model was used to calculate the free strain rates:[11]

$$\dot{\epsilon}_f = -\frac{1}{2}\left(\frac{4\pi}{3}\right)^{1/3}\frac{\gamma}{\eta l_o}\left(\frac{\rho_t}{\rho_o}\right)^{1/3}\left(\frac{\rho_t}{\rho} - 1\right)^{2/3} \tag{3.9}$$

Conservation of mass requires

$$\rho_M = \frac{(1 + \alpha)\rho_A\rho_B}{\alpha\rho_A + \rho_B} \tag{3.10}$$

where α is the weight ratio of component A to component B.[6] Therefore, the densification rate of the matrix depends on the densification rates of and the relative quantities of each of the regions:

$$\frac{\dot{\rho}_M}{\rho_M} = \frac{\rho_B}{\alpha\rho_A+\rho_B}\frac{\dot{\rho}_A}{\rho_A} + \frac{\alpha\rho_A}{\alpha\rho_A+\rho_B}\frac{\dot{\rho}_B}{\rho_B} \tag{3.11}$$

Since the strain rate is related to the densification rate by Equation 3.12,

$$\dot{\epsilon} = -\frac{1}{3}\frac{\dot{\rho}}{\rho} \tag{3.12}$$

Equations 3.6, 3.7, and 3.11 can be used to predict the densification rate of the matrix sample in terms of the materials properties of each region. A more detailed

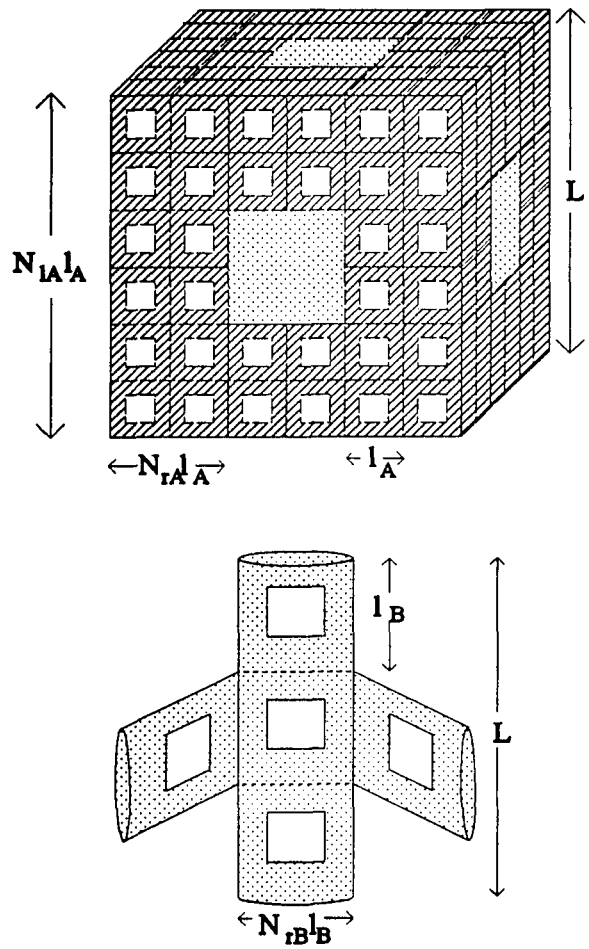

Figure 3.2: Geometry of the Interlocking Cell Model. For this diagram $N_{lA}=6$, $N_{rA}=2$, and $N_{rB}=1$.

mathematical derivation can be found in Scherer's paper describing the sintering behavior of samples with bimodal pore distribution.[6] The computer program used to do this modelling is given in Appendix A.

3.2 Interlocking Cell Model

The Interlocking Cell model was developed for this work as an alternative to the Self-Consistent model developed by Scherer.[6] Instead of calculating the stresses due to regions sintering at different rates, as in the Self-Consistent Model, the Interlocking Cell Model requires the entire sample to sinter at the same relative rate. This requirement occurs due to the geometry assumed by the model, hence the name Interlocking Cells, abbreviated as the IC model.

The assumed geometry for the IC model is depicted in Figure 3.2. A large Scherer unit cell[9] is constructed of smaller unit cells of Powder A. The pore in the center of the large Scherer cell is filled with small unit cells of Powder B. If Powder A normally sinters faster than Powder B, then as the large Scherer cell of Powder A tries to sinter, Powder B restricts the densification of the matrix. Therefore, if the entire sample is allowed to sinter without void formation, both the A and B Powders must sinter at a rate to maintain contact.

The mathematical equivalent of these geometrical restrictions can be derived in part by assuming that the length of the large Scherer cell, L, is composed of N_{lA} small unit cells of A:

$$L = N_{lA} l_A \tag{3.13}$$

as shown in Figure 3.2. The radius of the cylinders of the large Scherer unit cell accommodates N_{rA} small cells. If the diameter of the pore at the edge of the cell is N_{rB} small cells wide, then the length of the large Scherer cell can also be expressed as:

$$L = 2N_{rA} l_A + N_{rB} l_B \tag{3.14}$$

By setting Equations 3.13 and 3.14 equal to each other, the ratio of the dimensions for each type of small unit cell can be expressed in terms of the relative numbers of each type of cell:

$$\frac{l_A}{l_B} = \frac{N_{rB}}{N_{lA} - 2N_{rA}} \tag{3.15}$$

If the number and arrangement of the small cells of each powder does not change, then the total derivative of Equation 3.15 with respect to time is:

$$\frac{\frac{dl_A}{dt}}{l_A} = \frac{\frac{dl_B}{dt}}{l_B} \tag{3.16}$$

which implies that the relative changes in the unit cell dimensions are the same for each of the regions in the sample and the overall matrix.

Since the IC model doesn't require any additional stress analysis, Frenkel's basic assumption[10] that the rate of energy change due to the reduction in surface area ($\dot{E}_s$) must be equal to the rate energy is dissipated by viscous flow ($\dot{E}_v$) can be used. Flow of one component in the sample can result in a change in surface area of the other component and vice versa. This can be mathematically expressed as:

$$N_A\dot{E}_{V_A} + N_B\dot{E}_{V_B} = N_A\dot{E}_{S_A} + N_B\dot{E}_{S_B} \tag{3.17}$$

where N_A and N_B are the total numbers of small unit cells of each component in the sample.

The rate of energy loss of a cylinder through viscous flow is:

$$\dot{E}_v = \frac{3\pi\eta a^2}{h}\left(\frac{dh}{dt}\right)^2 \qquad (3.18)$$

where h is the height of the cylinder, a is the radius, and η is the viscosity of the material. The cylinders in the Scherer unit cell intersect at the corners, therefore the flow analysis is conducted on a simpler geometry - three cylinders with the same total volume as the Scherer unit cell. The height of this equivalent cylinder, with the same radius, a, as the cylinders in the Scherer unit cell, is:

$$h = l - \left(\frac{8\sqrt{2}}{3\pi}\right)a \qquad (3.19)$$

Therefore, the rate of energy loss through viscous flow in terms of the unit cell parameters is:

$$\dot{E}_V = \frac{4\pi^2\eta x^2 l^3}{\rho_r}\left(\frac{dx}{dt}\right)^2 \qquad (3.20)$$

where $x=a/l$ and $\rho_r = 3\pi x^2 - 8\sqrt{2}x^3$.

The rate of energy change in a cylinder due to a reduction in surface area is:

$$\dot{E}_S = \gamma\left(\frac{dS_c}{dt}\right) \tag{3.21}$$

where the surface area of the equivalent cylinder is $S_c = 2\pi al\text{-}8\sqrt{2}a^2$. This change in energy can be re-expressed as:

$$\dot{E}_S = -\frac{2\pi^2\gamma x^2 l^2}{\rho_r}\frac{dx}{dt} \tag{3.22}$$

Appendix B shows the complete derivation of Equations 3.20 and 3.22 and of the predicted densification rate using the IC model. After some manipulation the rate at which x_A changes, dx_A/dt, is found to be a function of α, η_A, η_B, ρ_A, ρ_B, γ_A, γ_B, x_A, x_B, l_A, and l_B. The rate at which the other component deforms, dx_B/dt, is a function of only x_A, x_B, and dx_A/dt. Since the relative densities of each region depend only on x, the relative densification rates of the two regions can be found through:

$$\frac{d\rho_i}{dt} = (6\pi x_i - 24\sqrt{2}x_i^2)\frac{dx_i}{dt} \tag{3.23}$$

The computer program used to model IC densification is in Appendix C.

Table 3.1 - Input Constants

Variable	Parameter Name	Value
η	Viscosity	Varied (see Table 3.2)
γ	Surface Energy	300 ergs/cm^2
d_o	Initial Pore Size	50 Å
ρ_o	Initial Relative Density	0.4
ρ_t	Theoretical Density	2.5 g/cc
α	Weight Ratio	1
(X)	(Mole Fraction - Important for calculating the homogeneous viscosity)	1

3.3 Parameterization

Both the Interlocking Cell (IC) and Self-Consistent (SC) models have been explored by varying the viscosities of each component in a heterogeneous sample. In order to study only the effects due to differences in viscosity, other important sintering parameters were kept constant. The values for these constants are listed in Table 3.1.

All of the modelled heterogenous sintering curves will be plotted against a normalized time, which includes the homogeneous viscosity. Therefore, it is necessary to calculate an effective homogeneous viscosity for the each modelled compositions, by assuming that two components in the sample are well mixed. Bottinga and Weill found that the logarithm of the viscosity of silicate melts depends linearly on composition over a relatively large range.[43] For this parameterization study the homogeneous viscosity was calculated using:

$$\ln\eta_h = X_A \ln\eta_A + X_B \ln\eta_B \qquad (3.24)$$

where X_A and X_B are the mole fractions of each component. Since both the SC and IC models require the weight ratio of the two components, instead of the mole fractions, it was assumed that the two components in the heterogeneous sample had

Table 3.2 - Viscosity Ratios

Viscosity Ratio	Homogeneous Viscosity (Poise)	Viscosity of A (Poise)	Viscosity of B (Poise)
1	10^{13}	10^{13}	10^{13}
2	10^{13}	$7.07*10^{12}$	$1.41*10^{13}$
3	10^{13}	$5.77*10^{12}$	$1.73*10^{13}$
5	10^{13}	$4.47*10^{12}$	$2.24*10^{13}$
10	10^{13}	$3.16*10^{12}$	$3.16*10^{13}$
100	10^{13}	10^{12}	10^{14}

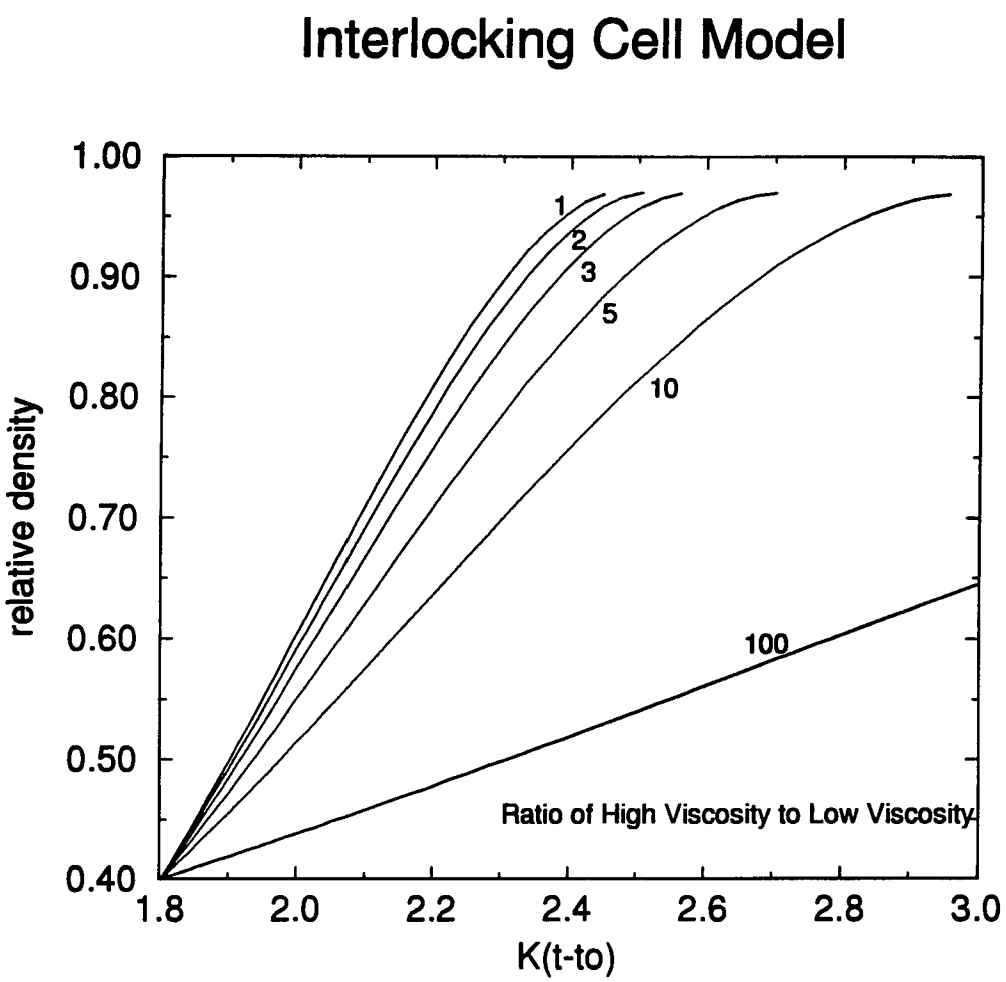

Figure 3.3: Densification behavior predicted by the Interlocking Cell Model for viscosity ratios of 1, 2, 3, 5, 10, and 100.

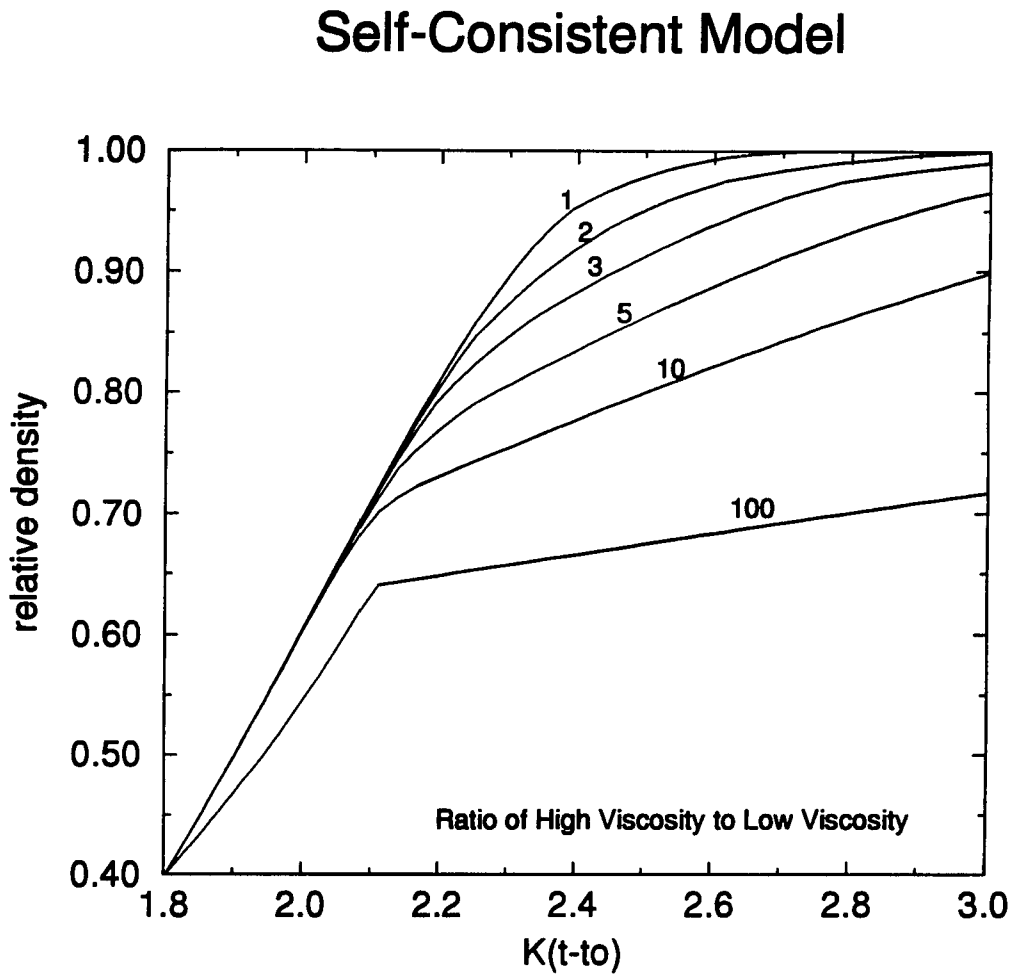

Figure 3.4: Densification behavior predicted by the Self-Consistent Model for viscosity ratios of 1, 2, 3, 5, 10, and 100.

similar densities and molecular weights. For equal amounts of the two components by weight ($\alpha = 1$), Equation 3.24 reduces to:

$$\eta_h = \sqrt{\eta_A \eta_B} \tag{3.25}$$

Table 3.2 contains the viscosities for each of the components used to explore both the IC and SC modelled sintering behaviors.

The IC and SC modelled behaviors depicted in Figures 3.3 and 3.4 and described below are plotted as relative density versus the homogeneous normalized time, $K(t-t_o)$. The normalized time parameter as defined by Scherer[9] is:

$$K(t-t_o) = \frac{\gamma}{\eta_h l_o \rho_{ro}^{1/3}}(t-t_o) \tag{3.26}$$

where t_o is the fictitious time when the relative density is zero. The homogeneous viscosity can be calculated using Equation 3.25. All of the parameters except the viscosity are the same in all the samples and are listed in Table 3.1.

3.3.1 Interlocking Cell Model

Figure 3.3 depicts the sintering behavior predicted by the IC model for viscosity ratios of 1, 2, 3, 5, 10, and 100, where a viscosity ratio of 1 represents a

homogeneous sample. The Scherer model[9] was used for the free strain rate over the entire range. Therefore, the sintering curves stop at a relative density of 0.94 beyond which the Scherer model is no longer valid.

For a given normalized time, $K(t-t_o)$, the homogeneous relative density is larger than for the heterogeneous sample. Heterogeneous samples with viscosity ratios significantly greater than 1 are predicted to sinter much slower than homogeneous powder compacts. A heterogeneous sample with a viscosity ratio of 10, will actually take 1.8 times longer to reach a relative density of 94% when compared to the corresponding homogeneous sample. Samples with larger viscosity ratios, possibly due to large differences in composition, require longer times to sinter.

While the heterogeneous samples are predicted to sinter slower than the corresponding homogeneous samples, the IC model predicts very similarly shaped curves. The initial sintering rate appears almost linear until relative densities of ~0.85. After that the densification rate slows and the relative density slowly approaches a value of one (if the Mackenzie-Shuttleworth model[11] were used to extend the range of the model).

Since the shapes of all the IC modelled curves are so similar, it may be possible to use a homogeneous sintering model to predict the heterogeneous densification behavior. However, in order to accomplish this, it is necessary to calculate an effective viscosity for these heterogeneous samples. Since the heterogeneous and homogeneous sintering curves do not lie on top of each other, the

Bottinga and Weill model[43] for computing viscosities of homogeneous glass melts does not appear to apply to mixtures of powders. However, some other model for extrapolating viscosity values based on composition may be useful.

In fact, Equation 3.17 may assist in finding that relationship. Deriving a generalized formula for the effective matrix viscosity is difficult. However, it is possible to look at the specialized case of two powders mixed together with the same dimensions for the small unit cells. Under these conditions Equation 3.17 reduces to:

$$\frac{3\pi a^2}{h}\left(\frac{dh}{dt}\right)^2[N_A\eta_A + N_B\eta_B] = \frac{2\pi^2\gamma x^2 l^2}{\rho_r}\frac{dx}{dt} \qquad (3.27)$$

or

$$\eta_m = N_A\eta_A + N_B\eta_B \qquad (3.28)$$

Therefore the matrix viscosity is simply a weighted average of the viscosities of the two components based on the number of each type of unit cell.

3.3.2 Self-Consistent Model

The heterogeneous sintering curves predicted by the SC model for viscosity ratios of 1, 2, 3, 5, 10, and 100 are shown in Figure 3.4. The x-axis corresponds to

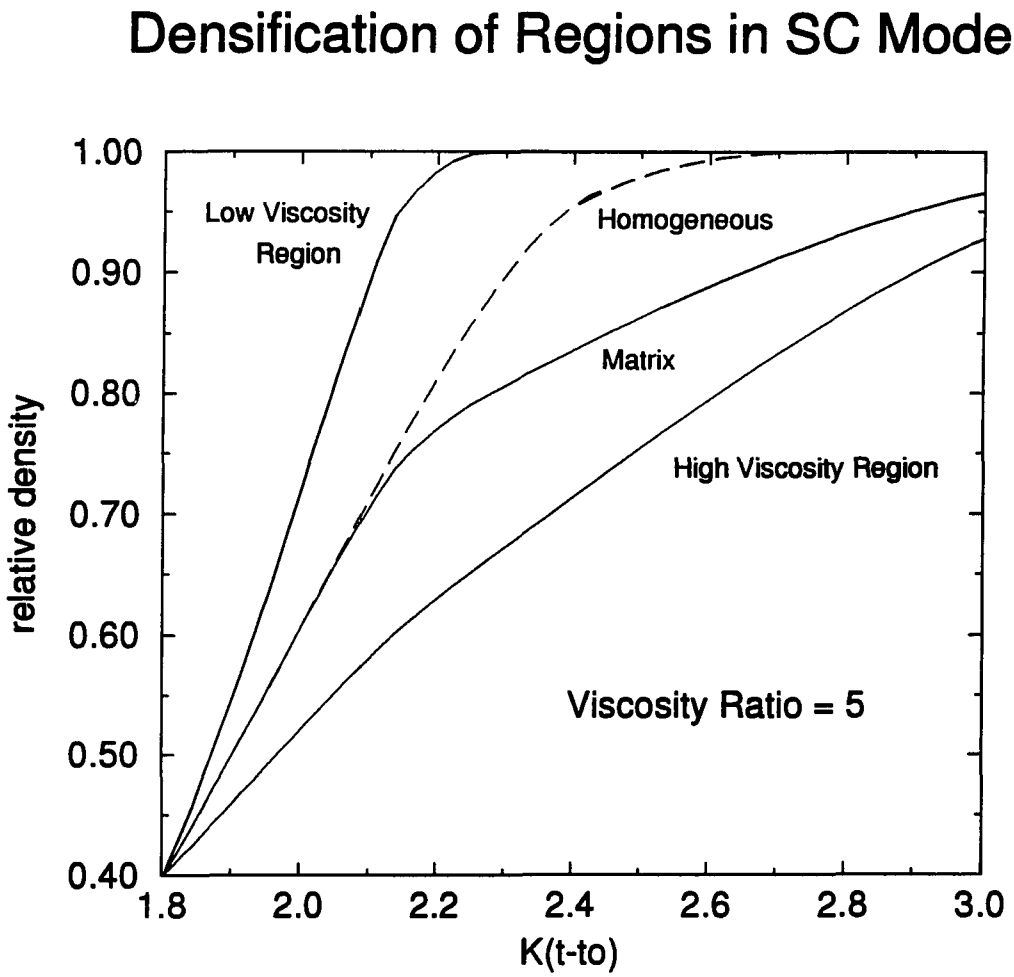

Figure 3.5: Densification behavior of the regions within a heterogeneous sample as predicted by the Self-Consistent model for a viscosity ratio of 5.

the normalized time for a homogeneous sample with a viscosity calculated using Bottinga and Weill's approach[43] and Equation 3.25. Just as was observed for the IC model, increasing the viscosity ratio from one to one hundred dramatically increases the time to reach full density.

However, unlike the IC model, the shapes of the SC modelled heterogeneous sintering curves are significantly different from the homogeneous sample. Figure 3.5 shows the densification behavior for each of the regions in a heterogeneous sample with a viscosity ratio of five. The low viscosity regions sinter much faster than the high viscosity regions, with the homogeneous and heterogeneous (matrix) sintering behaviors lying in between. The matrix and homogeneous sintering curves are very similar until the normalized time is approximately 2.1. The faster sintering low viscosity regions of the SC modelled sample initially help the bulk sample sinter. But once those regions are close to their full density, they act as inclusions and slow the densification of the bulk sample. This transition is observed in Figure 3.5 at a normalized time of approximately 2.2. As the faster sintering region approaches full density, the overall sintering slows considerably and the microstructural development of this heterogeneous sample is similar to one of a sintering compact with rigid inclusions. However, for most of the viscosity ratios explored, the sintering rate is initially fairly close to the homogeneous behavior, but then decreases significantly.

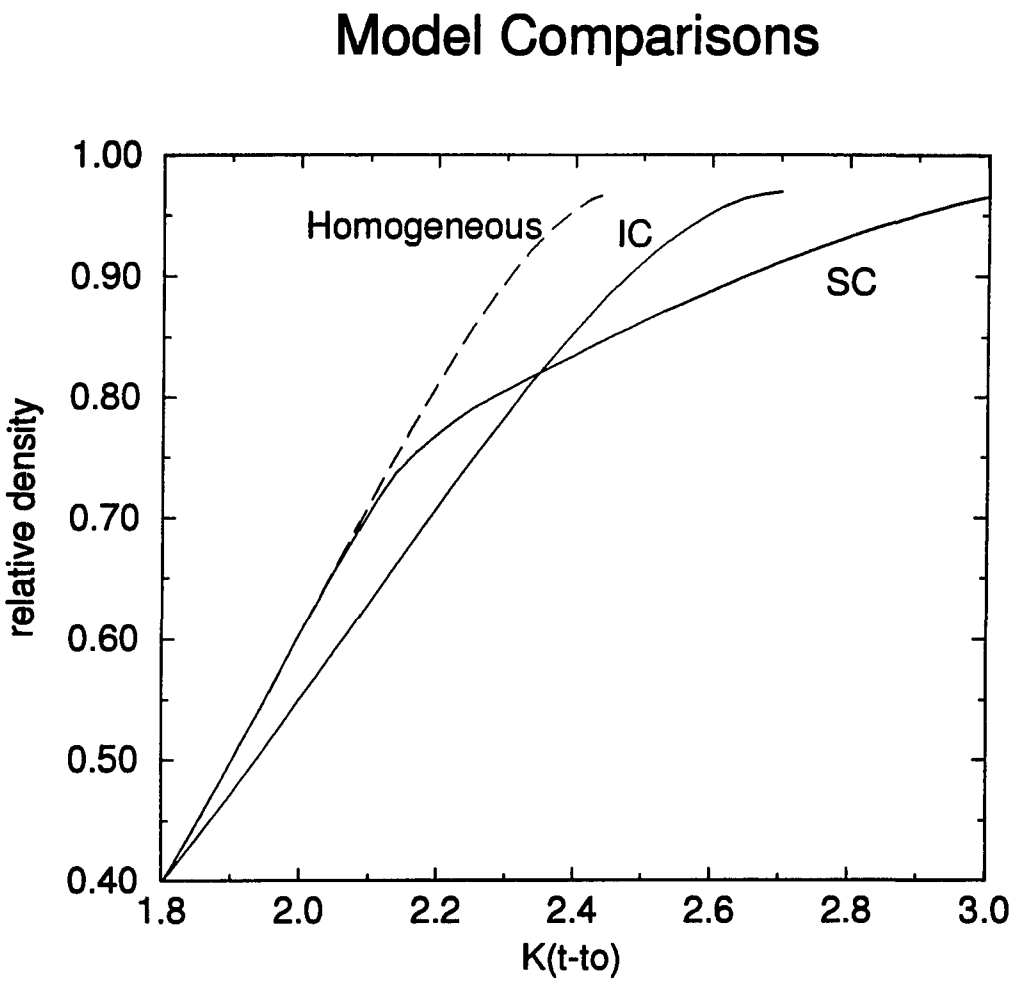

Figure 3.6: Densification behavior of a heterogeneous sample with a viscosity ratio of 5 as predicted by both the Self-Consistent and Interlocking Cell models.

3.4 Discussion

Figures 3.3 and 3.4 show the effect of the viscosity ratio on the sintering behavior of heterogeneous samples characterized using both the IC and SC models. Both of these models predict that by increasing the viscosity ratio of the two components in the heterogeneous sample, the time needed to sinter to a given density increases.

However, the overall sintering behavior predicted by each of these two models is very different, as shown in Figure 3.6 for a viscosity ratio of 5. The IC model has the same general shape as the homogeneous sample, but appears to have a higher effective viscosity. On the other hand, the SC model predicts initial sintering behaviors very similar to the homogeneous curve, but then deviates once the faster sintering regions approach full density.

Not only are the sintering curves for these two models different, but the assumptions about the developing microstructures are not the same. The basic geometrical assumptions of the IC model require all the Scherer cells, and therefore all the regions in a heterogeneous sample, to sinter at the same relative rate. The SC model allows each of the regions to sinter at a different rate, and then predicts the heterogeneous sintering behavior from the stresses that develop.

These two models assume very different microstructures during sintering. The IC model assumes that the two regions sinter at the same rate as the bulk, and the

SC model predicts different densification rates for each of the regions in the mixed sample. Therefore, only one of these models can accurately describe the changes in microstructure in a heterogeneous sample during sintering. Chapter 5 will explore which of these models fits the experimental sintering curves better.

While in this chapter both models were analyzed only for equal amounts of the two components, they do not mathematically fail for any amount of the faster sintering material from 0% to 100%. However, the IC model geometry does require a continuous network of both phases in order to generate the large interlocking unit cells as depicted in Figure 3.2. Therefore, the percolation threshold of 20% must be maintained for both regions.[44]

The SC model does not require a continuous network, but does impose a uniform hydrostatic stress on each of the regions. Therefore, the matrix around a given region should be compositionally uniform. This actually only occurs if neighboring regions do not interact, requiring a relatively low volume fraction of one of the components for the SC model to apply.

While sintering curves based on either the IC or SC model can be computed for any heterogeneous compact, geometrical assumptions suggest that the IC model should only be valid for approximately equal amounts of the two components and the SC model should apply when there is significantly more of one component than the other.

Both of these models have several other assumptions implicitly built in. One of these is that voids cannot form in the heterogeneous sample. In both the IC and SC models, the regions must maintain contact in order to transfer energy. However, if the stresses developing in the material due to differences in the free strain rates of the different compositions are extremely large, voids can form at the interface between the two regions.

Another factor which is not included in either of these models is bulk flow. The SC model implicitly assumes that flow occurs in order to maintain contact at the interface between the regions sintering at different rates. However, this term is not included in the energy rate equations. Bulk flow in the IC model implies that at the surface of the sample the lower viscosity composition would wick into the bulk through capillary flow. If this were to occur, the geometry requirements of the IC model would no longer apply at the surface since one of the regions would be absent.

However, as long as the viscosity ratio is not significant these two factors should not affect the applicability of these models to experimental data. In the next chapter a set of experiments will be described which were developed to test the validity of the IC and SC models. In Chapter 5, these two models will be compared to experimental heterogeneous sintering curves.

CHAPTER 4

EXPERIMENTAL PROCEDURE AND ANALYSIS

Densification curves can be used to characterize sintering behavior or test sintering models of either homogeneous or heterogeneous samples. In this chapter the experimental procedure and results will be outlined for the sintering studies of several different powders. Other characterization results, including porosimetry and X-ray diffraction analysis, will also be presented. The data analysis section, section 4.4, describes how the results from experimental sintering curves can be used to compare experimental and modelled sintering behaviors. Experimental viscosity and densification data will be obtained to test the two heterogeneous sintering models presented in Chapter 3.

4.1 Compositions

The compositions used for this study are shown in the MgO-Al_2O_3-SiO_2 phase diagram in Figure 4.1.[45] The exact compositions of the stoichiometric cordierite

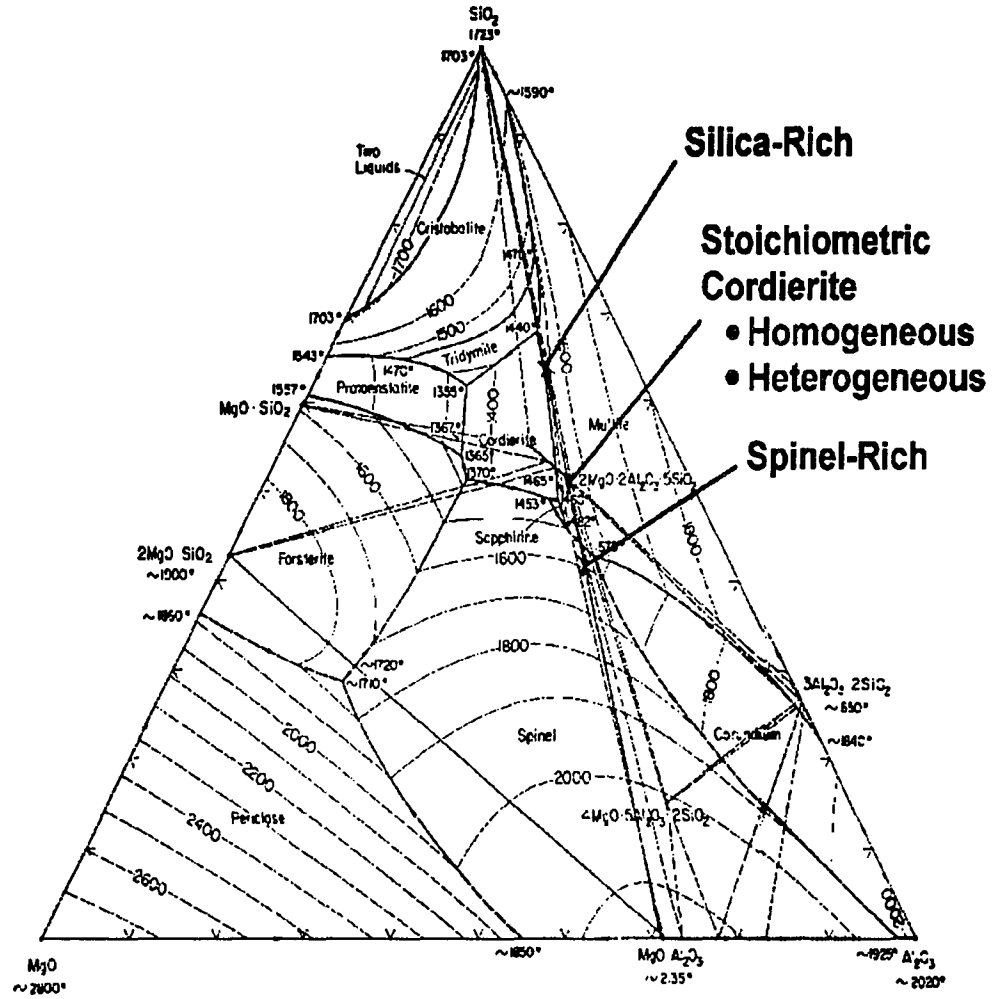

Figure 4.1: Phase Diagram of the $MgO\text{-}Al_2O_3\text{-}SiO_2$ system.[45]

powder (St) and the other homogeneous powders used in this study (Si and Sp) are listed in Table 4.1. Since these three compositions all lie along the silica-spinel tie line and vary by 10 mol% silica, they will be called stoichiometric, silica-rich, and spinel-rich, or abbreviated as St, Si, and Sp respectively.

Table 4.1 - Powder Compositions

Composition	Si (mol%)	St (mol%)	Sp (mol%)	M (mol%)
SiO_2	81.43	71.43	61.43	71.43
$MgAl_2O_4$	18.57	28.57	38.57	28.57

The three homogeneous powders listed in Table 4.1 were synthesized using an all alkoxide wet-chemical route as described by Aruchamy et al.[8] The only deviation from the procedure described[8] was that these powders were not spray-dried. The solvents were allowed to evaporate at room temperature producing a filter cake which was easily broken up into a powder in a mortar and pestle. The air-dried powder was then calcined at 700°C for two hours. This particular sol-gel route was selected because it can produce powders which are more homogeneous than other wet-chemical routes, and were found to have crystallization behaviors similar to very high purity melt glass powders.[8,12] Milled, melt-derived powders were not used because small particle sizes were preferred for the sintering studies. Smaller particle

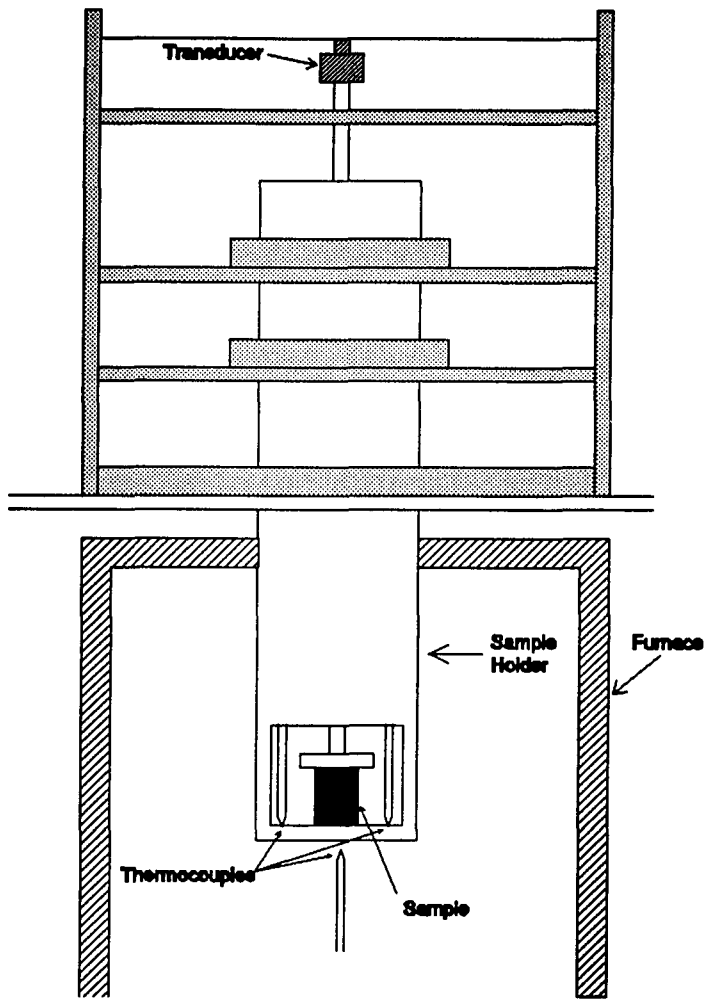

Figure 4.2: Experimental Sintering Apparatus - Dilatometer.

sizes allow powder compacts to sinter at lower temperatures and obtain higher densities before crystallization begins.

The heterogeneous sample, called mixed (M), was made by dry mixing the Sp and Si calcined powders in an alumina mortar and pestle for ten minutes. The resultant powder had the same overall composition as the homogeneous cordierite powder (St).

The approximate compositions of the Sp and Si powders were selected to provide a large enough difference in viscosity to distinguish between the Interlocking Cell and Self-Consistent models presented in Chapter 3. Viscosities for the Si and Sp compositions were computed according to the formalism developed by Bottinga and Weill.[43] As Appendix D shows, the ratio of the viscosity of the Si powder to the viscosity of the Sp powder is predicted to be approximately 52. This difference in viscosities should be large enough to distinguish between the two heterogenous sintering models.

4.2 Experimental Procedure

The dilatometer shown in Figure 4.2 and used for the experimental sintering studies requires the use of samples which are approximately 1 cm high. Therefore, cylindrical pellets were pressed using the air-dried powders described in section 4.1.

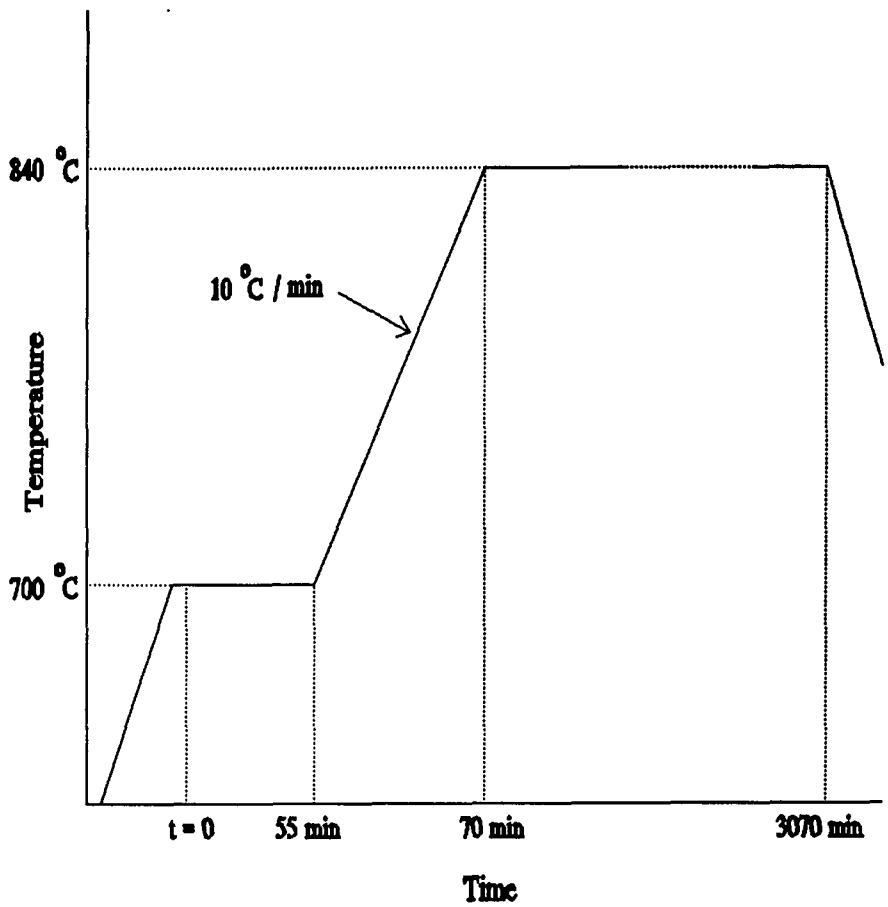

Figure 4.3: Heating Profile for Sintering Experiments.

In order to maintain some green strength, 20 drops of a saturated stearic acid/ethanol solution was added as a binder to approximately 0.20 g of powder before being pressed uniaxially to 1500 lbs in a 1/4" diameter cylindrical die. All samples were isostatically pressed at the same time to approximately 40,000 psi in order to ensure identical final pressing pressures.

Since the drying and pressing conditions significantly affect the green density and porosity, measurements of the initial pore size distribution were made. Mercury porosimetry was used to measure the pore size distribution for one sample of each composition before it had been sintered.

Densification curves for the three homogeneous compositions and the mixed powder were obtained using a dilatometer shown schematically in Figure 4.2. Dimensional changes in the pellets were measured with a displacement transducer positioned on top of a quartz rod which rested on the sample. The pellets were placed between two alumina plates in the sample chamber when the furnace was lowered. A motor was used to raise the preheated furnace to enclose the sample holder. The two thermocouples next to the powder compact were used to control the furnace and record the temperature.

The heating profile in Figure 4.3 was designed to provide reproducible heat treatments. Samples were inserted into the preheated 700°C furnace to allow the pellets and sample chamber to reach thermal equilibrium and the furnace control thermocouple was switched to one which is next to the sample. The 10°C/min ramp

up to the sintering temperature, 840°C, was rapid enough for only a small amount of densification to occur before reaching thermal stability. If a faster ramp rate had been selected the furnace would have overshot the desired temperature considerably.

Dimensional changes in the sample pellets were detected by the transducer and output to a chart recorder. The charts were digitized and mathematically converted into actual changes in length by a linear extrapolation of the initial and final voltages output by the transducer and the measured lengths before and after heating. The lengths and radii of the pellets were measured with a micrometer to ± 0.001 mm before and after sintering.

In order to convert from dimensional changes in length to densification curves, the length, radius, and mass of the pellets as a function of time must be known. The ratio of the relative change in length to the relative change in radius was between 1.02 and 1.07. Since none of the experimental samples slumped significantly (aspect ratios near 1.0), it was assumed that the changes in radius were linear with the changes in length. Since glasses of these compositions do not experience significant weight loss at these temperatures,[12] the mass lost during firing is due to the volatilization of the binder and residual organics from the processing. The mass after firing was used as a constant to calculate the glass density. The density, ρ, of a

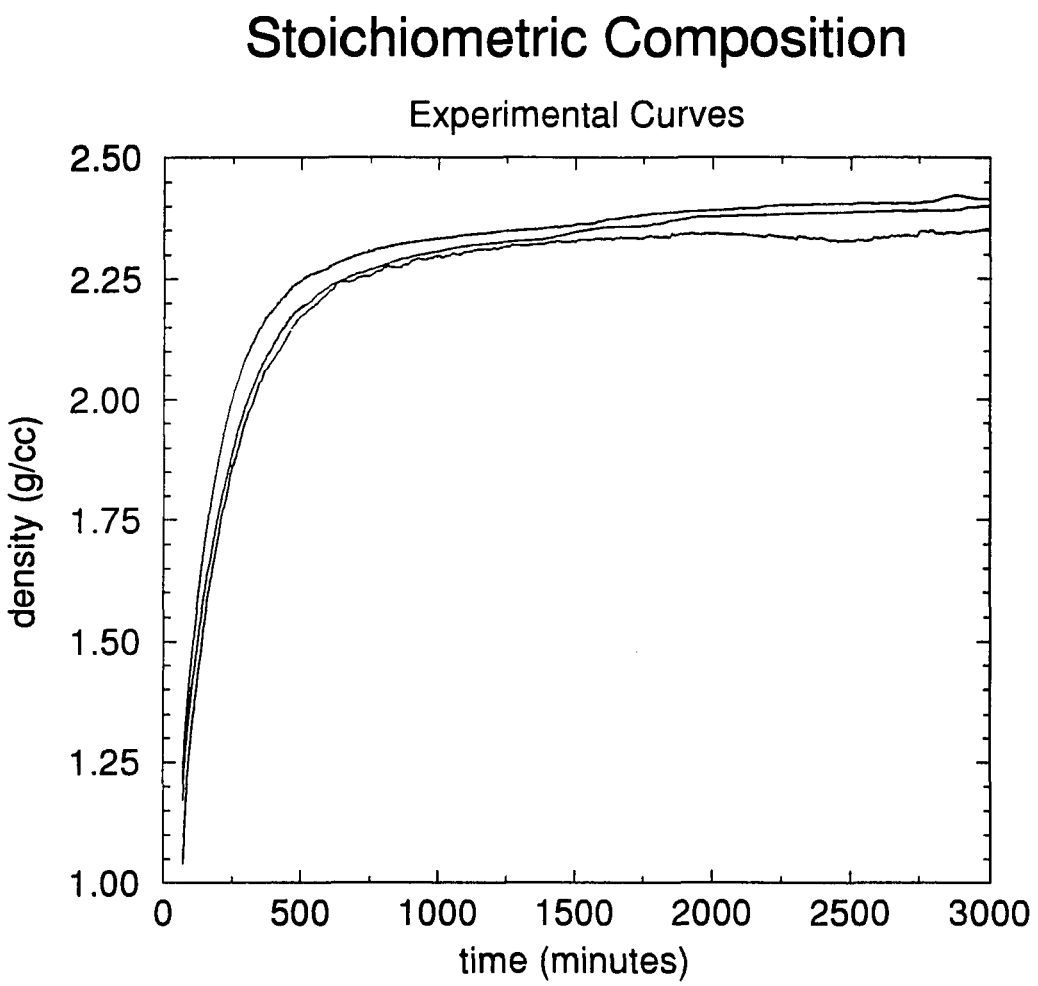

Figure 4.4: Experimental Sintering Curves for Stoichiometric Cordierite composition (St).

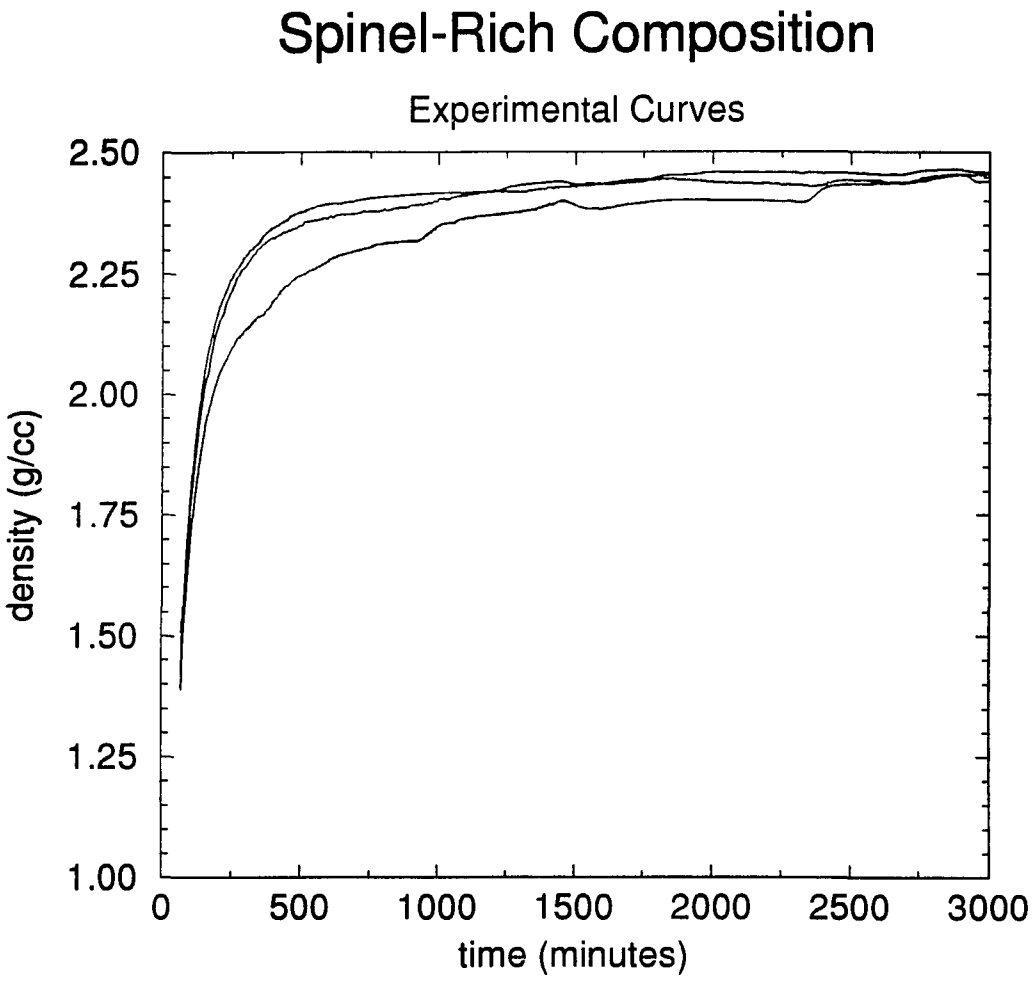

Figure 4.5: Experimental Sintering Curves for Spinel-Rich composition (Sp).

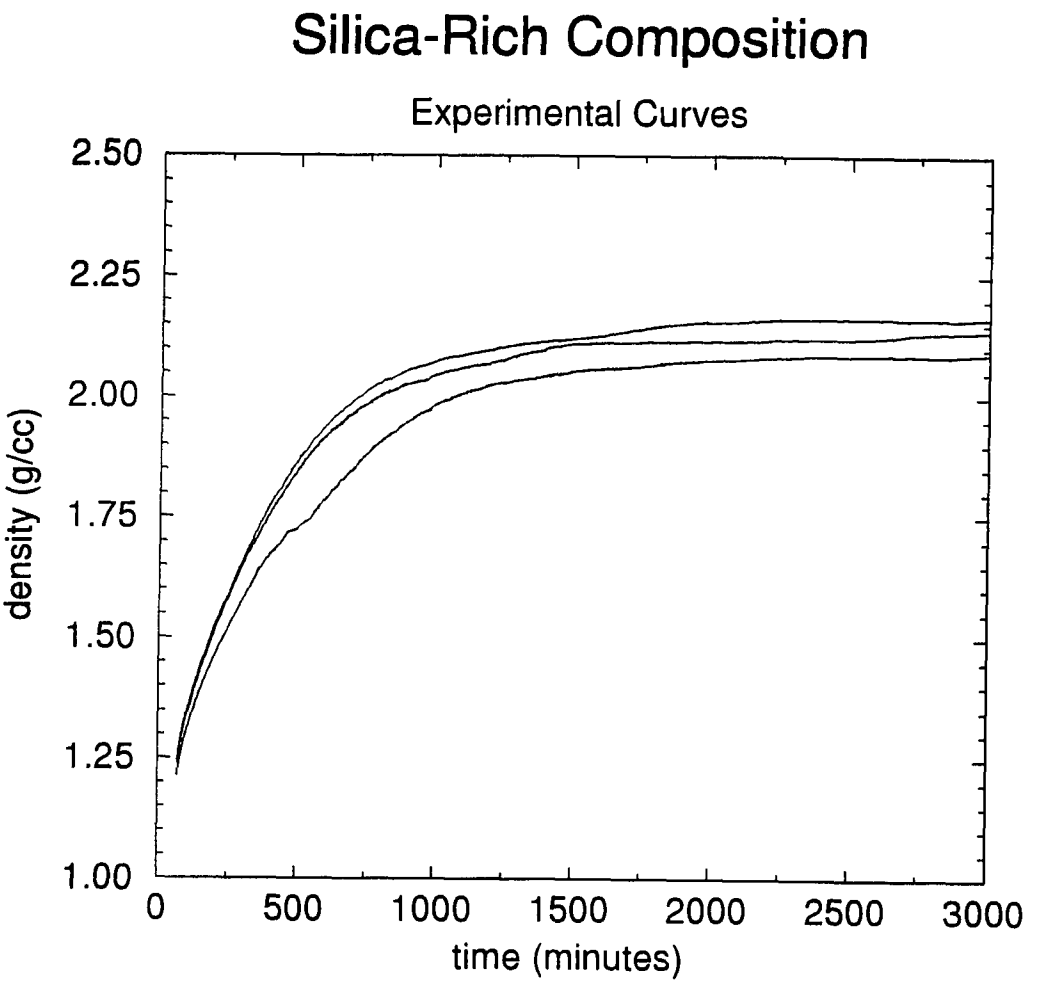

Figure 4.6: Experimental Sintering Curves for Silica-Rich composition (Si).

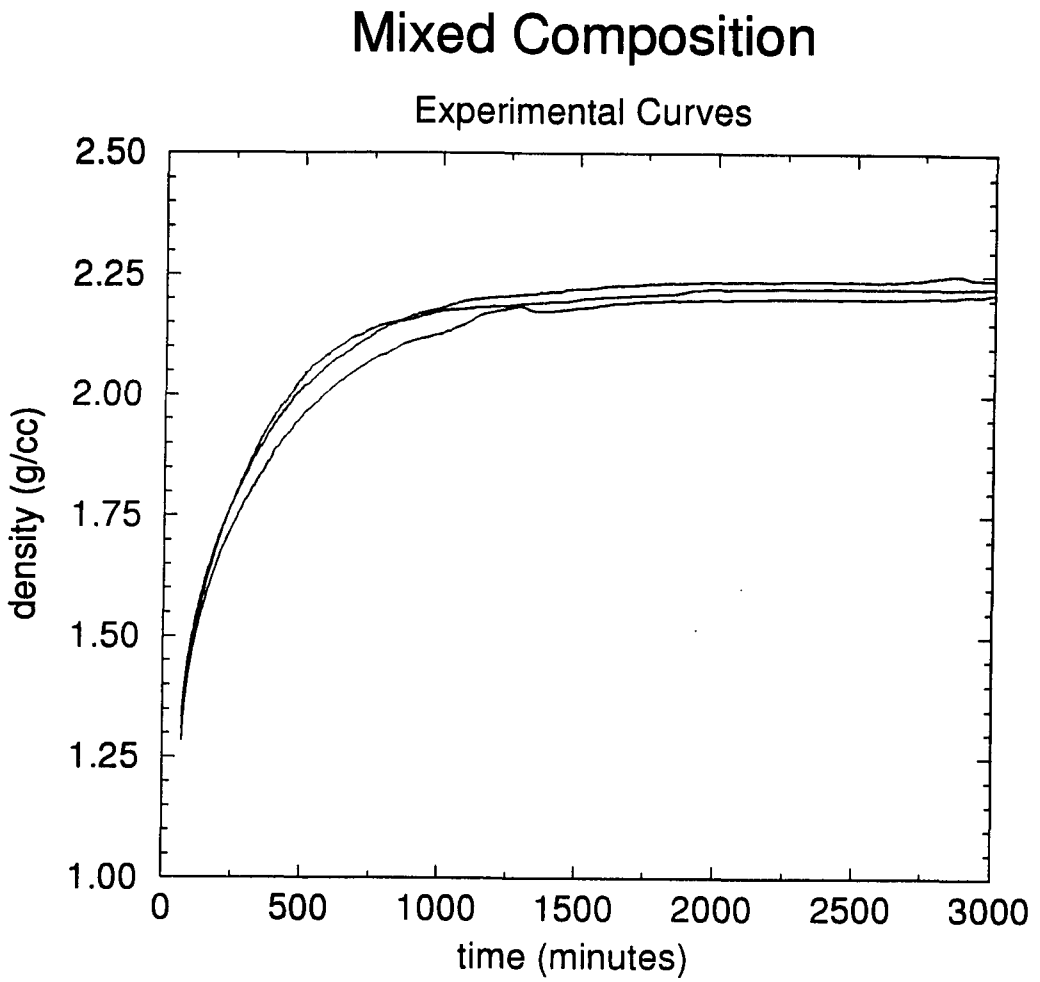

Figure 4.7: Experimental Sintering Curves for Mixed composition (M).

cylindrical pellet at any given time can be calculated:

$$\rho = \frac{4m}{\pi d^2 l} \tag{4.1}$$

where m is the mass of the pellet, d is the diameter, and l is the length. From chart recordings length as a function of time is obtained, therefore by using Equation 4.1 sintering curves can be plotted for each pellet.

4.3 Experimental Results

4.3.1 Densification Studies

The initial and final densities of all four of the powders studied are shown in Table 4.2, and their densification behaviors are depicted in Figures 4.4 through 4.7. Since t=0 corresponds to when the sample was inserted into the furnace, the density values for times less than 70 minutes have been omitted from these graphs because during this period the sample is not yet at the isothermal sintering temperature. The three curves on each graph represent individual sintering experiments conducted on the same composition to investigate the reproducibility of the densification behavior.

Table 4.2 - Initial and Final Densities

Composition	Initial Density (g/cc)		Final Density (g/cc)	
	Measured	Average	Measured	Average
St	0.987 0.992 0.997	0.992	2.359 2.404 2.415	2.393
Sp	1.073 1.069 1.063	1.068	2.465 2.456 2.460	2.460
Si	1.036 1.042 1.025	1.035	2.149 2.166 2.098	2.138
M	1.048 1.063 1.054	1.055	2.229 2.246 2.216	2.230

The densification behavior of the homogeneous stoichiometric powder (St) is shown in Figure 4.4. The three samples initially had densities of 0.987, 0.992, and 0.997, as shown in Table 4.2, and maintained their relative positions throughout the entire densification region, i.e. the sample starting out with a density of 0.997 always had the highest density. However, the differences in density between the curves vary with time. The magnitude of these differences fluctuates some, but the final densities, as shown in Table 4.2, differ by only 0.022 g/cc, which is less than 1%.

Table 4.2 also shows that the initial and final densities of the different Spinel-Rich (Sp) samples are closer to each other than for the St pellets. However, Figure 4.5 indicates that all the Sp pellets do not sinter identically. From 70 to

1000 minutes the differences in density are between 0.037 and 0.161 g/cc peaking at 365 minutes and with the density of one sample significantly lower than the other two. Then at about 930 minutes the densification rate of the same sample suddenly increases and its curve lies close to the others.

Table 4.2 shows that all three Silica-Rich (Si) samples have initial densities within 0.001 g/cc of the average. While two of the curves in Figure 4.6 are very similar throughout the sintering region, the third appears to sinter much slower than the other two and has a significantly lower density over the time range of 500 to 1000 minutes.

Figure 4.7 shows that the mixed samples (M) generally have very smooth densification curves; except, there appears to be an apparent deviation from a smooth curve for one sample around 1200 minutes. The variations in sintering behavior between the three curves is fairly constant over the entire experiment, unlike the Si and Sp compositions where there seems to be two curves that are the same and one that is significantly different.

One factor which all the compositions have in common is the appearance of discontinuities in the densification rate (Figure 4.5 and Figure 4.6) or even decreases in density (Figure 4.4). These apparent changes in density are due to power fluctuations in the transducer output and do not represent real changes in the sample. Experiments with no sample in the dilatometer revealed that discrepancies on the order of 0.08 g/cc may be attributed to the experimental apparatus alone.

These power instabilities may account for a large portion of the differences observed between the individual sintering curves of a given composition.

However, these power fluctuations do not account for the different initial and final densities of the various compositions shown in Table 4.2, since the initial and final dimensions were measured using a micrometer. The initial densities of the St powders are significantly lower than the others. This may be due the stoichiometric composition being produced at a different time which may have resulted in different drying conditions than the others. The initial densities of all the other compositions (Sp, Si, and M) are within 0.04 g/cc of each other.

The final densities of these four compositions are significantly different and these variations may be due to composition. As will be discussed later in this chapter, other authors have found that glasses along the silica-spinel tie line containing higher concentrations of silica have lower densities than those compositions with higher amounts of spinel.[41] Therefore, of the compositions studied the Sp pellets should have the highest final densities, as is observed in Table 4.2. This compositional argument may also explain the small variations between the initial densities of the Sp, M, and Si samples.

Since the St and M powder compacts have the same overall composition, they should reach the same final density, but instead varied by 0.16 g/cc. Crystallization has been known to arrest the further densification of glass powders, but X-ray diffraction analysis of these powders indicates that all four of these compositions

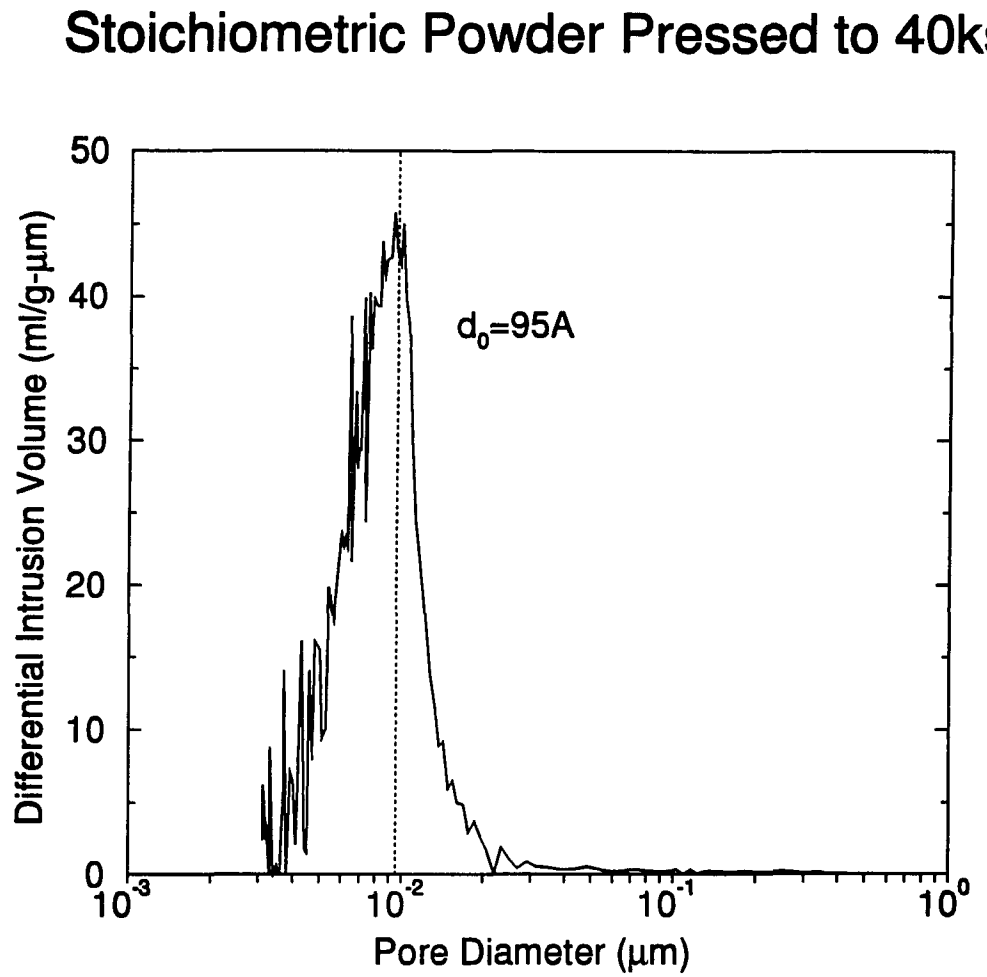

Figure 4.8A: Porosimetry Data for Stoichiometric Cordierite powder (St) pressed to 40 ksi.

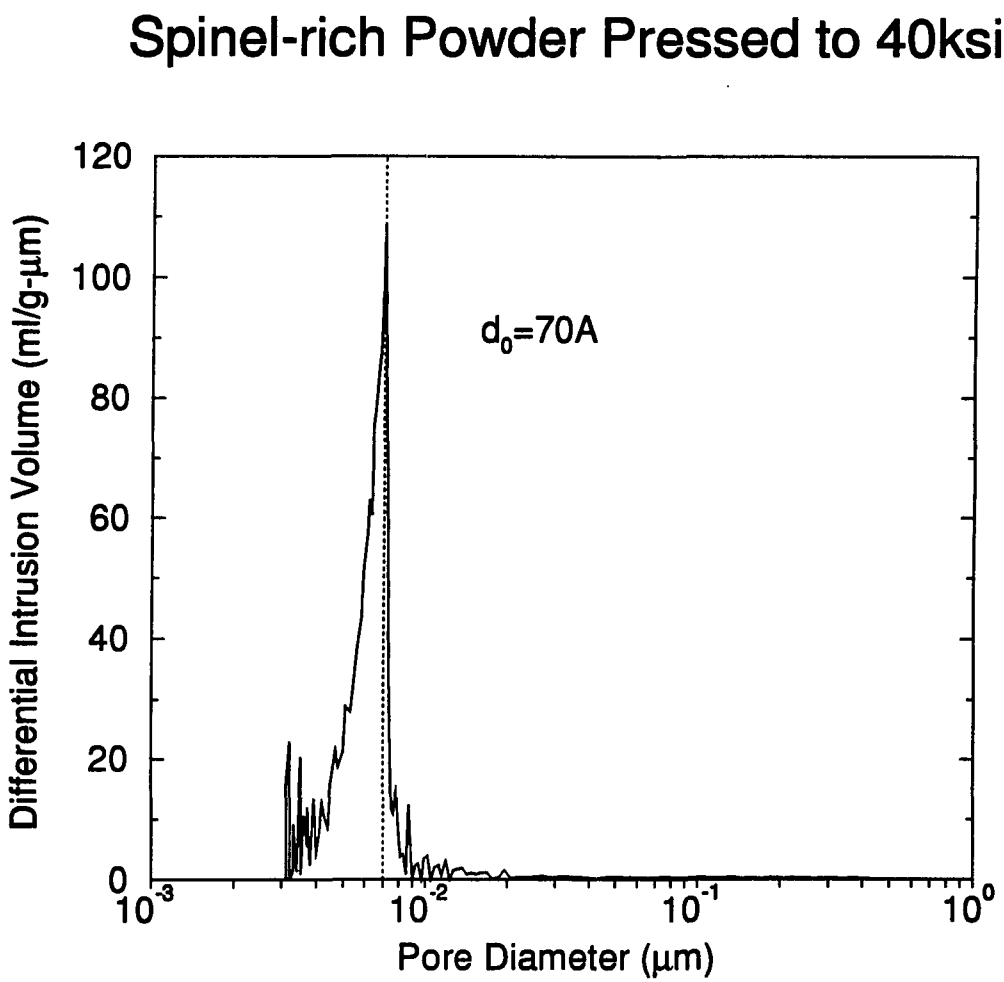

Figure 4.8B: Porosimetry Data for Spinel-Rich powder (Sp) pressed to 40 ksi.

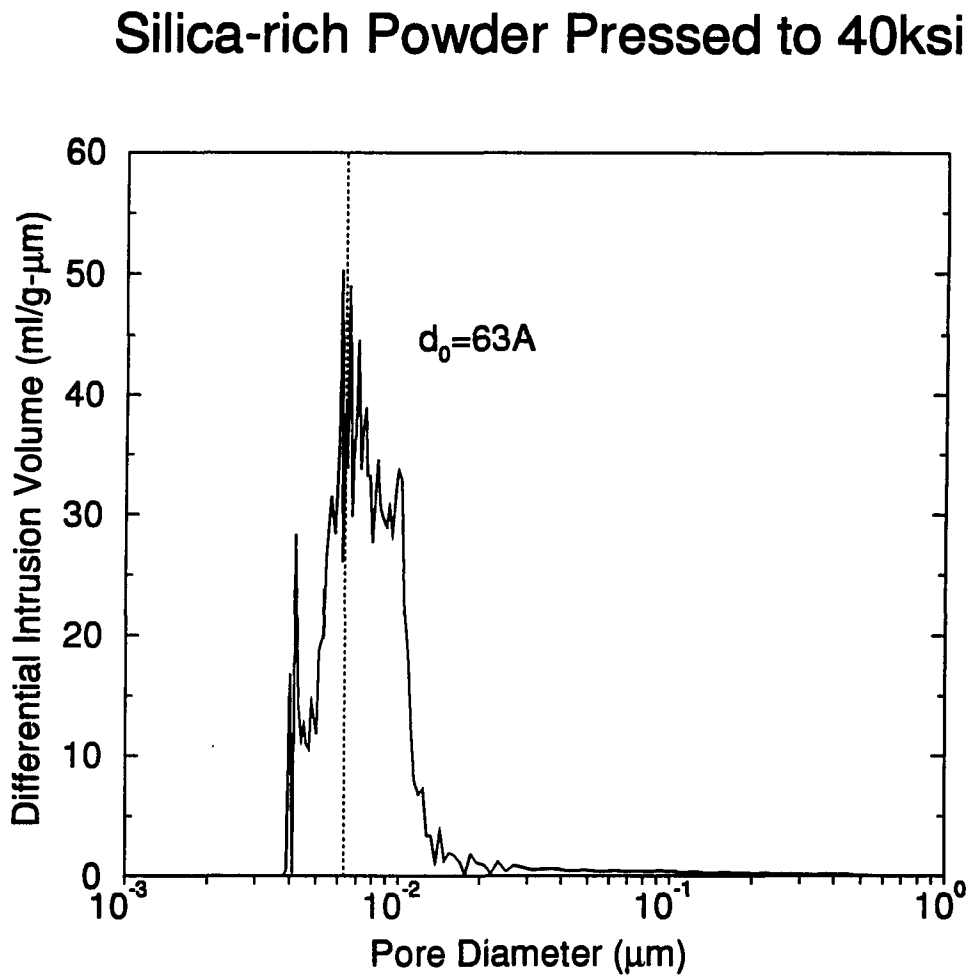

Figure 4.8C: Porosimetry Data for Silica-Rich powder (Si) pressed to 40 ksi.

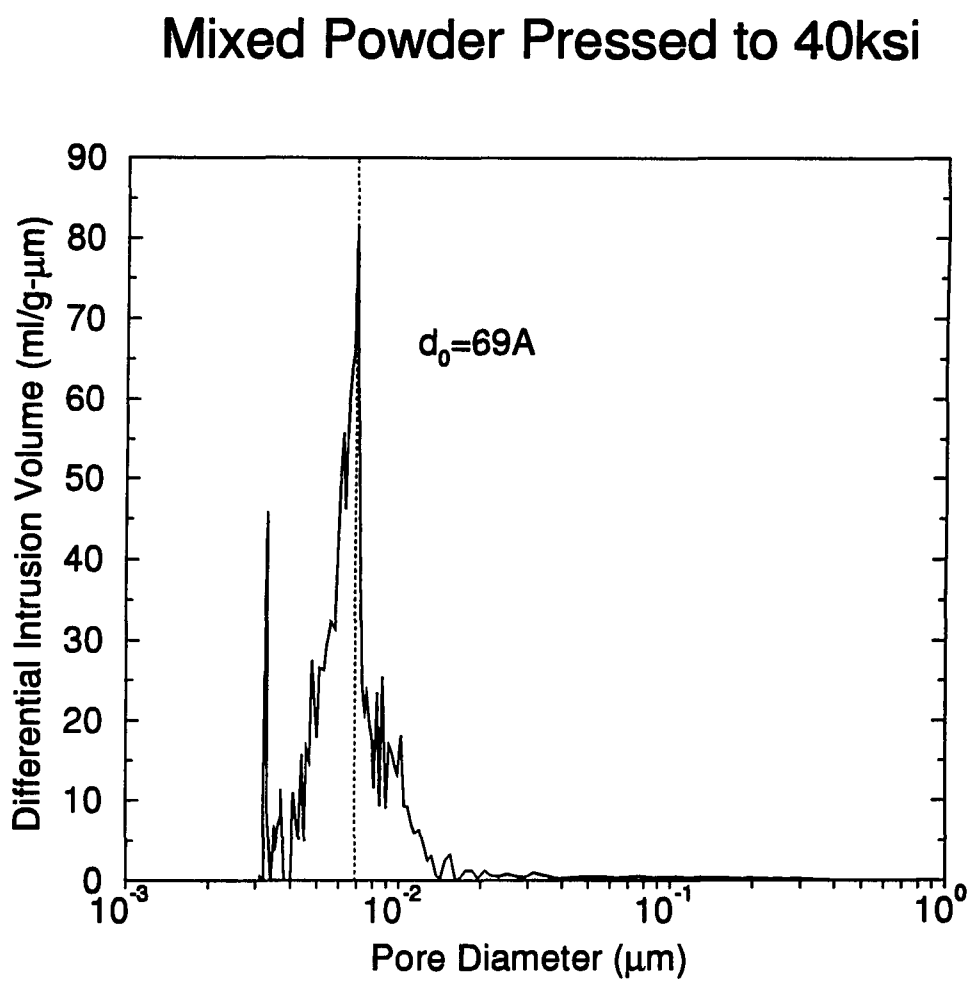

Figure 4.8D: Porosimetry Data for Mixed powder (M) pressed to 40 ksi.

were still amorphous after the sintering experiment was complete. Thus the differences between the final densities of the St and M compositions cannot be attributed to crystallization alone.

4.3.2 Porosity Results

Characterization of the initial porosities of the four compositions investigated revealed some significant differences. The data obtained from mercury porosimetry is depicted in Figures 4.8A through 4.8D and summarized in Table 4.3. The peak of the differential intrusion volume versus pore diameter indicates the maximum number of pores of the same size, which will be denoted as the pore size.

Table 4.3 - Porosimetry Data

Composition	Pore Size (Å)
St	95
Sp	70
Si	63
M	69

As can be observed in Figure 4.8 or in Table 4.3, the St composition has significantly larger pores than the other three compositions. The smaller pores may be due to different drying conditions of the powder and may also be the reason the

initial densities of the St pellets are significantly lower than for the other compositions (Table 4.2). Both the initial pore size and the initial density affect the densification rate, and therefore, will affect the resulting sintering curves.

Special care was taken for this study to ensure that all of the powders were pressed and heated under similar conditions. Even though precautions were taken, the initial sintering parameters, d_o and ρ_o, were different for the four compositions investigated. Therefore, in order to compare the sintering behavior of these powders under identical processing conditions, it is necessary to normalize the curves using sintering models.

4.4 Data Analysis

In order to model the sintering of homogeneous or heterogeneous samples, the viscosities and porosities of each of the components must be characterized. This section will describe how representative viscosity data was obtained from the three individual experimental densification curves of each composition. In the next chapter these extrapolated viscosities will be used to predict the sintering behaviors of homogeneous powders with identical initial conditions and to produce modelled sintering curves for heterogeneous powders.

4.4.1 Obtaining Average Sintering Behavior

The first step in modelling the viscosity is to characterize the sintering behavior of each composition. In order to use experimental data and discuss expected results from a given composition, the average or typical behavior must be determined. For this study the average behavior was determined by fitting all three experimental sintering curves of one composition to a function. The sintering behavior of each powder can therefore be represented by a time-dependent equation having a set of coefficients.

Equations of the form:

$$\rho = - \exp(At+B) - \exp(Ct+D) + Et+F \qquad (4.2)$$

were manually found to match the experimental sintering curves well. The program in Appendix E was written to fit experimental data to Equation 4.2 using non-linear least squares regression. The least squares approach attempts to minimize χ^2, which is the sum of the squares of the differences between a fitted curve and the experimental data points. The regression algorithm developed by Marquardt and Levenburg[46] was selected due to the relatively rapid rate with which χ^2 converges to a minimum.

The digitized experimental data files did not have the same number of points. Since the least squares routine applies equal importance to every input data point,

Table 4.4 - Experimental Fitting Coefficients

Fitted Parameters	St		Sp		Si		M	
	Value	Error	Value	Error	Value	Error	Value	Error
A	4.022e-4	0.010e-4	-3.062e-3	0.038e-3	-2.436e-3	0.011e-3	-2.947e-3	0.001e-3
B	-2.066	0.002	-1.022	0.011	2.747e-3	3.726e-3	-0.1086	0.0026
C	-6.363e-3	0.023e-3	-1.623e-2	0.011e-2	-0.1149	0.0782	-3.439e-2	0.071e-2
D	0.4811	0.0039	0.6760	0.0110	4.649	0.568	0.3463	0.0557
E	1.498e-4	0.004	2.320e-5	0.040e-5	6.708e-6	0.441e-6	9.830e-6	0.245e-6
F	2.352	0.001	2.385	0.001	2.111	0.001	2.198	0.0004
$\sigma_{\rho\ exp}$	2.993e-2		3.335e-2		3.734e-2		2.026e-2	
χ^2	1.881		2.335		2.931		0.8623	

it was necessary to "weight" each of the experimental curves in order to avoid the average sintering curve being skewed towards the curve with the most digitized points. Each digitized curve was converted using an interpolation program into 700 equally spaced data points between 70 and 3000 minutes. A single data file which contained the interpolated outputs from all three sintering curves was input into the least squares program given in Appendix E. The program outputs a set of coefficients for Equation 4.2 (A through F), the coefficients' associated errors, the experimental error, and χ^2.

Since non-linear regression routines, including the Marquardt/Levenburg algorithm,[46] can converge to local minima as well as global minima, a grid of initial coefficients was constructed as input for the least squares program. Each grid contained four to seven values for at least four of the six coefficients. After executing the least squares program for each set of coefficients, another grid was constructed. The new set of coefficients would span a smaller range and be centered around the least squares output values which produced the smallest χ^2. New grids would be constructed until the least squares program output the same set of best fitting coefficients for several of the input sets. The best fitting coefficients and their errors are listed in Table 4.4 for the St, Sp, Si, and M powders. Sintering curves plotted using Equation 4.2 and Table 4.4 will be called fitted sintering curves and represent the average sintering behavior of the three experimental sintering curves for each composition.

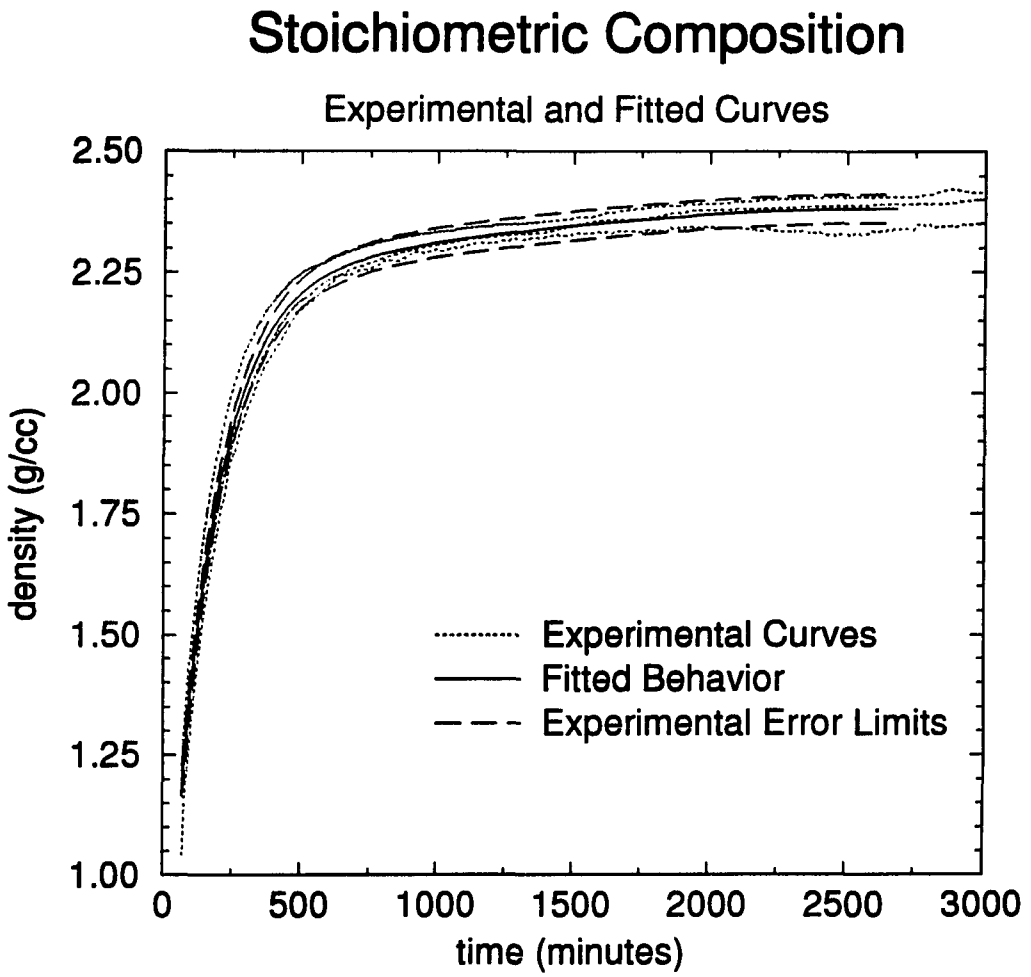

Figure 4.9: Experimental and Fitted Sintering Curves for Stoichiometric Cordierite powder (St).

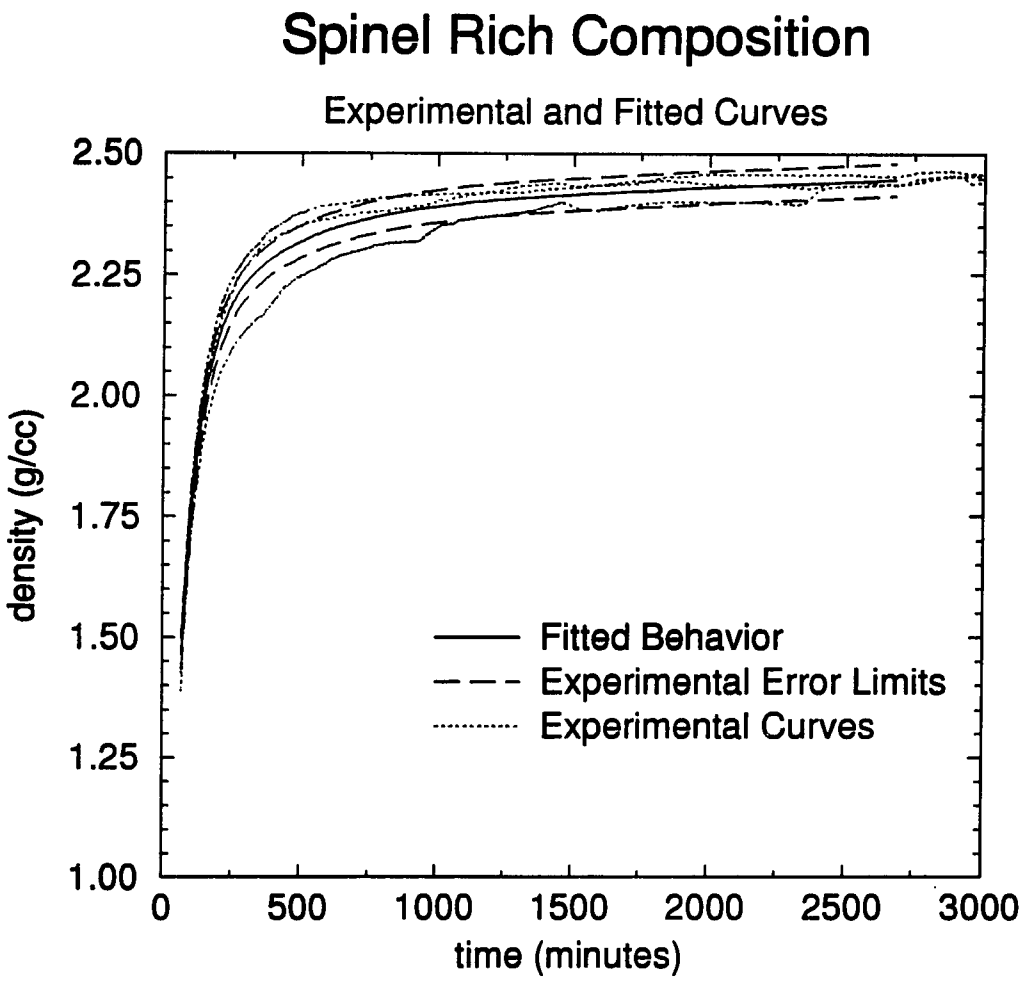

Figure 4.10: Experimental and Fitted Sintering Curves for Spinel-Rich powder (Sp).

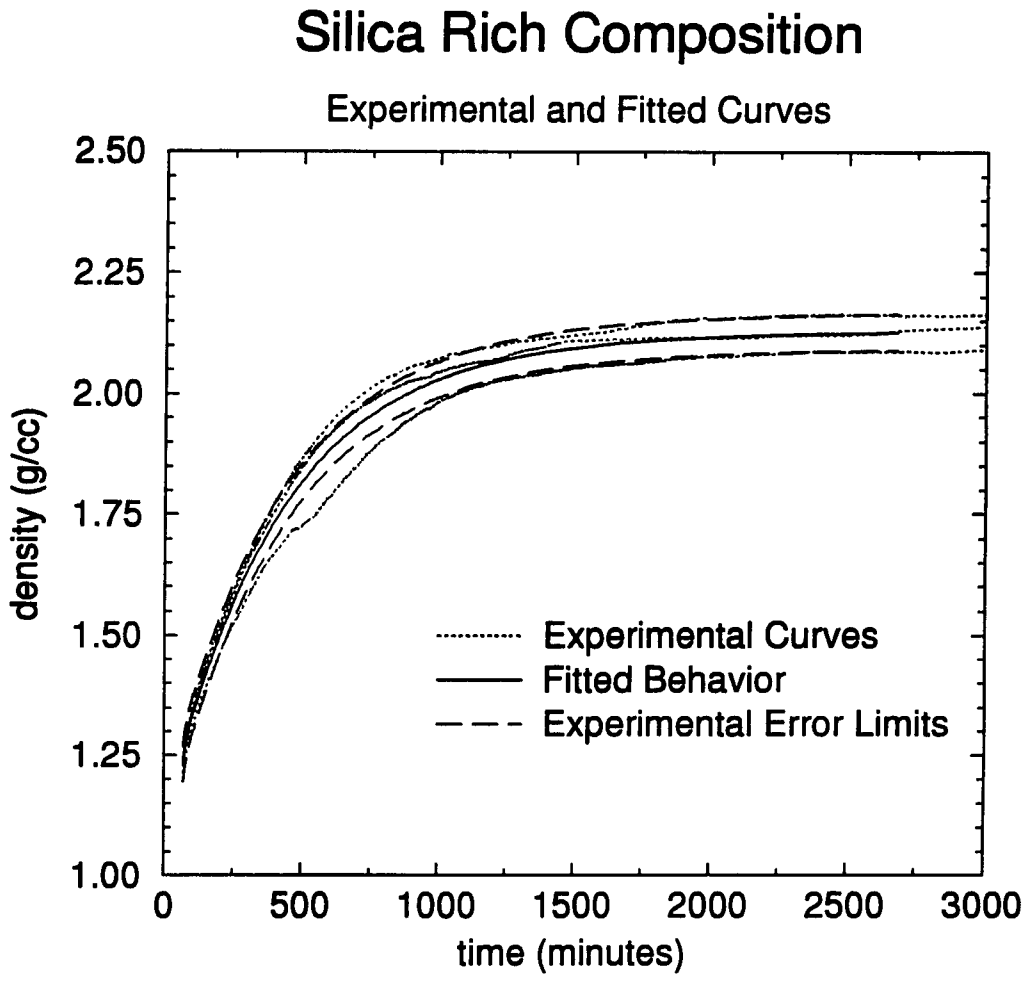

Figure 4.11: Experimental and Fitted Sintering Curves for Silica-Rich powder (Si).

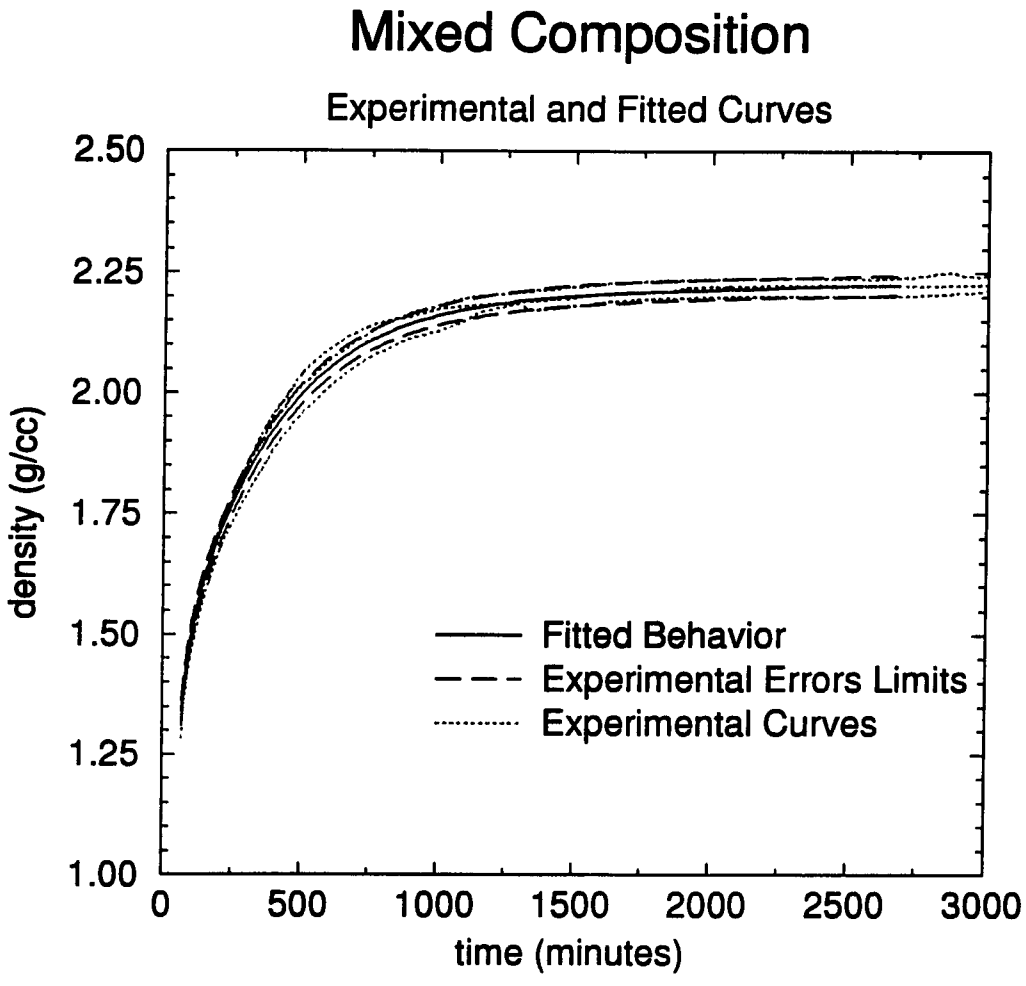

Figure 4.12: Experimental and Fitted Sintering Curves for Mixed powder (M).

Figures 4.9, 4.10, 4.11, and 4.12 show the fitted sintering curves, the three experimental sintering curves, and the experimental errors for each of the compositions (Sp, Si, St, and M). As can be seen in these figures, the fitted curve appears to be a fairly accurate representation of the average sintering behavior. The value $\sigma_{\rho\ exp}$ listed in Table 4.2 represents how well the experimental data points correlate with the fitted curve, and will be called the experimental error. Assuming the three experimental sintering curves are in a Gaussian distribution centered around the fitted curve, then another new experimental sintering curve will with 68% confidence lie within the experimental error bars, $\rho_{fit} \pm \sigma_{\rho\ exp}$.

However, the use of a series of grids as inputs for the least squares routine does not ensure that the absolute global minimum for χ^2 has been found, or that Equation 4.2 provides the best fit to the data. Using the error associated with each of the coefficients, it is possible to determine the reliability of Equation 4.2 and whether the best fit coefficients are representative of the average sintering behavior. A measure of the accuracy to which the fitted curve is known can be expressed as:

$$\sigma_{\rho_{fit}} = \sqrt{(\frac{\partial \rho_{fit}}{\partial A})^2\sigma_A^2+(\frac{\partial \rho_{fit}}{\partial B})^2\sigma_B^2+(\frac{\partial \rho_{fit}}{\partial C})^2\sigma_C^2+(\frac{\partial \rho_{fit}}{\partial D})^2\sigma_D^2+(\frac{\partial \rho_{fit}}{\partial E})^2\sigma_E^2+(\frac{\partial \rho_{fit}}{\partial F})^2\sigma_F^2} \quad (4.3)$$

which is the uncertainty in the average behavior.

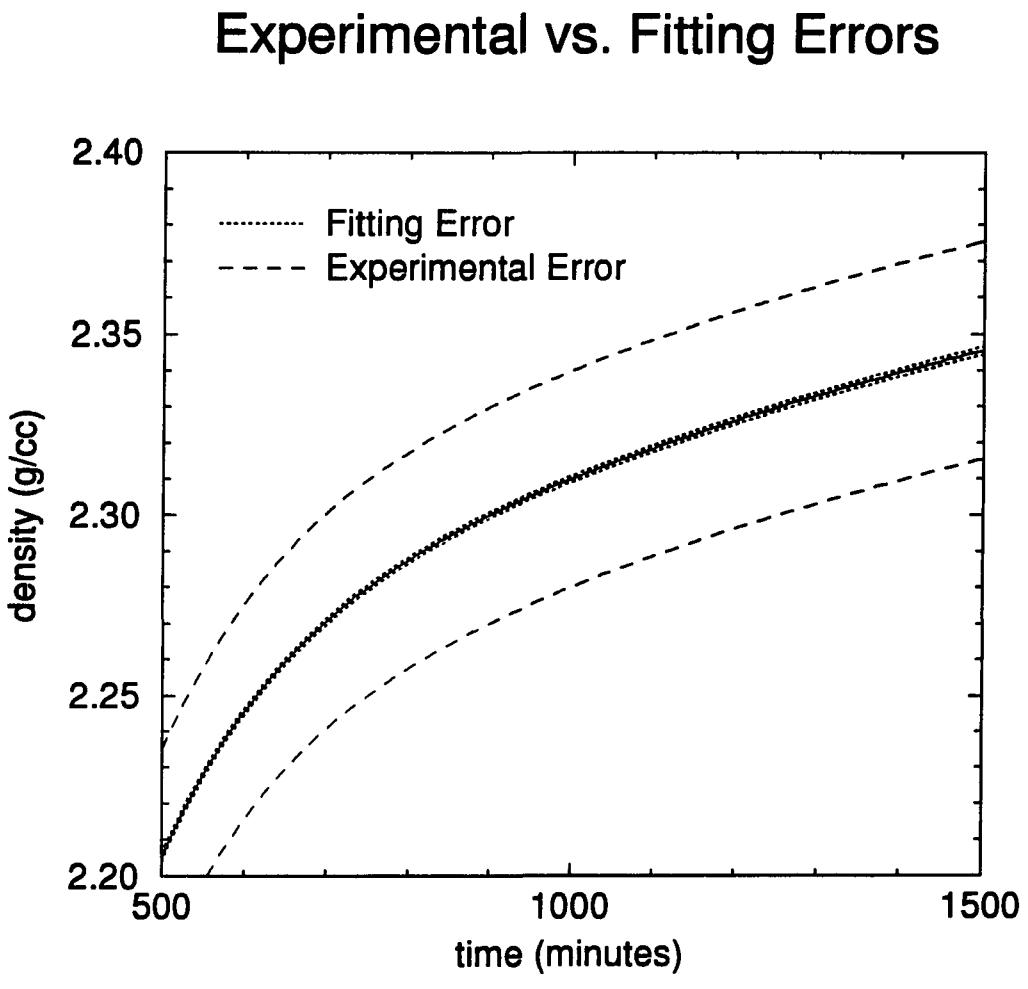

Figure 4.13: Comparison of Experimental and Fitted Errors.

The experimental error, $\sigma_{\rho\ exp}$, is a measure of how close the individual sintering curves lie. As can be seen in Figure 4.13 for the St powder, the error in the experimental data is significantly larger than the uncertainty in the fitted curve, $\sigma_{\rho\ fit}$. Therefore, even though the equation and coefficients may not give the absolute best fit, the uncertainty in determining the true average sintering behavior is significantly less than the experimental deviations from it.

4.4.2 Applying Scherer's Model[9] to Homogeneous Powders

The fitted sintering curves, as calculated from Equation 4.2 and Table 4.4, will be used to model the viscosity of the homogeneous powders. The curves depicted in Figures 4.9 through 4.11 are plots of the density as a function of time and the experimental error for each of the three homogeneous compositions investigated. However, most sintering models use relative density as the modelling parameter,[9,11] which is the density at any given time divided by the density after the sample has been fully sintered (the theoretical density).

$$\rho_r = \frac{\rho}{\rho_t} \tag{4.4}$$

Since the theoretical densities of the compositions in this study were not experimentally determined, values were extrapolated from densities published in the literature. The densities for a variety of compositions along the silica-spinel tie line

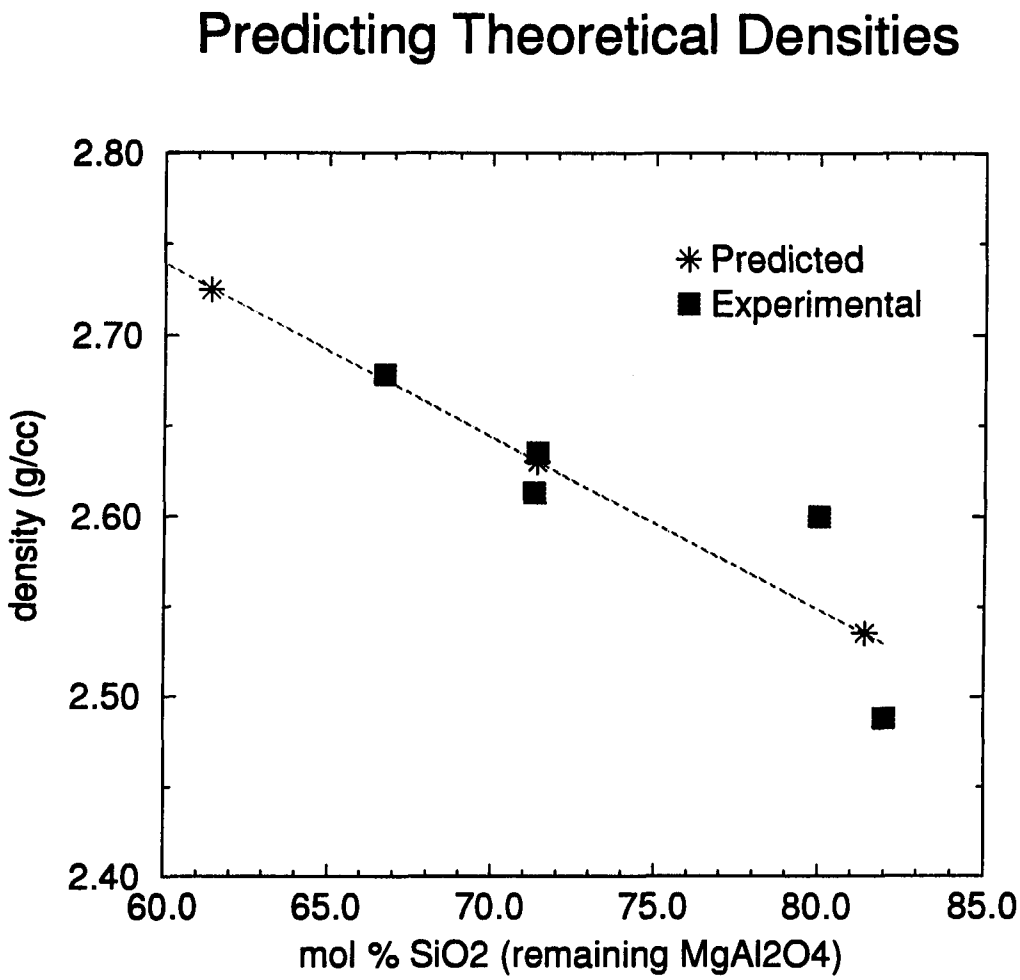

Figure 4.14: Predicted Theoretical Densities calculated by fitting a line to Glass Densities From the Literature.[41]

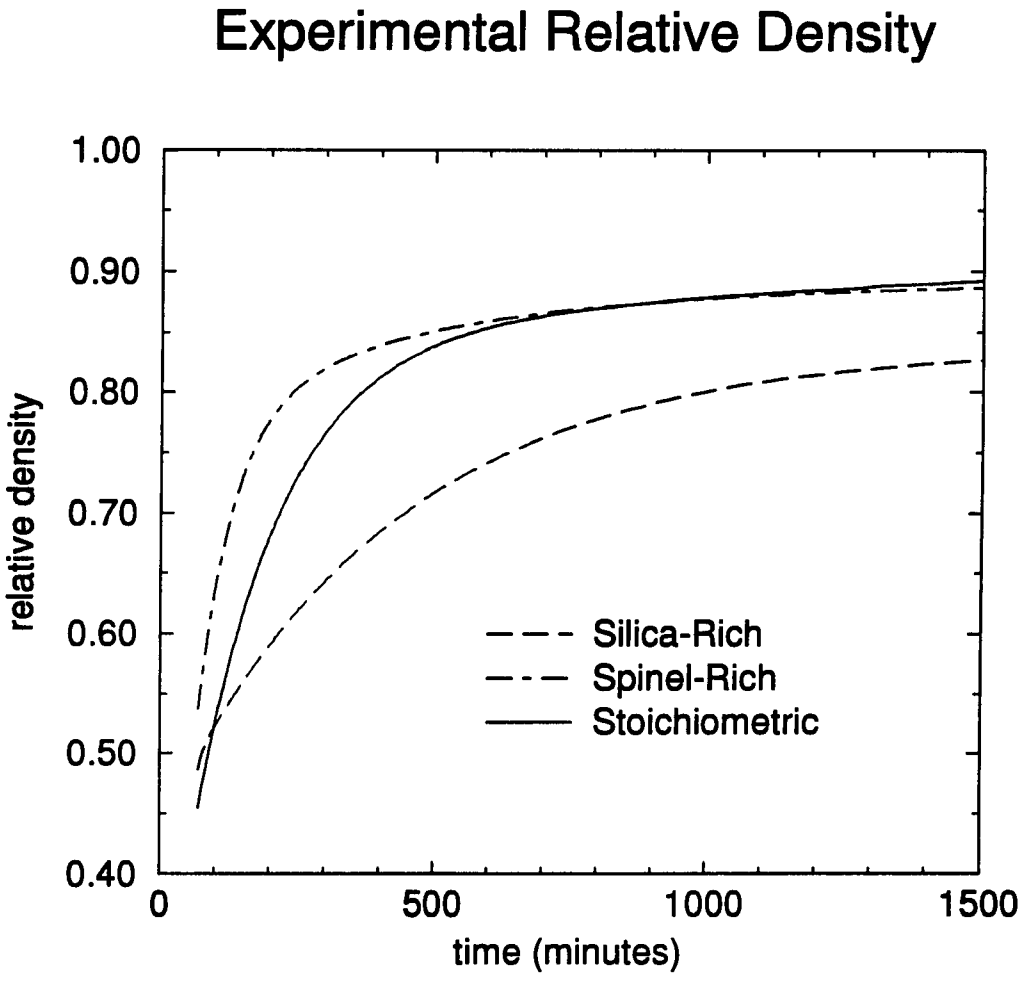

Figure 4.15: Plots of Relative Density versus time for all the homogeneous compositions.

are shown in Figure 4.14 and Table 4.5.[41] As the amount of spinel increases, so does the density. The theoretical densities of the compositions studied in this document have been calculated by linear extrapolation of the densities in Table 4.5 as a function of mol% SiO_2. These extrapolated values are listed in Table 4.6.

Table 4.5 - Literature Values for Glass Densities[41]

Composition (mol%)		Density (g/cc)
SiO_2	$MgAl_2O_4$	
66.7	33.3	2.6128
71.3	28.7	2.678
71.4	28.6	2.635
80.0	20.0	2.60
82.0	18.0	2.488

Table 4.6 - Extrapolated Theoretical Densities

Name	Composition (mol%)		Density (g/cc)
	SiO_2	$MgAl_2O_4$	
Sp	61.43	38.57	2.725
St	71.43	28.57	2.630
Si	81.43	18.57	2.535

Figure 4.15 shows the average relative densification behavior of all three homogeneous compositions investigated in this study. One reason the three compositions sinter differently is because they do not have the same materials properties, i.e. viscosities. Comparisons of the sintering behaviors of these powders are complicated by the fact that the initial conditions are different. By extrapolating the viscosity from the relative density plots using Scherer's model for homogeneous sintering,[9] densification curves with the same initial conditions can be generated and compared. While Scherer's homogeneous sintering model was originally tested for soot preforms and aerogels, it has since been used to model a variety of other powders, including sol-gel.[47] Scherer's model[9] will be used in this document to normalize the homogeneous sintering curves and to extrapolate the viscosities of these cordierite-based sol-gel powders.

Chapter 2 describes Scherer's homogeneous sintering model and the normalized time parameter, $K(t-t_o)$.[9] Since the relative density is a function of time, Equation 4.5 listed below cannot be solved explicitly for viscosity. Therefore, the viscosity as a function of time has been calculated by numerical integration for small time intervals.

$$K(t-t_o) = \int_{t_o}^{t} \frac{\gamma}{\eta l_o \rho_o^{1/3}} dt = \int_0^x \frac{2\,dx}{(3\pi - 8\sqrt{2}x)^{1/3} x^{2/3}} \qquad (4.5)$$

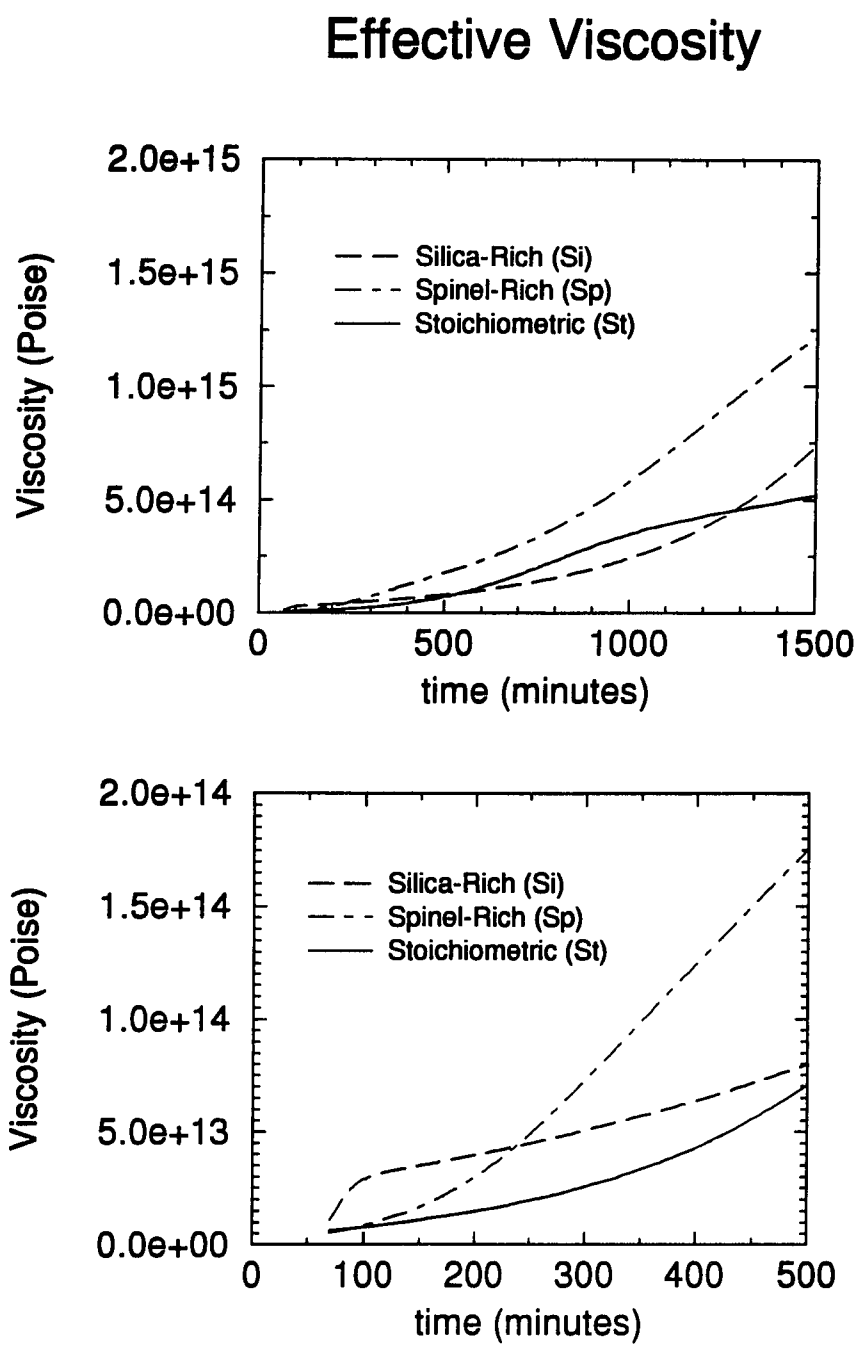

Figure 4.16: Extrapolated Homogeneous Viscosities.

Since the viscosity is inversely proportional to the densification rate, as the sample stops sintering the error in the viscosity increases. Once the sintering stops, the effective viscosity is infinite. Experimentally it is not possible to detect the very small changes in density at long times, therefore the data will be cutoff once the slowest sintering sample reaches a relative densification rate of less than $2*10^{-7}$/min. According to this criteria, the Sp densification rates for times greater than approximately 1500 minutes should not be used.

The extrapolated viscosities for the St, Sp, and Si compositions are shown in Figure 4.16, where it is apparent that all the compositions have effective viscosities with transient behaviors. Basic assumptions about the relative values of the viscosity, based on composition, do not appear to apply to these sintering samples. While the Sp powder initially has the lowest viscosity, as would be expected based on composition, it crosses the St viscosity curve after 90 minutes and has a viscosity even higher than the Si composition after 250 minutes. This will have a significant impact on the modelled sintering curves which will be discussed in Chapter 5.

The fact that extrapolated viscosities are time-dependent raises the question of the applicability of Scherer's model[9] to these powders. However, other authors[46] have extrapolated transient viscosities from sintering curves using Scherer's model and believed the data to be valid. By experimentally determining the effective sintering viscosities, normalized sintering curves can be generated. Therefore,

Scherer's sintering model[9] will be used to predict the homogeneous sintering behavior of these compositions.

Modelled behavior of the St, Si, and Sp compositions can be constructed and compared using identical initial conditions and the effective viscosities shown in Figure 4.16. It is also possible to use the effective viscosities of the Si and Sp compositions to model the behavior of different regions in a heterogeneous sample, such as the mixed powder. Modelling of the sintering behavior of both homogeneous and heterogeneous powders with these compositions will be explored in Chapter 5.

CHAPTER 5

INTERPRETATION OF SINTERING MODELS

In Chapter 2, several models which have been published in the literature were outlined for both homogeneous and heterogeneous sintering of powder compacts. To describe the sintering of heterogeneous glasses, the Interlocking Cell model was developed and the Self-Consistent model was presented in Chapter 3. These two models were also compared for a variety of input conditions. The sintering behavior of several homogeneous (St, Sp, and Si) and heterogeneous (M) compositions were investigated, and the results were presented in Chapter 4. However, since the investigated powders had a variety of initial densities and porosities, comparisons of the sintering behaviors which have not been normalized are difficult. Therefore, the last half of Chapter 4 was devoted to extrapolating useful data from the sintering curves so that the three homogeneous compositions, the heterogeneous composition, and the sintering models can be compared.

In this chapter, the viscosities extrapolated from the sintering curves of the St, Sp, and Si powders in Chapter 4 will be used to generate modelled sintering curves. The term "modelled" sintering curve only applies to those sintering plots generated

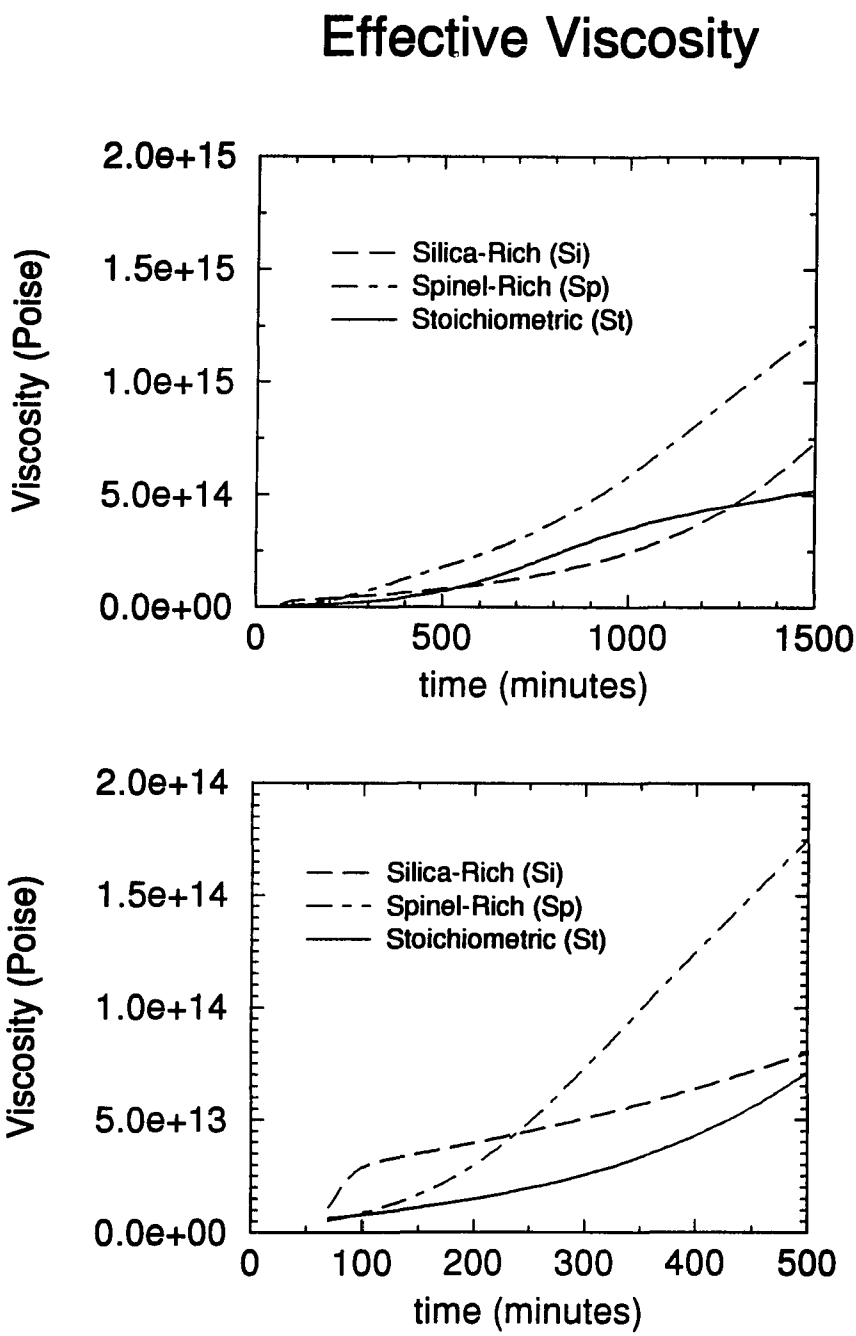

Figure 5.1: Extrapolated Homogeneous Viscosities.

using extrapolated viscosities and either Scherer's homogeneous sintering model[9] or the IC or SC heterogeneous sintering models. All of the modelled curves were normalized to have the same initial porosities and relative densities.

By using identical initial conditions, the normalized sintering behavior of these three homogeneous powders can be compared. The effect of heterogeneities can also be studied by comparing the normalized St and the fitted M sintering curves. The densification behaviors modelled using the SC and IC algorithms will also be compared to the M powder.

5.1 Using Extrapolated Viscosities

In Chapter 4, viscosities for the homogeneous powders were extrapolated from the densification curves using Scherer's homogeneous sintering model. As Figure 5.1 shows, the obtained viscosities exhibit time-dependent behavior during much of the sintering. These transient viscosities can change by up to two orders of magnitude during the two days of sintering. Therefore, constant viscosity values can not be used for these powders to model sintering behavior.

The extrapolated viscosities shown in Figure 5.1 do not seem to obey normal composition correlations. Generally samples rich in spinel have relatively low viscosities.[43] But the Sp composition has the lowest viscosity of the compositions

studied for only the first 90 minutes, after which the St composition has a lower viscosity.

The fact that these powders were produced using a wet-chemical route may contribute to the observed transient viscosity behavior in Figure 5.1 and to other observed differences between the powders. Wet-chemically derived powders retain some water and residual organics from the processing, which may evaporate during sintering. The incorporation of hydroxyls or carbonaceous species in the glass forms non-bridging oxygens and a more open glass network. The glass viscosity increases as water evaporates forming more bridging oxygens.

The formation of necks between the particles has been proposed[44] to describe the factor of 100 increase in viscosity observed by Rahaman et al.[16,38] However, the viscosity values from this work vary continuously throughout the sintering range, well past the point where necks would form. Rearrangement of the particles into a more dense structure has also been postulated as the cause of observed increases in viscosity for liquid phase sintering. However, once necks form in a glass sample, particle rearrangement must be accompanied by bulk flow which occurs on the same or longer time scales as viscous sintering. Therefore, the rearrangement of particles does not explain the transient behavior observed in this study.

All of the powders exhibited transient behavior; however, the St composition sintered faster than even the Sp powder, as shown in Figure 4.15. This indicates that more than just composition affects the viscosity. The St also had a larger pore size

than the other powders investigated. Both of these facts suggest that either the St powder was processed in a different manner or reacted differently to the same processing procedure.

The stoichiometric composition, when made homogeneously is a grey powder; but powders with a slightly different composition appear white. Varying the calcining procedure does not appear to change the powder's appearance.[48] It is possible that under the same processing conditions the stoichiometric cordierite composition, St, retains more carbon which cannot be removed. Also the final products of the condensation reaction may be different for the St, Sp, and Si powders, causing various amounts of water to remain incorporated in each of the glasses. By heating the powders and removing the residual water or carbon, the viscosity will increase. These reactions may not have been complete in the St powder, since a viscosity increase of a factor almost 100 is observed during sintering. The incomplete reaction may have been caused by different processing conditions or different chemical kinetics of this composition.

Since the effective sintering viscosities do not appear to depend only on composition, but also on other factors such as processing, it is difficult to model or predict viscosities for these powders. Therefore, the extrapolated viscosities depicted in Figure 5.1 will be used for all of the modelled sintering curves in this chapter. Applying these values is appropriate so long as the effective materials properties, i.e.

the viscosities, are not affected by changes in initial density or porosity and Scherer's homogeneous sintering model[9] can be applied to these sol-gel powders.

5.2 Homogeneous Sintering - Effect of Composition

Scherer's homogeneous sintering model[9] can be used to plot a modelled homogeneous sintering curve, given an effective sintering viscosity and the initial microstructure. The relative densification rate as outlined in Chapter 2 is:

$$\frac{d\rho_r}{dt} = (6\pi x - 24\sqrt{2}x^2)\frac{dx}{dt} = (6\pi x - 24\sqrt{2}x^2)\left(\frac{\gamma}{2\eta l_o}\frac{\rho_r^{1/3}}{\rho_{r_o}^{1/3}}\right) \qquad (5.1)$$

The modelled sintering curves for the homogeneous compositions in this study can be generated using the extrapolated viscosities in Figure 5.1, Equation 5.1, and by applying a constant relative densification rate over a small time interval, Δt.

$$\rho_{r_{i-1}} = \rho_{r_i} + \left(\frac{d\rho_r}{dt}\right)_i \Delta t \qquad (5.2)$$

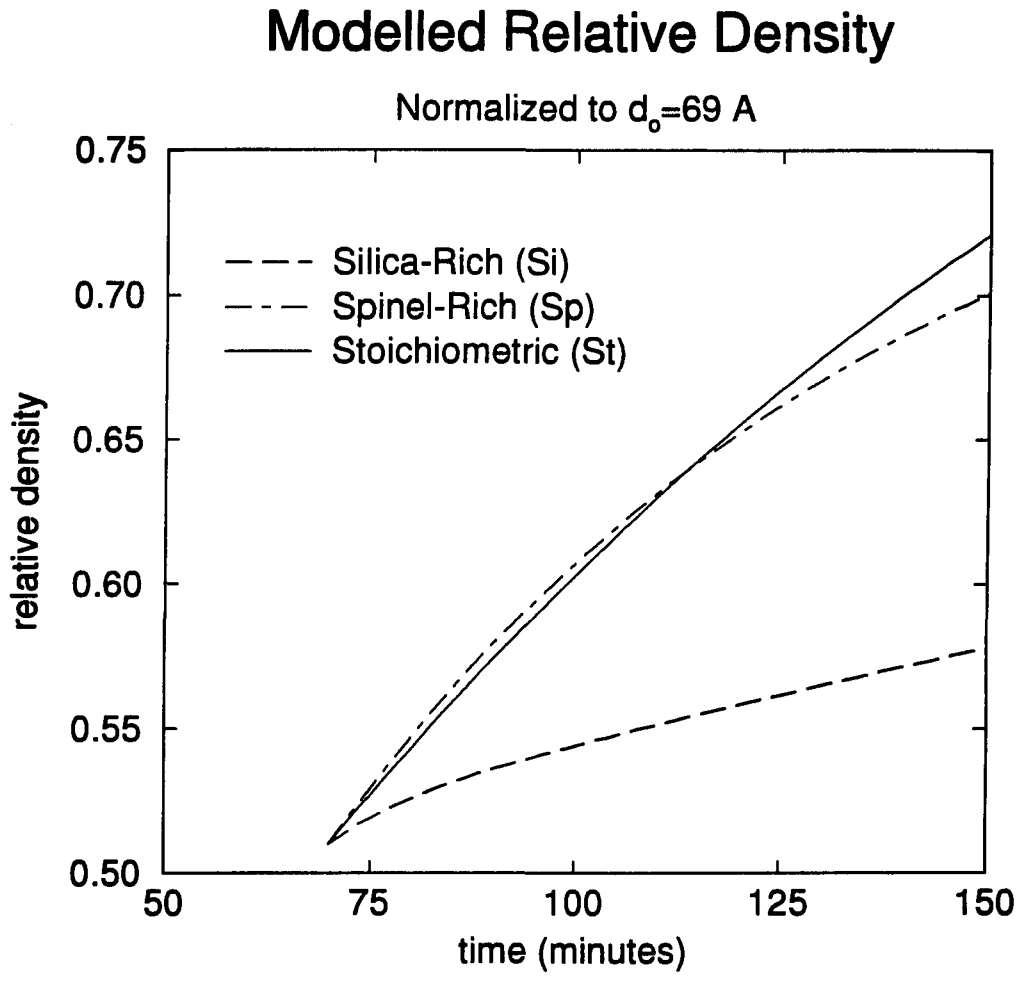

Figure 5.2A: Modelled Sintering Behavior for the homogeneous compositions (50 to 150 minutes).

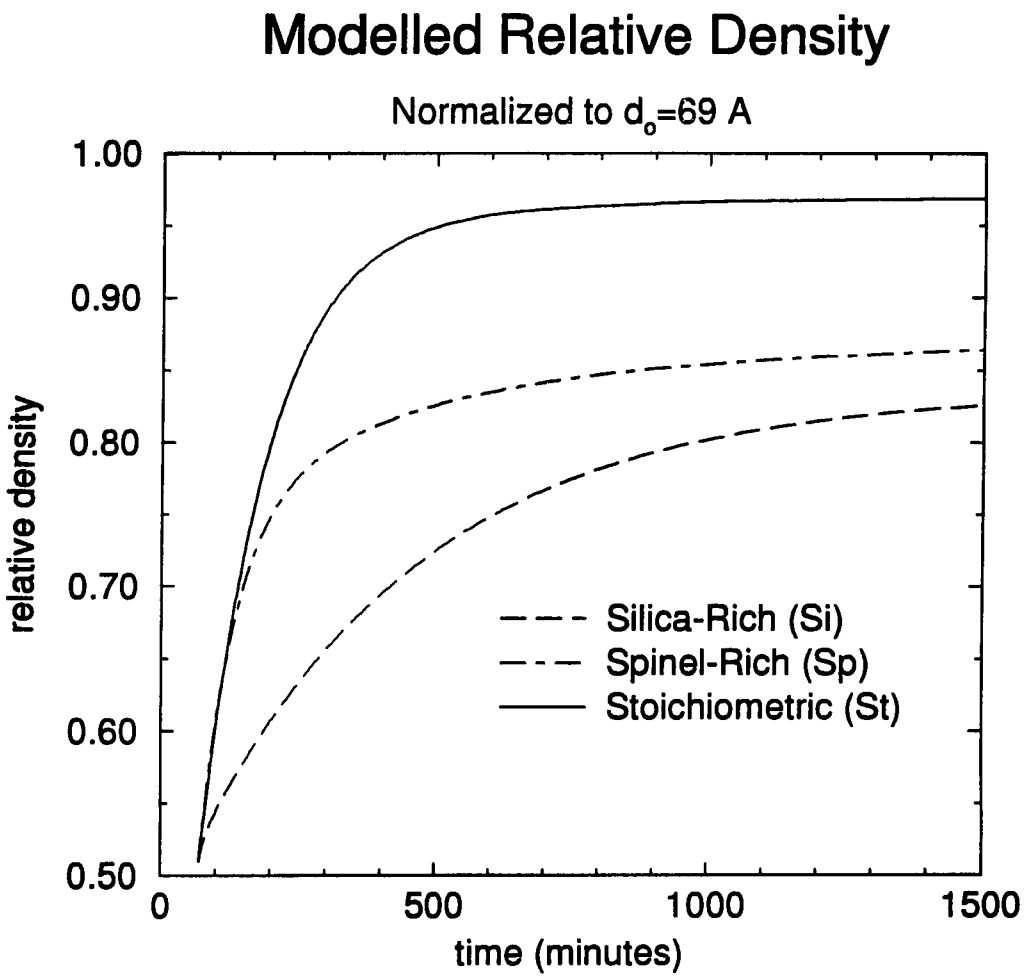

Figure 5.2B: Modelled Sintering Behavior for the homogeneous compositions (0 to 1500 minutes).

Since this algorithm applies a constant value for the transient viscosity over the time interval, small time steps should be used. The normalized, modelled sintering curves for the St, Sp, and Si compositions are shown in Figures 5.2A and 5.2B.

One of the factors which limited comparisons of the original fitted homogeneous sintering curves was different initial relative densities. All of the graphs in this chapter have been normalized as described at the beginning of this chapter. The initial conditions for all the samples are the same as was found in Chapter 4 for the mixed samples. Therefore, the values for the constants for Equation 1 are: γ = 300 ergs/cm^2, ρ_{ro} = 0.51, and l_o = 144 Å (d_o = 69 Å). Curves generated using Scherer's homogeneous sintering model or the heterogeneous Interlocking Cell or Self-Consistent models will be called modelled curves, while the densification behavior represented by Equation 5.3 will still be indicated as fitted behavior.

$$\rho = -\exp(At+B) - \exp(Ct+D) + Et + F \qquad (5.3)$$

The modelled sintering curves of all three homogeneous compositions depicted in Figure 5.2 have initial relative densities of 0.51. The Sp powder has a higher modelled relative density than the Si powder over the entire sintering range. Based on composition, samples richer in spinel are expected to sinter faster than those with more silica, as is observed when the Si and Sp modelled behaviors are

compared. However, over almost the entire sintering range the St powder has a higher modelled relative density than either the Sp or Si compositions.

The behavior observed in Figures 5.2A and 5.2B can be explained using the time-dependent viscosities for each of these powders found in Figure 5.1. The Sp powder has the lowest viscosity of the three compositions until about 90 minutes, which is why it has the highest modelled relative density for times less than 113 minutes. However, for times between 90 and 550 minutes the St powder has the lowest viscosity and therefore sinters the fastest in this range.

By 550 minutes where the Si composition becomes the powder with the lowest viscosity, the St powder has already reached a relative density of 0.954. By approximately 1000 minutes the transient viscosities of all the compositions have reached a value, of approximately $2*10^{15}$ Poise, which makes sintering on the time scale of days extremely difficult. While on a time scale of years the Sp and Si samples may continue to sinter, the high viscosities have essentially halted densification.

The Sp powder sinters faster than the Si powder as expected but not faster than the St composition. As described in Section 5.1, the different processing conditions probably enable the St powder to reach a higher final relative density. Composition alone can not be used to predict the relative sintering rates observed for these powders. The relationships between the modelled densification curves of

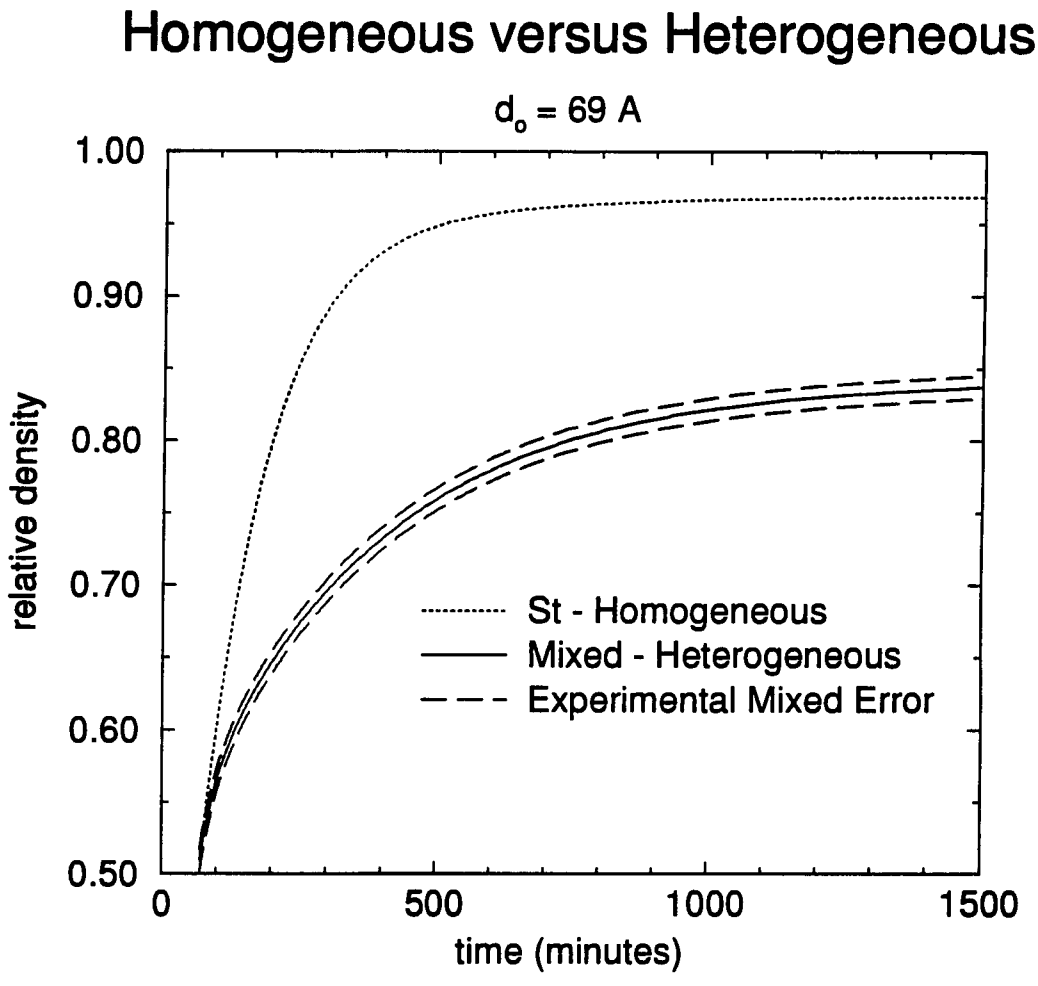

Figure 5.3: Modelled Sintering Behavior for the homogeneous and heterogeneous cordierite compositions (St and M).

the various compositions are a direct consequence of the extrapolated viscosities used to generate them.

5.3 Homogeneous versus Heterogeneous Sintering

One of the purposes of this study was to investigate the effect of heterogeneity on sintering. The St and M powders have the same bulk compositions; however, the M powder is composed of a mixture of the Si and Sp powders and is not a homogeneous compound like the St powder. Therefore, the primary difference between the St and M powders is the extent of homogeneity.

The mixed composition cannot be normalized to account for differences in initial relative density and porosity because the appropriate heterogeneous sintering model has not yet been determined. In order to compare the St and M powders, the St sintering curve in Figure 5.3 was normalized to the initial conditions of the M powder using Scherer's model[9] and the extrapolated viscosity shown in Figure 5.1. The fitted curve of the M sample can be used for comparison since it represents the observed average heterogeneous sintering behavior. Since the St composition has been normalized to agree with the initial conditions of the M sample, the modelled St and fitted M curves can be plotted and compared.

Figure 5.3 shows that the sintering behavior of the St powder lies well outside the experimental error bars of the mixed sintering curve. Even though both of these curves have the same initial conditions, the St powder initially sinters much faster and reaches a higher final modelled relative density. When sintering curves are plotted as a function of normalized time with effective viscosities computed according to Bottinga and Weill,[43] both the IC and SC models predict faster densification rates when both regions have the same viscosity instead of different viscosities.

However, some of the differences between the St and M sintering behaviors may be attributed to more than simply the presence or absence of heterogeneities. As described in the previous section and depicted in Figure 5.2A, the St sample sinters faster than even the Sp powder. Since the St normalized composition sinters faster than each of the components of the mixed sample, the St powder would be expected to sinter faster than the heterogeneous mixture.

However, the St composition may not be expected to have a sintering behavior between the Si and Sp powders. As discussed in Section 5.1, the St powder may have reacted or been processed differently. Another possibility is that the viscosity of the St composition should not be an average of the Si and Sp powders. This would be the case if a peak in the viscosity versus composition plot occurred around the stoichiometric cordierite composition. It may not be reasonable to assume that the sintering behavior of the St powder should be between the Si and Sp behaviors.

So even though the sintering curves have been normalized to account for small initial microstructural differences, such as porosity and relative density, broad statements based on composition or homogeneity cannot be made about effective sintering viscosities or densification behavior. The large observed differences between the St and M powders are probably due to variations in water or carbon content. Even if these factors could be eliminated, perhaps by producing the powders through a melt process, it is possible that the St powder would still have a lower viscosity, and therefore sinter faster than either the Si or Sp powders.

Even though this experimental study of the St and M powders may not have revealed significant differences due to heterogeneities, it did prove the importance of powder processing on the viscosity and sintering behaviors. This experimental densification study has also revealed the importance of transient viscosities and their effect on sintering behavior. Just because the St composition lies between the Sp and Si compositions on the phase diagram, does not mean the sintering behavior of the St composition will have an intermediate behavior. However, the question remains whether or not the mixed sintering behavior is expected to lie between its two components. Therefore, the experimentally determined sintering curves for the mixed sample will be compared to two different heterogeneous sintering models.

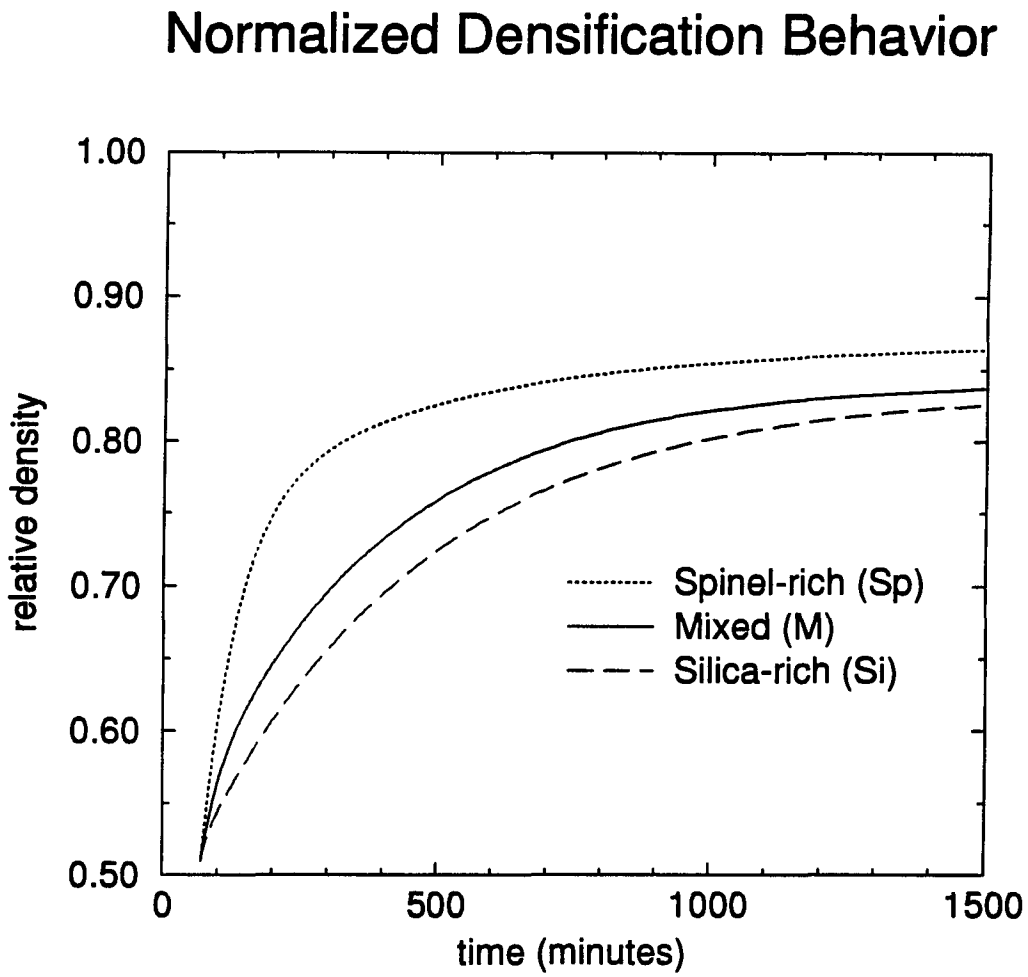

Figure 5.4: Normalized Sintering Behavior for the Spinel-Rich (Sp), Silica-Rich (Si), and Mixed (M) powders.

5.4 Heterogeneous Sintering Models

One of the tasks of this study was to determine whether the Interlocking Cell or Self-Consistent model corresponds better with the observed heterogeneous sintering behavior. These two models were outlined in Chapter 3. The modelled heterogeneous sintering curves for the mixed composition were generated using both the IC and SC models and are presented in Sections 5.4.1 and 5.4.2. The viscosities for this modelling study were extrapolated from the homogeneous sintering curves of the Sp and Si compositions and are depicted in Figure 5.1. The initial conditions for each of the regions were the same as for the overall mixed sample. Therefore, it has been assumed that pores, which are 69 Å in diameter, have been distributed evenly in both the high and low viscosity regions, and the initial relative density everywhere is 0.51. The normalized sintering curves for the Sp, Si, and M powders are depicted in Figure 5.4.

Throughout this document it has been assumed that the Sp and Si powders have been processed in the same manner. However, similar processing conditions were not a requirement of the two powders used to test the IC and SC models. The only assumption was that the powder properties of the components remain the same in both the homogeneous and mixed samples. Homogenization, chemical reactions, and some types of physical mixing may alter the viscosity of the regions and were assumed not to occur in the investigated mixed sample. This document maintains the

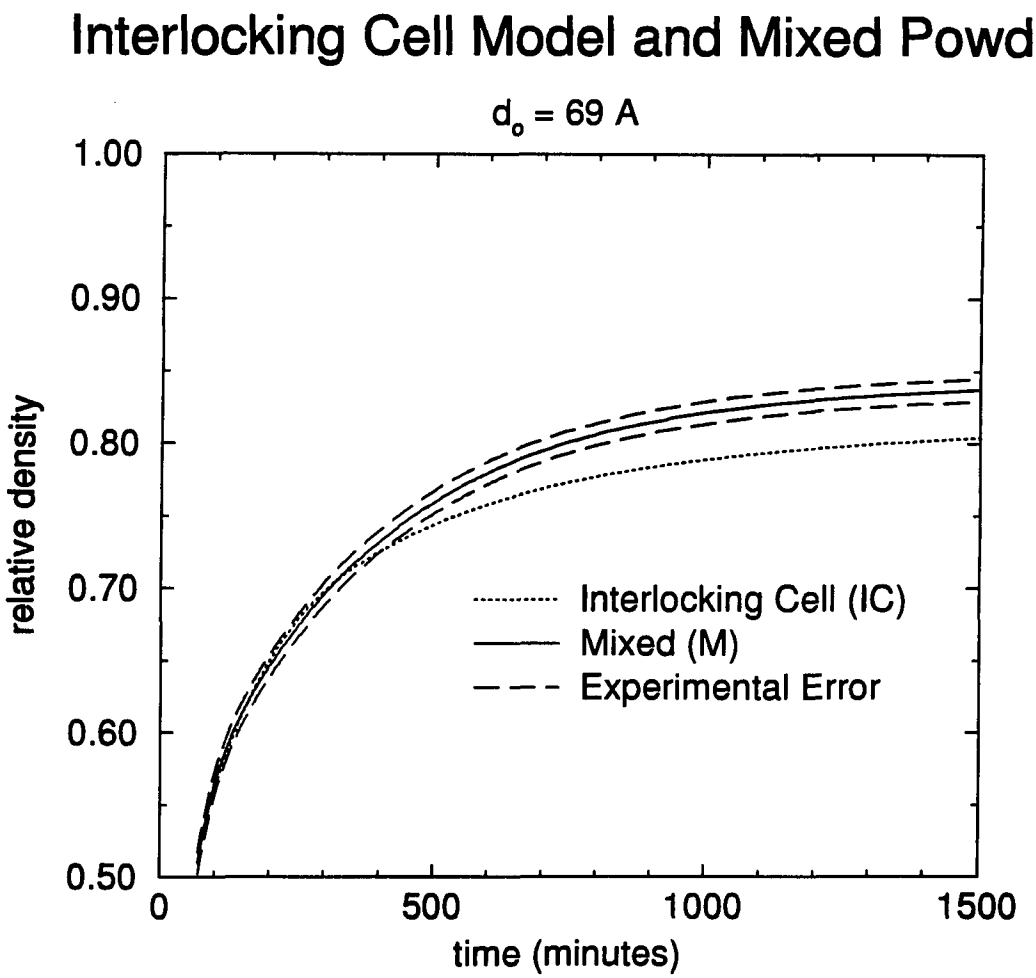

Figure 5.5: Comparison of the experimental Mixed powder and the modelled Interlocking Cell sintering curves.

assumption that the effective sintering viscosities do not change due to the sintering behavior of the neighboring regions.

5.4.1 Interlocking Cell Model

The IC model geometry assumes that a cell of right circular cylinders of one of the components in the mixture is intertwined with another unit cell of the other component. Figure 5.5 shows the IC modelled and fitted sintering behaviors of the mixed composition investigated in this study. This figure shows that the IC modelled sintering curve lies well within the experimental error for times less than 400 minutes.

For sintering times longer than about 500 minutes the IC modelled curve is significantly lower than the experimental sintering data, and eventually differs from the fitted curve by over three times the expected experimental error. The effective sintering viscosity predicted by the IC model is significantly higher than is observed experimentally. This implies that either the IC model does not apply to this system or the effective viscosities of the regions are different in the heterogeneous mixture than in the homogeneous Sp and Si sintering compacts.

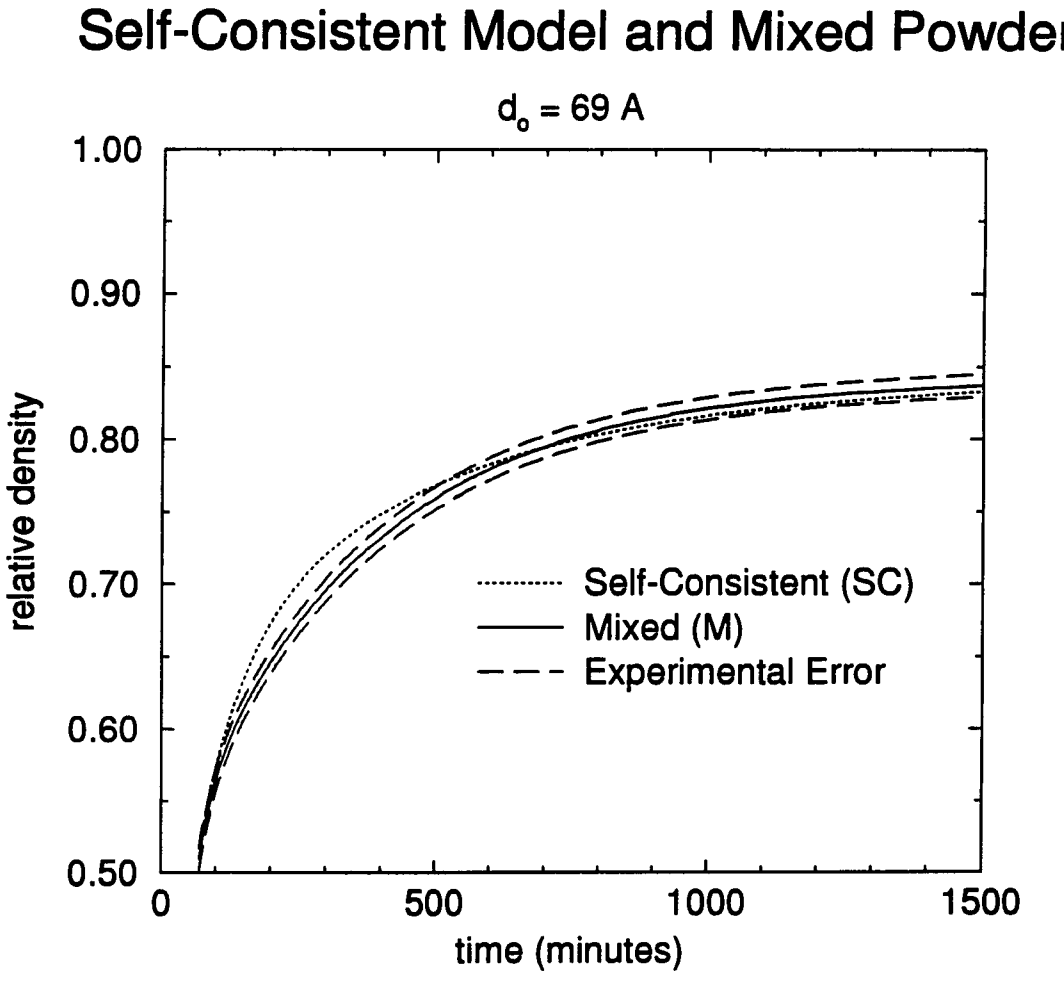

Figure 5.6: Comparison of the experimental Mixed powder and the modelled Self-Consistent sintering curves.

5.4.2 Self-Consistent Model

The SC modelled sintering curve for the M powder is shown in Figure 5.6. The SC model assumes that the matrix constrains the sintering of both the high and low viscosity regions, but allows each to sinter at a different rate. The SC modelled curve appears to fit the experimental data better than the IC model, and applies exceptionally well for long times. The final density predicted by the SC model differs from the fitted value by less than 0.1%.

The time interval over which the SC model lies outside one experimental standard deviation is between 90 and 510 minutes (coincidentally, the same region over which the IC model fits the experimental data best). Over this region the SC modelled curve predicts faster densification rates and higher relative densities than is experimentally observed. The largest deviation between the fitted and SC modelled curves is 3.6 times one standard deviation, but occurs over a very short time interval.

The SC model may at short times predict a relative density different from that which is experimentally observed because the extrapolated viscosity from the homogeneous Sp and Si curves was different than what was experienced in the mixed sample. This would be true if a) the powder properties changed when mixed, or b) not enough experimental data was obtained to extrapolate a viscosity which is representative of the homogeneous powders. One interesting observation is that two of the Sp sintering curves shown in Figure 4.10 are significantly higher than the third.

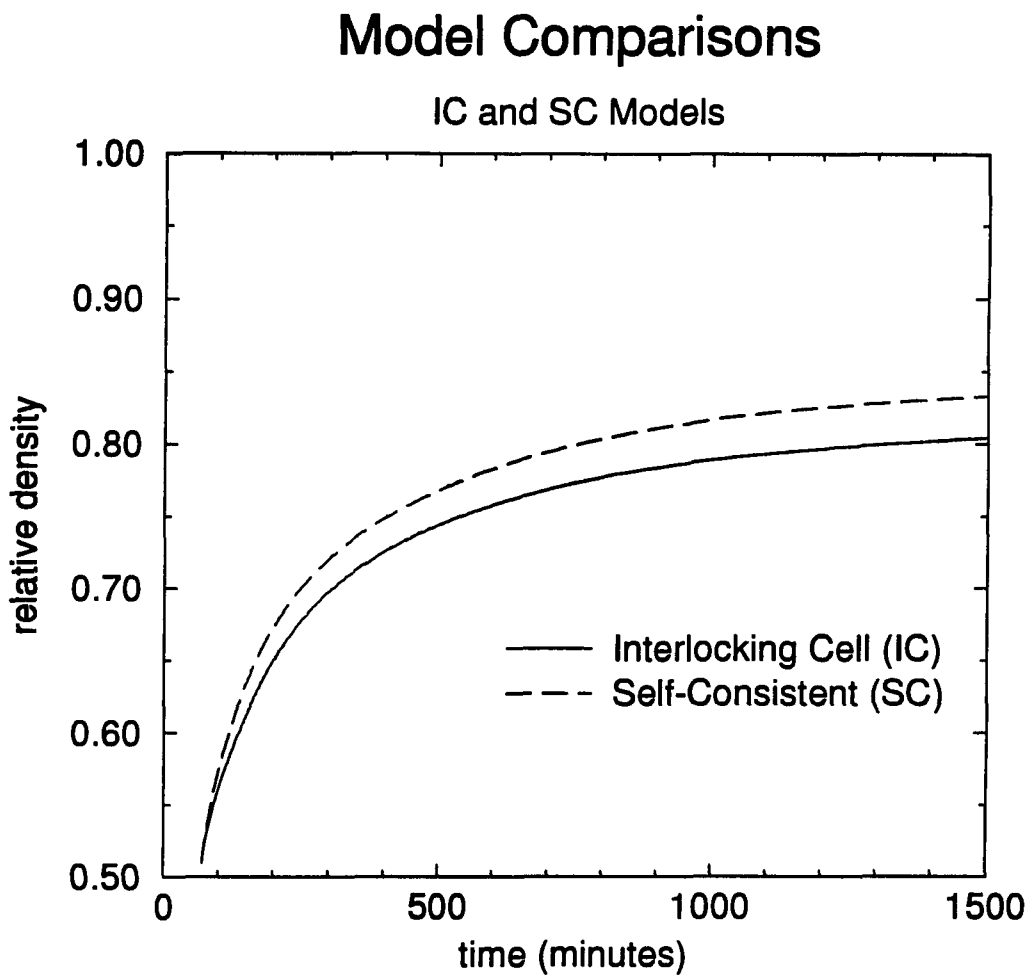

Figure 5.7: Comparison of the Interlocking Cell and Self-Consistent Models with experimental viscosities.

Since all three curves were weighted equally when computing the fitted sintering behavior, the resulting fitted sintering curves for both the St and Si powders may have been artificially shifted towards the two faster sintering curves. This would effectively shift the viscosities to lower than average values. Since these effective viscosities are used in the SC model, the modelled curve may be higher than the true average sintering behavior. This problem could be resolved by using a larger number of homogeneous experimental sintering curves resulting in higher confidences in the extrapolated viscosities.

5.5 General Discussion

For constant viscosity ratios, the SC model predicts faster initial sintering rates than the IC model. Figure 5.7 shows this also to be the case for the mixed composition, which was modelled based on the effective sintering viscosities of the Sp and Si powders. However, for compositions with a time-independent viscosity, the IC modelled sintering curve eventually reaches a higher modelled relative density than is predicted by the SC model. In this study, the IC modelled sintering curve using experimentally determined viscosities is lower than the SC modelled behavior over the entire densification range. Near 1000 minutes the time-dependent viscosity reaches a large enough value to significantly inhibit sintering. The IC modelled

powder has effectively stopped sintering due to these large viscosities, before it had a chance to cross the SC predicted curves as is observed for constant viscosity powders.

While the observed differences in sintering behavior between the IC and SC models can be explained for either constant or time-dependent viscosities, only one of these models can appropriately characterize the microstructure of any particular sintering powder compact. The SC model appears to fit the experimental data of this study better, even though it was postulated in Chapter 3 that the IC model was more likely to apply to samples with approximately equal volume fractions of the two components. Except over the time range of 90 to 510 minutes the SC modelled sintering curve lies within the 68% confidence limits of the mixed sample, while the final density predicted by the IC model was underestimated by over 3%. However, due to the relatively large errors associated with the sintering data, the differences between these two models can just be distinguished experimentally.

With our experimental set-up, individual sintering curves can vary significantly, therefore a method for finding the average densification behavior was developed. Some of the difficulties in defining the typical behavior were due to power fluctuations in the recording transducer, which caused sudden changes in the apparent densification rate or even decreases in density. Without this source of error, more representative experimental sintering curves could be plotted without artifacts of the experimental apparatus superimposed.

Eliminating the power fluctuations will reduce the experimental error by up to a factor of 2. However, some experimental errors will still exist and the variations between individual samples can not be eliminated. Table 4.2 shows that the initial and final densities vary from sample to sample, which will result in slightly different sintering curves. Therefore, in addition to eliminating the power fluctuations, a larger number of experiments should be conducted on each composition to ensure that the extrapolated viscosity is representative of the powder.

While it appears that the SC model fits the experimental sintering behavior of the mixed sample better than the IC model, both models lie within the 95% confidence limit. Therefore, more experimental work should be conducted to verify the applicability of the SC model to heterogeneous sintering samples. One of the things that should be attempted is reducing the magnitude of the experimental error so that the differences between the models can be distinguished. For the powders in this study, the size of the 95% error bars should be less than 0.1 in the relative density. Other experiments which can be conducted to verify which model applies to sintering glass compacts with heterogeneities will be discussed in the next chapter.

CHAPTER 6

SUMMARY, CONCLUSIONS, AND FUTURE WORK

This document has explored the sintering of homogeneous and heterogeneous samples. Two new heterogeneous sintering models have been presented and explored theoretically. In order to investigate the utility of these two models, experimental sintering curves of both homogeneous and heterogeneous samples near the cordierite composition were studied. Data from the experimental sintering curves and porosimeter were reduced mathematically so that comparisons between the typical behavior of a given composition and other compositions or sintering models could be made.

6.1 Summary

6.1.1 Models

Both the Interlocking Cell (IC) and the Self-Consistent (SC) models, presented in Chapter 3, predicted slower sintering behavior of the heterogeneous sample when compared to a homogeneous sample of the same composition. For this

study, the homogeneous viscosity was calculated using Bottinga and Weill's formalism[43] for silicate melts. The differences in relative density between the heterogeneous and homogeneous sintering curves depend primarily on how large of a difference in viscosity exists between the two components in the heterogeneous sample. Different shapes for the sintering curves are predicted by each of the models. The SC model predicts faster initial sintering than the IC model, but then suddenly the densification rate slows once the faster sintering regions reach full density. The time to reach 95% of the theoretical density is predicted to be 1.4 times longer for the SC model than for the IC model for a sample with a constant viscosity ratio of 5.

Both of the heterogeneous sintering models presented in Chapter 3 of this document can not apply to sintering powder compacts at the same time. The IC model assumes that each of the components forms a continuous network, which intertwine with each other. The assumed geometry of two interlocking Scherer unit cells requires that all of the regions densify at the same rate. The SC model, developed originally by Scherer for bimodal pore distributions,[6] allows the two regions to sinter at different rates and then computes the stresses in the matrix which develop. On a microscopic level, the homogeneous regions within a heterogeneous sample can not sinter at the same rate as the IC model predicts, and at the same time at different rates as the SC model assumes.

6.1.2 Viscosity

To examine which model better explains heterogeneous sintering behavior, homogeneous sintering curves for several glass compositions in the $MgO-Al_2O_3-SiO_2$ system were obtained. After mathematically computing the average sintering behavior for each powder, viscosities were extrapolated and used to describe the behavior of the regions within the mixed sample. All of the computed viscosities were time-dependent and changed by up to three orders of magnitude.

Since the experimental homogeneous sintering curves were obtained isothermally at 840°C, the transient viscosity had the effect of halting further densification. Increases in viscosity are known to occur when water or residual organics are removed from powders produced using wet-chemical techniques.[47] Independent of the source of the increased viscosity, sintering on the order of days essentially stops after an effective viscosity of $2*10^{15}$ Poise is reached.

The time-dependent viscosity depends on the processing conditions of the powder. Typically powders richer in spinel would have lower viscosities,[43] but for this study the Spinel-rich powder had the lowest viscosity for only the first 90 minutes of sintering. The transient behavior allowed the viscosity of this powder to increase significantly, even exceeding the value for the Silica-rich composition.

6.1.3 Sintering

Since all of the sintering conditions, including the heat treatment, were identical for all of the samples, it is possible to use the homogeneous extrapolated viscosities to model sintering behaviors. However, the initial conditions (i.e. porosities and initial relative densities) were not the same, so the sintering curves were normalized using Scherer's homogeneous sintering model[9] to the initial conditions of the mixed sample. The observed normalized sintering behavior correlated well with the experimentally determined viscosity relationships.

The stoichiometric composition sintered significantly faster than any of the other powders, and was the only powder modelled to reach a relative density greater than 0.95. The Stoichiometric cordierite composition also had the lowest viscosity over a large portion of the sintering region. Since this powder had a significantly larger initial porosity and lower initial density under the same pressing conditions as the other powders, it is believed that the St composition may have hydrolyzed or dried differently. This may also explain why the St powder has more of a transient effect initially, and why the densification curve does not lie between the Spinel-rich and Silica-rich compositions, even though all three were produced under similar conditions.

The homogeneous stoichiometric cordierite sinters faster than the heterogeneous sample, as both the Interlocking Cell and Self-Consistent models predict; but it also sinters faster than either one of the components in the mixed

powder. Comparisons between the experimental mixed sintering behavior and the heterogeneous sintering models can be made even if the Spinel-rich and Silica-rich powders have retained different amounts of residual water and/or organics. The only assumption about the behavior of the individual components is that homogenization and chemical reactions between the regions do not occur in the mixed sample.

The modelled and experimental sintering curves seem to indicate that the Self-Consistent model can be used to describe the densification behavior of the mixed powder. The Self-Consistent model predicts a density after 3000 minutes of sintering to within 0.1% of the experimental value. However, both the Self-Consistent and Interlocking Cell models appear to fit the data at short times as well as any given experimental curve. Comparisons of the two models at long times are difficult to make since the high transient viscosities halt densification. Therefore, further studies should be conducted to verify the conclusion that the Self-Consistent model can be used to describe the densification behavior of heterogeneous samples over the entire sintering range.

6.2 Conclusions

This study of the three homogeneous compositions revealed some very important facts about effective transient viscosities. If the transient viscosity

increases quickly to large values, obtaining fully dense samples on the desired time scale may be impossible. Therefore, manufacturers must pay particular attention to the processing conditions of glass powders. Even relative viscosity relationships between powders processed under the same or similar conditions, such as the Spinel-rich and Silica-rich compositions, vary with time and cannot be predicted based on composition. However, experimental viscosity curves can be useful in predicting sintering behavior.

The transient viscosities in this study limited comparisons of the Self-Consistent and Interlocking Cell models because sintering stopped before the samples reached full density. Therefore, for studies with experimental errors of ± 0.03 in the relative density, a ratio of the high to low viscosities must be at least 5 over the entire sintering range in order to distinguish between the two heterogeneous sintering models presented in this document. Powders with transient viscosities can be used for this type of study; however, changes in viscosity of more than two orders of magnitude require extended experimental sintering times to allow the powders to fully sinter. Therefore, for this type of study it is desirable to produce homogeneous powders with small particle sizes which do not have a large transient component to their viscosity.

While the transient viscosity behaviors prohibited the exploration of the two heterogeneous models at high relative densities, some preliminary conclusions from this study can be drawn. The Self-Consistent model fits the experimental sintering

behavior of the heterogeneous sample better and over a larger time interval than the Interlocking Cell model. Therefore, the Self-Consistent model can be used to describe the microstructural developments within a heterogeneous sample during densification.

6.3 Future Work

This study has uncovered some very interesting results, which only emphasizes the amount of work yet to be done to explain heterogeneous sintering behavior. Specific areas which deserve more research include correlations between existing heterogeneous sintering models and experimental data, the effect of initial microstructure on sintering, and basic studies on transient viscosity behavior.

It may be useful to correlate the effective sintering viscosities with values obtained from other measurement techniques, such as a viscometer. If the values agree, it may be possible to use viscosity functions found using these other techniques to model sintering behavior, since they often have smaller associated errors. At low temperatures, sintering experiments may be a useful technique for obtaining viscosity data on powders which could not be measured by other techniques.

However, the source of the transient viscosity has not been fully explained. Several authors have postulated that the transient viscosity in sol-gel powders is due

to chemical changes, either the loss of water or oxidation of residual carbon.[47] Sintering experiments involving different firing atmospheres or calcining heat treatments should result in different observed transient behavior, if chemical changes in the sample are the cause. Thermogravimetric Analysis or Mass Spectroscopy may also assist in characterizing the source of the transient viscosity behavior. Other authors have suggested that rearrangement and structural relaxation will result in time-dependent viscosities. Existing relaxation models may be applied to sintering data, such as that which is presented in this document, to study transient behaviors.

These types of experiments may also help explain the effect of processing on the sintering and extrapolated viscosities of glass powders. Even though the homogeneous samples in this study were processed under very similar conditions, they appeared to have differences due to the manner in which they were produced. Thermogravimetric Analysis combined with sintering experiments may indicate the critical steps of the processing. Also, by studying powders with intentionally different processing conditions such as the work conducted by Aruchamy et al.,[8] the level of heterogeneities which can be tolerated for a given application can be explored.

While transient viscosities may effectively halt the densification of samples heated isothermally, constant heating rate experiments could be used to investigate the sintering behavior of samples near their theoretical densities. By using heating rate studies the entire range of relative densities can be investigated. However, the compositions must still be carefully selected so that the effective sintering viscosities

of the components do not cross in the region of interest. In order to distinguish between different heterogeneous sintering models - in particular between the Interlocking Cell and Self-Consistent models - a viscosity ratio of at least 5 must be maintained throughout the sintering experiment.

Both the Interlocking Cell and Self-Consistent models should also be explored using pore size distributions as the source of heterogeneities instead of chemical variations. Scherer has already published theoretical work on the expected behavior of a powder with a bimodal pore size distribution; however, very little experimental work on this type of powder has been conducted. Particle size distributions, and therefore pore size distributions, can be generated by spray-drying sol-gel powders at different temperatures. By using one homogeneous composition with different pore sizes, the difficulties associated with calculating the ratio of two time-dependent viscosities is eliminated.

The effect of the distribution of the heterogeneities on sintering should also be researched. This type of experiment could involve simply mixing two powders of different compositions either chemically or physically to obtain different spatial distributions of the heterogeneities. At one extreme the powder could be homogeneous on an atomic scale, while at the other extreme the experiment would involve two pellets of different compositions resting on top of each other. This study should also include the effect of the relative amounts of each component by varying the volume percent from 0% to 50%.

This study has not discussed the impact of the sintering models or sintering behavior on other properties or on manufacturing products. One of the main problems with powder processing is obtaining a fully dense sample with the desired dimensions and mechanical properties. Improper selection of the heat treatment or compositions of the heterogeneous compact can cause voids to form either from chemical reactions between the two components or simply residual stresses. The developing stresses in a sintering sample can be predicted using sintering models. Further work should be conducted on the magnitude of the stresses which develop as a function of the scale of heterogeneities and how they affect mechanical properties.

APPENDIX A

PROGRAM FOR THE SELF-CONSISTENT MODEL

A.1 Analytical Approach for the Self-Consistent Model

The following pages containing the code used to generate theoretical sintering curves using the Self-Consistent Model developed by Scherer.[6] The algorithm used is very similar to Scherer's, however, viscosity or porosity can be the source of the heterogeneities in the mixed sample. The original pore size and relative density for a homogeneous sample, each of the components, and for the heterogeneous sample must initially be entered. From these parameters, the initial dimensions for the Scherer unit cells[9] can be computed. The viscosity as a function of time is also read from a file.

Once the initial unit cell parameters have been computed, the free strain rates for both of the regions in the mixed sample are computed along with their sintering properties, F and N, using the input viscosities. Using the Hashin-Shtrikman approach, the matrix values of F and N can be calculated and used to compute the densification rates of each of the regions in the matrix, as described by Scherer.[6] The matrix densification rate is then simply a weighted average of the densification rates

of the two regions. By multiplying the densification rate by the time interval, the new relative density at a given time can be computed and the cycle repeated with a new set of viscosity values.

A.2 Self-Consistent Model Program

```
c     **********************************************************************
c     scdata - This program calculates the time in units of K(t-to)
c     (where K is for the homogeneous sample) for inhomogeneous samples
c     to sinter.
      character finput*14, foutput*14
      real lmo, lso, llo, lho
      write(*,'(a/)') ' Enter input filename, with apostrophies'
      read(*,*) finput
      write(*,'(a/)') ' Enter output filename, with apostrophies'
      read(*,*) foutput
        open(1,file=finput, status = 'old')
        open(2,file=foutput,status = 'new')
      read(1,*) time,rrhohi,rrhosi,rrholi,rrhomi
      read(1,*) time,doh,dos,dol,dom
      gammah=300.
      gammas=300.
      gammal=300.
      gammam=300.
      write(*,'(a/)') ' Enter alpha, wt. ratio of large viscosity to
     1small viscosity cells'
      read(*,*) alpha
c     Calculate K(t-to) for homogeneous for where we want to start
      read(1,*) time, rrhoh, rrhos, rrhol, rrhom
      errpi = 0.
      call fx(rrhohi,errpi,xho,errxo)
      errp = 0.0
      call fx(rrhoh,errp,xh,errx)
      call fkt(xh,errx,calh,ecalh)
c     Initialize the relative densities and K(t-to)
```

```
      sumhint = calh
c     calculate the lo for all
      call fx(rrhosi,errpi,xso,errxso)
      lso = dos*0.88623/(1.-2.*xso)
      call fx(rrholi,errpi,xlo,errxlo)
      llo = dol*0.88623/(1.-2.*xlo)
      lho = doh*0.88623/(1.-2.*xho)
c     The coefficient ( gamma/(lo*rrho**(1/3)) ) is given below
      coeffh = gammah/(lho*rrhohi**(1./3.))*10.**8.
      vl = 1./((alpha*rrhos/rrhol)**(-1.)+1.)
      sig1 = (alpha*rrhos/(rrhol+alpha*rrhos)**2.)**2.*errpl**2.
      sig2 = (alpha*rrhol/(rrhol+alpha*rrhos)**2.)**2.*errps**2.
      sigvl = sig1+sig2
      vs = 1.-vl
      sigvs = sigvl
      rrhom = vl*rrhol+vs*rrhos
      sigpm = rrhol**2.*sigvl+vl**2.*sigpl+rrhos**2.*sigvs+vs**2.*sigps
      read(1,*) time, etah, etas, etal
        etaho = etah
        etaso = etas
        etalo = etal
        evisho = evish
        evislo = evisl
        evisso = eviss
      write(2,130) time, rrhoh, rrhom, rrhos, rrhol
  130 format(f10.2, 4(f7.4))
  150 timeold=time
      sigps = eps**2.
      sigpl = epl**2.
      sigpm = epm**2.
      etash = etaso/etaho
      etalh = etalo/etaho
      sigsh = 1/etaho**2.*evisso**2.+(etaso/etaho**2.)**2.*evisho**2.
      siglh = 1/etaho**2.*evislo**2.+(etalo/etaho**2.)**2.*evisho**2.
      vl = 1./((alpha*rrhos/rrhol)**(-1.)+1.)
      sig1 = (alpha*rrhos/(rrhol+alpha*rrhos)**2.)**2.*sigpl
      sig2 = (alpha*rrhol/(rrhol+alpha*rrhos)**2.)**2.*sigps
      sigvl = sig1+sig2
      call frstrr(rrhos,eps,etash,sigsh,lho,lso,rrhohi,rrhosi,fsrs,
     1sigfsrs)
      call frstrr(rrhol,epl,etalh,siglh,lho,llo,rrhohi,rrholi,fsrl,
```

```
     1sigfsrl)
      fs = f(rrhos,etash)
      fl = f(rrhol,etalh)
        sigfs = (3.*rrhos/(3.-2.*rrhos))**2.*sigsh
     1         +(9.*etash/(3.-2.*rrhos)**2.)**2.*sigps
        sigfl = (3.*rrhol/(3.-2.*rrhol))**2.*siglh
     1         +(9.*etalh/(3.-2.*rrhol)**2.)**2.*sigpl
      sns = sn(rrhos,etash)
      snl = sn(rrhol,etalh)
        t1 = 0.5*.507949*(rrhos/(3.-1.968*rrhos))**(-.5)
        t2 = 3./(3.-1.968*rrhos)**2.
        signs = (t1*t2)**2.*sigps
        t1 = 0.5*.507949*(rrhol/(3.-1.968*rrhol))**(-.5)
        t2 = 3./(3.-1.968*rrhol)**2.
        signl = (t1*t2)**2.*sigpl
      call fnm(sns,snl,signs,signl,fs,fl,sigfs,sigfl,vl,sigvl,rrhom,
     1sigpm,etamh,sigmh,fm,sigfm,snm,signm)
      a = 1./(1.+.5*(fs/(1.-2.*sns))*((1.+snm)/fm))
        siga = ferr(a,fs,sns,sigfs,signs,fm,snm,sigfm,signm)
      b = 1./(1.+.5*(fl/(1.-2.*snl))*((1.+snm)/fm))
        sigb = ferr(b,fl,snl,sigfl,signl,fm,snm,sigfm,signm)
      term1 = 3.*(1.-a)*((1.-b)*alpha*rrhos+rrhol)*fsrs
        ta = (-3.*((1.-b)*alpha*rrhos+rrhol)*fsrs)**2.*siga
        tb = (3.*(1.-a)*fsrs*(-alpha*rrhos))**2.*sigb
        ts = (3.*(1.-a)*fsrs*(1.-b)*alpha)**2.*sigps
        tl = (3.*(1.-a)*fsrs)**2.*sigpl
        tf = (3.*(1.-a)*((1.-b)*alpha*rrhos+rrhol))**2.*sigfsrs
        sigt1 = ta+tb+ts+tl+tf
      term2 = 3.*(1.-b)*a*alpha*rrhos*fsrl
        ta = (3.*(1.-b)*alpha*rrhos*fsrl)**2.*siga
        tb = (-3.*a*alpha*rrhos*fsrl)**2.*sigb
        ts = (3.*(1.-b)*a*alpha*fsrl)**2.*sigps
        tf = (3.*(1.-b)*a*alpha*rrhos)**2.*sigfsrl
        sigt2 = ta+tb+ts+tf
      term3 = (b-1.)*alpha*rrhos+(a-1.)*rrhol
        ta = rrhol**2.*siga
        tb = (alpha*rrhos)**2.*sigb
        ts = ((b-1.)*alpha)**2.*sigps
        tl = (a-1.)**2.*sigpl
        sigt3 = ta+tb+ts+tl
c     drrhosdt and drrholdt are from eq. 24 and 25 but are divided
```

```
c     by K homogeneous as is drrhomdt
      drrhosdt = (term1+term2)/term3
        sigds = (1./term3)**2.*(sigt1+sigt2)
         sigds = sigds+(drrhosdt/term3)**2.*sigt3
      term1 = 3.*(1.-b)*(alpha*rrhos+(1.-a)*rrhol)*fsrl
        ta = (3.*(1.-b)*(-rrhol)*fsrl)**2.*siga
        tb = (-3.*(alpha*rrhos+(1.-a)*rrhol)*fsrl)**2.*sigb
        ts = (3.*(1.-b)*fsrl*alpha)**2.*sigps
        tl = (3.*(1.-b)*fsrl*(1.-a))**2.*sigpl
        tf = (3.*(1.-b)*(alpha*rrhos+(1.-a)*rrhol))**2.*sigfsrl
        sigt1 = ta+tb+ts+tl+tf
      term2 = 3.*(1.-a)*b*rrhol*fsrs
        ta = (-3.*b*rrhol*fsrs)**2.*siga
        tb = (3.*(1.-a)*rrhol*fsrs)**2.*sigb
        tl = (3.*(1.-a)*b*fsrs)**2.*sigpl
        tf = (3.*(1.-a)*b*rrhol)**2.*sigfsrs
        sigt2 = ta+tb+tl+tf
      term3 = (b-1.)*alpha*rrhos+(a-1.)*rrhol
        ta = rrhol**2.*siga
        tb = (alpha*rrhos)**2.*sigb
        ts = ((b-1.)*alpha)**2.*sigps
        tl = (a-1.)**2.*sigpl
        sigt3 = ta+tb+ts+tl
      drrholdt = (term1+term2)/term3
        sigdl = 1/term3**2.*(sigt1+sigt2)+(drrholdt/term3)**2.*sigt3
      terms = (rrhol/(alpha*rrhos+rrhol))*drrhosdt
        denom = alpha*rrhos+rrhol
        tl = (alpha*rrhos*drrhosdt/denom**2.)**2.*sigpl
        ts = (alpha*rrhol*drrhosdt/denom**2.)**2.*sigps
        td = (rrhol/denom)**2.*sigds
        sigts = tl+ts+td
      terml = (alpha*rrhos/(alpha*rrhos+rrhol))*drrholdt
        tl = (alpha*rrhos*drrholdt/denom**2.)**2.*sigpl
        ts = (alpha*rrhol*drrholdt/denom**2.)**2.*sigps
        td = (alpha*rrhos/denom)**2.*sigdl
        sigtl = tl+ts+td
      drrhomdt = terms+terml
        sigdm = sigts+sigtl
      etaho=etah
        etaso=etas
        etalo=etal
```

```
      evisho = evish
      evisso = eviss
      evislo = evisl
     read(1,*) time, etah, etas, etal
     dt=(time-timeold)*60.
     delktto = coeffh*dt/etaho
c      sigkt = (delktto/etaho)**2.*evisho**2.
c     calh = calh + delktto
c      sigcalh = sigcalh+sigkt
c    step change all of the individual densities
c     call rdense(rrhoh,sigph,calh,sigcalh)
      call fx(rrhoh, eph, xh, errx)
      dxh = delktto*rrhoh**(1./3.)/2.
      dph = (6.*3.14159*xh-24.*2.**.5*xh**2.)*dxh
      rrhoh = rrhoh + dph
     rrhomo = rrhom
    rrhom = rrhom*(1.0+delktto*drrhomdt)
     t1 = (1.0+delktto*drrhomdt)**2.*sigpm
     t2 = (rrhomo*drrhomdt)**2.*sigkt
     t3 = (rrhomo*delktto)**2.*sigdm
     sigpm = t1+t2+t3
    if(rrhom.gt.1.) rrhom = 1.0
     rrhoso = rrhos
    rrhos = rrhos*(1.0+delktto*drrhosdt)
     t1 = (1.0+delktto*drrhosdt)**2.*sigps
     t2 = (rrhoso*drrhosdt)**2.*sigkt
     t3 = (rrhoso*delktto)**2.*sigds
     sigps = t1+t2+t3
    if(rrhos.gt.1.) rrhos=1.
     rrholo = rrhol
    rrhol = rrhol*(1.0+delktto*drrholdt)
     t1 = (1.0+delktto*drrholdt)**2.*sigpl
     t2 = (rrholo*drrholdt)**2.*sigkt
     t3 = (rrholo*delktto)**2.*sigds
     sigpl = t1+t2+t3
    if(rrhol.gt.1.) rrhol=1.
     eph = sigph**.5
     epm = sigpm**.5
     eps = sigps**.5
     epl = sigpl**.5
    write(2,200) time,rrhoh,rrhom,rrhos,rrhol
```

```
 200  format(f10.2,4(f7.4),f8.4)
      if(rrhol.eq.1.0) go to 550
       go to 150
 500  continue
 550  continue
      end
c     ***************************************************************
c     This calculates the values of G/etah,N,F/etah, and eta for the
c     matrix
      subroutine fnm(sns,snl,signs,signl,fs,fl,sigfs,sigfl,vl,sigvl,
     1rrhom,sigpm,etamh,sigmh,fm,sigfm,snm,signm)
        gs = fs/(2.*(1.+sns))
        gl = fl/(2.*(1.+snl))
           siggs = (gs/fs)**2.*sigfs+(gs/(1.+sns))**2.*signs
           siggl = (gl/fl)**2.*sigfl+(gl/(1.+snl))**2.*signl
        bs = fs/(3.*(1.-2.*sns))
        bl = fl/(3.*(1.-2.*snl))
           sigbs = (bs/fs)**2.*sigfs+(2.*bs/(1.-2.*sns))**2.*signs
           sigbl = (bl/fl)**2.*sigfl+(2.*bl/(1.-2.*snl))**2.*signl
        term1 = (gl-gs)*vl
           sigt1 = vl**2.*(siggl+siggs)+(gl-gs)**2.*sigvl
        term2 = 6.*(bs+2.*gs)*(1.-vl)*(gl-gs)
           t1 = ((1.-vl)*(gl-gs))**2.*sigbs
           t2 = (2.*(1.-vl)*(gl-gs)-(bs+2.*gs)*(1.-vl))**2.*siggs
           t3 = ((bs+2.*gs)*(gl-gs))**2.*sigvl
           t4 = ((bs+2.*gs)*(1.-vl))**2.*siggl
           sigt2 = 36.*(t1+t2+t3+t4)
        term3 = 5.*gs*(3.*bs+4.*gs)
           sigt3 = (15.*bs+40.*gs)**2.*siggs+(15.*gs)**2.*sigbs
        glow = gs+term1/(1.+term2/term3)
           t1 = siggs
           t2 = 1./(1.+term2/term3)**2.*sigt1
           t3 = (term1/(term3*(1.+term2/term3)**2.))**2.*sigt2
           t4 = (-term1*term2/(term3+term2)**2.)**2.*sigt3
           siglow = t1+t2+t3+t4
        term1 = (gs-gl)*(1.-vl)
           sigt1 = (1.-vl)**2.*(siggs+siggl)+(gs-gl)**2.*sigvl
        term2 = 6.*(bl+2.*gl)*vl*(gs-gl)
           t1 = (vl*(gs-gl))**2.*sigbl
           t2 = (2.*vl*(gs-gl)-(bl+2.*gl)*vl)**2.*siggl
           t3 = ((bl+2.*gl)*(gs-gl))**2.*sigvl
```

```
          t4 = ((bl+2.*gl)*vl)**2.*siggs
          sigt2 = 36.*(t1+t2+t3+t4)
        term3 = 5.*gl*(3.*bl+4.*gl)
          sigt3 = (15.*bl+40.*gl)**2.*siggl+(15.*gl)**2.*sigbl
        ghigh = gl+term1/(1.+term2/term3)
          t1 = siggl
          t2 = 1./(1.+term2/term3)**2.*sigt1
          t3 = (term1/(term3*(1.+term2/term3)**2.))**2.*sigt2
          t4 = (-term1*term2/(term3+term2)**2.)**2.*sigt3
          sighigh = t1+t2+t3+t4
        gm = .5*(ghigh+glow)
          siggm = 0.5*(sighigh+siglow)
        snm = .507949*(rrhom/(3.-1.968*rrhom))**.5
          t1 = 0.5*0.507949*(rrhom/(3.-1.968*rrhom))**(-.5)
          t2 = 3./(3.-1.968*rrhom)**2.
          signm = (t1*t2)**2.*sigpm
        fm = gm*2.*(1.+snm)
          sigfm = 4.*(1.+snm)**2.*siggm+4.*gm**2.*signm
        etamh = fm*(3.-2.*rrhom)/(3.*rrhom)
          sigmh = (etamh/fm)**2.*sigfm+(-fm/rrhom**2.)**2.*sigpm
      return
      end
c     ***********************************************************************
c     This function calculates the F divided by eta homogeneous values
      function f(rrho,etar)
      f = 3.*etar*rrho/(3.-2.*rrho)
      end
c
c     ***********************************************************************
c     This calculates the N values
      function sn(rrho,etar)
      sn = .507949*(rrho/(3.-1.968*rrho))**.5
      end
c     ***********************************************************************
c     This function calculates the free strain rate divided by Kh for
c     the small and large viscosities
      subroutine frstrr(rrho,ep,etar,sigvis,lho,lo,rrhohi,rrhoi,fsr,
     1sigfsr)
        real lho, lo
        if(rrho.lt..942)then
          c = 1.20042
```

```
          call fx(rrho,ep,x,errx)
c         write(m,10)  rrho, etar, lho, lo, rrhoi, x
c 10       format( 6(f8.4))
          term1 = (2.-3.*c*x)/(1.-c*x)**(2./3.)/x**(1./3.)
               sigt1 = 2./3.*(9.*c**2.*x**2.-1.)
               sigt1 = sigt1/(x**(4./3.)*(1.-c*x)**(5./3.))
               sigt1 = (sigt1)**2.*errx**2.
          const = -0.352051*(1./etar)*(lho/lo)*(rrhohi/rrhoi)**(1./3.)
          fsr = const*term1
             sigfsr = const**2.*sigt1
        else
          x = 100
             sigfsr =  100.
          fsr = -0.805996*(1.-rrho)**(2./3.)*rrho**(1./3.)
          fsr = fsr*(1./etar)*(lho/lo)*(rrhohi/rrhoi)**(1./3.)
        endif
      return
      end
c     ***********************************************************************
c     This function calculates the value of x = ratio of cylinder radius
c     to length associated with a given value of the relative density
c     for a unit cell consisting of intersecting right cylinders
c     (Scherer model).
c
      subroutine fx(rrho,ep,x,ex)
        hnumer = 2.**.5*(3.14159**3.-64.*rrho)
               sighn = (64.*2.**.5*ep)**2.
        hdenom = 16.*(rrho*(3.14159**3.-32.*rrho))**.5
              ta = 8.*(rrho*(3.14159**3.-32*rrho))**(-.5)
              tb =  3.14159**3.-64.*rrho
              sighd = (ta*tb)**2.*ep**2.
        term1 = atan(hnumer/hdenom)
               ta = 1./(1.+(hnumer/hdenom)**2.)
               tb = ta/hdenom
               sigtc = tb**2.*sighn
               td = -hnumer/(hnumer**2.+hdenom**2.)
               sigte = (td)**2.*sighd
               sigt1 = sigtc + sigte
        term2 = 3.14159*2.**.5*sin(term1/3.)/8.
             sigt2 = (3.14159*2.**.5/24*cos(term1/3.))**2.*sigt1
        term3 = 3.14159*2.**.5/16.
```

```
      x = term3-term2
            sigx = sigt2
            ex = sigx**.5
      return
     end
c    **********************************************************************
c    This function calculates K(t-to) for a given value of x.
c    It essentially calculates the definite integral (so it does not
c    substract the portion for x=0).
     subroutine fkt(x,ex,calint,ecal)
       y = (3.*3.14159/x-8.*2.**.5)**(1./3.)
             sigy = 3.14159/x**2.*(3.*3.14159/x-8*2.**.5)**(-2./3.)
            sigy = sigy**2.*ex**2.
      beta = (8.*2.**.5)**(1./3.)
      term1 = beta**2.-beta*y+y**2.
            sigt1 = (-beta+2.*y)**2.*sigy
      term2 = (beta+y)**2.
            sigt2 = (2.*(beta+y))**2.*sigy
      term3 = (2.*y-beta)/(beta*3.**.5)
            sigt3 = (2./(beta*3.**.5))**2.*sigy
      term4 = .5*alog(term1/term2)
            sigt4 = (.5/term1)**2.*sigt1+(.5/term2)**2.*sigt2
      term5 = 3.**.5*atan(term3)
            sigt5 = (3.**.5/(1+term3**2.))**2.*sigt3
      calint = -2.*(term4+term5)/beta
            sigcal = 4./beta*(sigt4+sigt5)
            ecal = sigcal**.5
      return
     end
c    **********************************************************************
c    This subroutine determines the relative density for a given value
c    of K(t-to). It uses Scherer's model at low densities and the MS
c    model at higher densities. The rrho switchover point is 0.942.
     subroutine rdense(rrho,sigp,sumhint,sigint)
     if(sumhint.lt.2.407) then
c      THIS FUNCTION CALCULATES THE VALUE OF X = RATIO OF
CYLINDER RADIUS
C      LENGTH WHICH CORRESPONDS TO INPUTTED VALUE OF K(t-to)
USING THE
C      SCHERER SINTERING MODEL.
c
```

```
      ytest = 1.9674
   50 gamma = 2.244924 + ytest
      beta = (11.31371 + ytest**3.)/gamma
      delta = .51436*(gamma - 3.36739)
      hnum = -sumhint + .44545*alog(gamma**2./beta) -
     11.54308*atan(delta)
      hdenom = -(1.33635/beta/gamma**2.)*(beta-(gamma - 2.244924)**2.)+
     1.7937/(1. + delta**2.)
      hn = hnum/hdenom
        sighn = sigint/hdenom**2.
      ytest = ytest + hn
        sigy = sighn
      if(hn.le..0001.and.hn.ge.-.0001) go to 60
      go to 50
   60 oldy = ytest
      caly = ytest
      subx = 9.42478/(caly**3. + 11.31371)
        sigx = (9.42478/(caly**3.+11.31371)**2.*3.*caly**2.)**2.*sigy
      rrho = 9.42478*subx**2. - 11.31371*subx**3.
        sigp = (6.*3.14159*subx-24.*2.**.5*subx**2.)**2.*sigx
      else
      If(rrho.ge.1.0) go to 62
c     Here the reduced time must be adjusted by a constant determined
c     by the changeover density for the MS and Scherer models. At rrho
c     of .942, Kt for Scherer is 2.407 and that of MS is 1.0176. Note
c     we still retain sumhint to keep track of absolute time.
      rdtims = sumhint - 2.407 + 1.0176
        sigp = 100.
      rrho = densms(rdtims)
   62 continue
      endif
      return
      end
```

```
c     ***********************************************************************
c
      function ferr(const,f,sn,sigf,signi,fm,snm,sigfm,signm)
        t1 = ((1+snm)/(2.*(1.-2.*sns)*fm))**2.*sigfs
        t2 = (fs*(1.+snm)/((1.-2*sns)**2.*fm))**2.*signs
        t3 = (fs/(2.*(1.-2.*sns)*fm))**2.*signm
        t4 = (-fs*(1.+snm)/(2.*(1.-2.*sns)*fm**2.))**2.*sigfm
        ferr = 1/a**2.*(t1+t2+t3+t4)
      end


c     ***********************************************************************
c     THIS FUNCTION CALCULATES THE RELATIVE DENSITY OF A UNIT
CELL WITH
C     K(t-to) VALUE OF PKMS USING THE MACKENZIE-SHUTTLEWORTH
MODEL.  IT
C     USES BOTH BISECTION AND NEWTON-RAPHSON TECHNIQUES FOR
FINDING THE
C       ROOT.  THE ALGORITHIM IS BASED ON PROGRAM RTSAFE IN
"NUMERICAL
C     RECIPES".  NOTE THAT THE PROGRAM FINDS THE ROOT X WHERE

C      X = ((1-RD)/RD)**(1/3).
C
      FUNCTION densms(pkms)
      data MAXIT/100/
      x1 = 2.5
      x2 = 0.0
      xacc = 0.0001
      calL FUNCD(X1,pkms,FL,DF)
      CALL FUNCD(X2,pkms,FH,DF)
      IF(FL*FH.GE.0.) PAUSE 'root must be bracketed'
      IF(FL.LT.0.)THEN
        XL=X1
        XH=X2
      ELSE
        XH=X1
        XL=X2
        SWAP=FL
        FL=FH
```

```
      FH=SWAP
     ENDIF
     yden=.5*(X1+X2)
     DXOLD=ABS(X2-X1)
     DX=DXOLD
     CALL FUNCD(yden,pkms,F,DF)
     DO 11 J=1,MAXIT
      IF(((yden-XH)*DF-F)*((yden-XL)*DF-F).GE.0.
    *     .OR. ABS(2.*F).GT.ABS(DXOLD*DF) ) THEN
       DXOLD=DX
       DX=0.5*(XH-XL)
       yden=XL+DX
       IF(XL.EQ.yden)goto 50
      ELSE
       DXOLD=DX
       DX=F/DF
       TEMP=yden
       yden=yden-DX
       IF(TEMP.EQ.yden)goto 50
      ENDIF
      IF(ABS(DX).LT.XACC) goto 50
      CALL FUNCD(yden,pkms,F,DF)
      IF(F.LT.0.) THEN
       XL=yden
       FL=F
      ELSE
       XH=yden
       FH=F
      ENDIF
 11  CONTINUE
     PAUSE 'yden exceeding maximum iterations'
 50  continue
     densms = 1/(1+yden**3)
     RETURN
     END
c
     subroutine funcd(y,pkms,fn,df)
     alpha = 1 + y**3
     beta = (1 + y)**3
     delta = (2*y-1)/1.73205
     fn=0.413567*(0.5*alog(alpha/beta)-1.73205*atan(delta)+2.720699)
```

```
      fn = fn - pkms
      df=0.413567*(1.5*(y-1)/alpha - 2/(1+delta**2))
      return
      end
C     ***********************************************************************
```

APPENDIX B

DERIVATION OF THE EQUATIONS FOR THE INTERLOCKING CELL MODEL

Starting with Equations 3.17, 3.18, and 3.21 an expression for the densification rate for each of the regions will be presented.

The rate of energy dissipated through viscous flow can be re-expressed in terms of x. The length of the equivalent flowing cylinders, h, is

$$h=l-(\frac{8\sqrt{2}}{3\pi})a=l(1-\frac{8\sqrt{2}}{3\pi}x)=\frac{l_o\rho_o^{\frac{1}{3}}}{(3\pi x^2-8\sqrt{2}x^3)^{\frac{1}{3}}}\frac{1}{3\pi x^2}(3\pi x^2-8\sqrt{2}x^3) \qquad \textbf{(B.1)}$$

therefore,

$$h = \frac{l_o\rho_o^{\frac{1}{3}}}{3\pi x^2}(3\pi x^2-8\sqrt{2}x^3)^{\frac{2}{3}} \qquad \textbf{(B.2)}$$

or

$$h=\frac{l}{3\pi x^2}\rho \tag{B.3}$$

Then dh/dt can be calculated as

$$\frac{dh}{dt}=\frac{l_o\rho_o^{\frac{1}{3}}}{3\pi}[-2x^{-3}(3\pi x^2-8\sqrt{2}x^3)^{\frac{2}{3}}+\frac{2}{3}x^{-2}(3\pi x^2-8\sqrt{2}x^3)^{-\frac{1}{3}}(6\pi x-24\sqrt{2}x^2)]\frac{dx}{dt} \tag{B.4}$$

$$\frac{dh}{dt}=\frac{l_o\rho_o^{\frac{1}{3}}}{3\pi}\frac{1}{x^3(3\pi x^2-8\sqrt{2}x^3)^{\frac{1}{3}}}[-2(3\pi x^2-8\sqrt{2}x^3)+\frac{2}{3}x(6\pi x-24\sqrt{2}x^2)]\frac{dx}{dt} \tag{B.5}$$

$$\frac{dh}{dt}=\frac{l_o\rho_o^{\frac{1}{3}}}{3\pi}\frac{-2\pi x^2}{x^3(3\pi x^2-8\sqrt{2}x^3)^{\frac{1}{3}}}\frac{dx}{dt} \tag{B.6}$$

$$\frac{dh}{dt}=-\frac{2}{3}\frac{l_o\rho_o^{\frac{1}{3}}}{x\rho^{\frac{1}{3}}}\frac{dx}{dt}=-\frac{2}{3}\frac{l}{x}\frac{dx}{dt} \tag{B.7}$$

Since the change in energy due to flow depends on dh/dt and h, it can now be expressed as

$$\dot{E}_v=\frac{3\pi\eta a^2}{h}\left(\frac{dh}{dt}\right)^2=\frac{3\pi\eta x^2 l^2}{\frac{l\rho}{3\pi x^2}}\left(-\frac{2}{3}\frac{l}{x}\frac{dx}{dt}\right)^2 \qquad \textbf{(B.8)}$$

$$\dot{E}_v = \frac{9\pi^2\eta x^4 l}{\rho}\frac{4l^2}{9x^2}\left(\frac{dx}{dt}\right)^2 \qquad \textbf{(B.9)}$$

and finally

$$\dot{E}_v = \frac{4\pi^2\eta x^2 l^3}{\rho}\left(\frac{dx}{dt}\right)^2 \qquad \textbf{(B.10)}$$

Similarly, the rate of energy reduction due to a change in surface area can be expressed in terms of x:

$$S=2\pi al-8\sqrt{2}a^2=l^2(2\pi x-8\sqrt{2}x^2)=\frac{l_o^2\rho_o^{\frac{2}{3}}(2\pi x-8\sqrt{2}x^2)}{(3\pi x^2-8\sqrt{2}x^3)^{\frac{2}{3}}} \qquad \textbf{(B.11)}$$

Therefore, dS/dt is

$$\frac{dS}{dt} = \frac{l_o^2 \rho_o^{\frac{2}{3}}}{(3\pi x^2 - 8\sqrt{2}x^3)^{\frac{5}{3}}}[-2\pi^2 x^2]\frac{dx}{dt} \qquad \textbf{(B.12)}$$

or

$$\frac{dS}{dt} = -\frac{2\pi^2 x^2 l^2}{\rho}\frac{dx}{dt} \qquad \textbf{(B.13)}$$

and the change in surface energy is

$$\dot{E}_s = \frac{2\pi^2 \gamma x^2 l^2}{\rho}\frac{dx}{dt} \qquad \textbf{(B.14)}$$

The ratio of the number of small unit cells of each component is

$$\frac{N_B}{N_A} = \alpha \frac{\rho_A}{\rho_B}\frac{l_A^3}{l_B^3} \qquad \textbf{(B.15)}$$

The energy rate balance can be used to obtain

$$\alpha\frac{\rho_A l_A^3}{\rho_B l_B^3}\dot{E}_{vB}+\dot{E}_{vA}=\alpha\frac{\rho_A l_A^3}{\rho_B l_B^3}\dot{E}_{sB}+\dot{E}_{sA} \tag{B.16}$$

$$\alpha\frac{\rho_A l_A^3}{\rho_B l_B^3}\frac{4\pi^2\eta_B x_B^2 l_B^3}{\rho_B}\left(\frac{dx_B}{dt}\right)^2+\frac{4\pi^2\eta_A x_A^2 l_A^3}{\rho_A}\left(\frac{dx_A}{dt}\right)^2=\alpha\frac{\rho_A l_A^3}{\rho_B l_B^3}\frac{2\pi^2\gamma_B x_B^2 l_B^2}{\rho_B}\frac{dx_B}{dt}+\frac{2\pi^2\gamma_A x_A^2 l_A^2}{\rho_A}\frac{dx_A}{dt} \tag{B.17}$$

$$\alpha\frac{2\eta_B x_B^2 l_A \rho_A}{\rho_B^2}\left(\frac{dx_B}{dt}\right)^2+\frac{2\eta_A x_A^2 l_A}{\rho_A}\left(\frac{dx_A}{dt}\right)^2=\alpha\frac{\rho_A}{\rho_B^2}\frac{\gamma_B x_B^2 l_A}{l_B}\frac{dx_B}{dt}+\frac{\gamma_A x_A^2}{\rho_A}\frac{dx_A}{dt} \tag{B.18}$$

From geometric constraints

$$\frac{1}{l_B}\frac{dl_B}{dt}=\frac{1}{l_A}\frac{dl_A}{dt} \tag{B.19}$$

Since

$$\frac{dl}{dt}=\frac{d}{dt}\left(\frac{l_o\rho_o^{\frac{1}{3}}}{(3\pi x^2-8\sqrt{2}x^3)^{\frac{1}{3}}}\right)=-\frac{1}{3}\frac{l_o\rho_o^{\frac{1}{3}}}{(3\pi x^2-8\sqrt{2}x^3)^{\frac{4}{3}}}(6\pi x-24\sqrt{2}x^2)\frac{dx}{dt} \qquad \textbf{(B.20)}$$

$$\frac{dl}{dt}=-\frac{1}{3}\frac{l}{\rho}(6\pi x-24\sqrt{2}x^2)\frac{dx}{dt} \qquad \textbf{(B.21)}$$

then

$$-\frac{1}{3}\frac{1}{l_B}\frac{l_B}{\rho_B}(6\pi x_B-24\sqrt{2}x_B)\frac{dx_B}{dt}=-\frac{1}{3}\frac{1}{l_A}\frac{l_A}{\rho_A}(6\pi x_A-24\sqrt{2}x_A)\frac{dx_A}{dt} \qquad \textbf{(B.22)}$$

The change in x with time is

$$\frac{dx_B}{dt}=\frac{\rho_B}{\rho_A}\left(\frac{6\pi x_A-24\sqrt{2}x_A^2}{6\pi x_B-24\sqrt{2}x_B^2}\right)\frac{dx_A}{dt} \qquad \textbf{(B.23)}$$

based strictly on geometry. This also means that the relative densification rates of the two regions must be the same,

$$\frac{1}{\rho_B}\frac{d\rho_B}{dt}=\frac{1}{\rho_A}\frac{d\rho_A}{dt} \tag{B.24}$$

Using Equation B.23 for the change in x, and Equation B.18 as the rate equation

$$\frac{2\alpha\eta_B x_B^2 l_A \rho_A}{\rho_A^2}\left(\frac{6\pi x_A-24\sqrt{2}x_A^2}{6\pi x_B-24\sqrt{2}x_B^2}\right)^2\left(\frac{dx_A}{dt}\right)^2+\frac{2\eta_A x_A^2 l_A}{\rho_A}\left(\frac{dx_A}{dt}\right)^2=\alpha\frac{\rho_A}{\rho_B}\frac{\gamma_B x_B^2 l_A}{l_B\rho_A}\frac{(6\pi x_A-24\sqrt{2}x_A^2)}{6\pi x_B-24\sqrt{2}x_B^2}\frac{dx_A}{dt}+\frac{\gamma_A x_A^2}{\rho_A}\frac{dx_A}{dt} \tag{B.25}$$

Finally,

$$\frac{dx_A}{dt}=\frac{1}{2}\frac{\alpha\frac{\rho_A}{\rho_B}\frac{\gamma_B x_B^2}{l_B}\left(\frac{6\pi x_A-24\sqrt{2}x_A^2}{6\pi x_B-24\sqrt{2}x_B^2}\right)+\frac{\gamma_A x_A^2}{l_A}}{\alpha\eta_B x_B^2\left(\frac{6\pi x_A-24\sqrt{2}x_A^2}{6\pi x_B-24\sqrt{2}x_B^2}\right)+\eta_A x_A^2} \tag{B.26}$$

Therefore,

$$\frac{dx_A}{dt} = f(\alpha,\eta_B,\eta_A,\gamma_B,\gamma_A,x_B,x_A,l_B,l_A,\rho_B,\rho_A) \qquad \textbf{(B.27)}$$

and using Equation B.23

$$\frac{dx_B}{dt} = f(\rho_A,\rho_B,x_A,x_B,\frac{dx_A}{dt}) \qquad \textbf{(B.28)}$$

Since the densification rate of each region is related to x

$$\frac{d\rho}{dt} = (6\pi x - 24\sqrt{2}x^2)\frac{dx}{dt} \qquad \textbf{(B.29)}$$

the densification rates may also be calculated.

APPENDIX C

PROGRAM FOR THE

INTERLOCKING CELL MODEL

C.1 Analytical Approach for the Interlocking Cell Model

Section C.2 contains the program used to calculate theoretical sintering curves based on the Interlocking Cell Model. The input file is the same as that for the Self-Consistent Model and contains the initial pore sizes and relative densities for the homogeneous powder, each of the components in the mixed sample, and the mixed sample itself, as well as the time dependent viscosities of the three homogeneous powders. After the initial cell dimensions are calculated, the change in x with respect to time for one of the components is computed using Equation B.26. From there the change in the cell dimensions of the other component and of the matrix can be computed. From the changes in x, the changes in relative density, and therefore the new relative densities, for each of the components and the matrix can be computed. This process is then repeated with next set of viscosities for each of the matrix components in the data file.

C.2 Interlocking Cell Model Program

```
c     ***********************************************************************
c                              iccor.FOR
c     This program will calculate the rrho for homogeneous and
c     inhomogeneous samples with a time dependent viscosity. The
c     program steps time. The viscosities are combined using the
c     interlocking cell model.
c       This is a revision of previous ic programs because the
c       assumptions starts at the beginning instead of working things
c       through for equal volume fractions of two different viscosities
c       While the program will be run for either bimodal pore size or
c       viscosity, the equations are such that it is valid for either.
c       So to change it we just need to change the input parameters.
c       We will be using the Scherer model since the MS analog to IC
c       is not clear.
      character foutput*14,finput*14
      real lom, loh, loha, loma, lohcm, lomcm,numer
      real lol, los, ll, ls
      real nh, ns, nl, nt
      write(*,'(a/)') ' Enter input filename, with apostrophies'
      read(*,*) finput
      write(*,'(a/)') ' Enter output filename, with apostrophies'
      read(*,*) foutput
      open(1,file=finput,status = 'old')
      open(2,file=foutput,status = 'new')
      read(1,*) time, rrhohi, rrhosi, rrholi, rrhomi
      read(1,*) time, doh, dos, dol, dom
      gammah = 300.
      gammam = 300.
      gammas = 300.
      gammal = 300.
      write(*,'(a/)') ' Enter the weight ratio of large to small'
      read(*,*) alpha
      write(*,'(a/)') ' Enter the small theoretical density '
      read(*,*) rhost
      write(*,'(a/)') ' Enter the large theoretical density '
      read(*,*) rholt
c       Calculate the initial lengths of the cells and x
        eph = 0.
      epm = 0.
```

```
      eps = 0.
      epl = 0.
        epm = 0.
      sigph = eph**2.
      sigpm = epm**2.
      sigps = eps**2.
      sigpl = epl**2.
      call fx(rrhohi,eph,xh,exh)
      call fx(rrhomi,epm,xm,exm)
      call fx(rrhosi,eps,xs,exs)
      call fx(rrholi,epl,xl,els)
      loh = 3.14159**0.5*doh/(2.*(1.-2.*xh))
      lom = 3.14159**0.5*dom/(2.*(1.-2.*xm))
      los = 3.14159**0.5*dos/(2.*(1.-2.*xs))
      lol = 3.14159**0.5*dol/(2.*(1.-2.*xl))
      read(1,*) time, rrhoh, rrhos, rrhol, rrhom
      call fx(rrhoh,eph,xh,exh)
      call fkt(xh,exh,calint,sigcalh)
c     Initialize the relative densities and K(t-to)
      sumhint = calint
      calh = calint
c       Since we are no longer stepping Ktto, we only want to keep
c       track of it for the homogeneous. The coefficient portion is
c       coeff = gamma/(lo*rrhoi^(1/3)*eta) but eta varies
      coeffh = gammah/(loh*rrhohi**(1./3.))*10.**8.
c      vl = 1./((alpha*rrhos/rrhol)**(-1.)+1.)
c      vs = 1.-vl
c      rrhom = vl*rrhol+vs*rrhos
      read(1,*) time, etah, etas, etal
      write(2,130) time,rrhoh,rrhom,rrhos,rrhol
  130 format(f10.0,4(f7.4),4(f7.4))
  150 timeold=time
c       I need to do this in three steps. First what happens to
c       the homogeneous. Then what happens to the small and large
c       cells. Then lastly, how these combine to affect the matrix.
c       What I mean by what happens is what do the length, x and
c       the density do.
      etaho = etah
      etaso = etas
      etalo = etal
      evisho = evish
```

```
      evisso = eviss
      evislo = evisl
      read(1,*) time, etah, etas, etal
      dt = (time-timeold)*60.
c       This part calculates the step in density for the homogeneous
c      delktto = coeffh * dt / etaho
c       sigkt = (coeffh*dt/etaho**2.)**2.*evisho**2.
c      sigcalho = sigcalh
c      calh = calh + delktto
c       sigcalh = sigcalho+sigkt
c      call rdense(rrhoh,sigph,calh,sigcalh)
       call fx(rrhoh,eph, xh, exh)
       dxhdt = gammah/(2.*etaho)*(rrhoh)**(1./3.)
       dxhdt = dxhdt/(loh*rrhohi**(1./3.))*10.**8.
       dphdt = (6.*3.14159*xh-24.*2.**.5*xh**2.)*dxhdt
       rrhoh = rrhoh + dphdt*dt
c       This part calculates the new parameters for the large and small
      call fx(rrhos,eps,xs,exs)
      call fx(rrhol,epl,xl,exl)
      ls = los*rrhosi**(1./3.)/(rrhos**(1./3.))
        sigls = (ls/(3.*rrhos))**2.*eps**2.
      ll = lol*rrholi**(1./3.)/(rrhol**(1./3.))
        sigll = (ll/(3.*rrhol))**2.*epl**2.
      rhos = rrhos*rhost
        sigdns = eps**2./rhost**2.
      rhol = rrhol*rholt
        sigdnl = epl**2./rholt**2.
      ratsa = (6.*3.14159*xs-24.*2.**0.5*xs**2.)/(6.*3.14159*xl-24.*
     12.**0.5*xl**2.)
        sigs = ((6.*3.14159-48.*2.**.5*xs)/(6.*3.14159*xl-24.*2.**.5
     1         *xl**2.))**2.*exs**2.
        sigl = (ratsa*(6.*3.14159-48.*2.**.5*xl)/(6.*3.14159*xl-24*
     1         2.**.5*xl**2.))**2.*exl**2.
        sigratsa = sigs+sigl
      term1 = gammas/(2.*etaso*ls)*10.**8.
        sigt1 = (term1/etaso)**2.*evisso**2.+(term1/ls)**2.*sigls
      term2 = alpha*rhos/rhol*xl/xs*ls/ll*gammal/gammas*ratsa+1.
        tds = ((term2-1.)/rhos)**2.*sigdns
        tdl = ((term2-1.)/rhol)**2.*sigdnl
        txl = ((term2-1.)/xl)**2.*exl**2.
        txs = ((term2-1.)/xs)**2.*exs**2.
```

```
      tls = ((term2-1.)/ls)**2.*sigls
      tll = ((term2-1.)/ll)**2.*sigll
      tr = ((term2-1.)/ratsa)**2.*sigratsa
      sigt2 = tds+tdl+txl+txs+tls+tll+tr
    term3 = alpha*rhost/rholt*etalo/etaso*ratsa**2.+1.
      tvl = ((term3-1.)/etalo)**2.*evislo**2.
      tvs = ((term3-1.)/etaso)**2.*evisso**2.
      tr = (2.*(term3-1.)/ratsa)**2.*sigratsa
      sigt3 = tvl+tvs+tr
    dxsdt = term1*term2/term3
      sigdxs = (term2/term3)**2.*sigt1+(term1/term3)**2.*sigt2
      sigdxs = sigdxs+(dxsdt/term3)**2.*sigt3
    dpsdt = (6.*3.14159*xs-24.*2.**0.5*xs**2.)*dxsdt
      tx = ((6.*3.14159-48.*2.**.5*xs)*dxsdt)**2.*exs**2.
      tdx = (6.*3.14159*xs-24.*2.**.5*xs**2.)**2.*sigdxs
      sigdps = tx+tdx
    dpldt = rrhol/rrhos*dpsdt
      sigdpl = (dpldt/rrhol)**2.*epl**2.+(dpldt/rrhos)**2.*eps**2.
      sigdpl = sigdpl + (dpldt/dpsdt)**2.*sigdps
    dpmdt = rrhom/rrhos*dpsdt
      sigdpm = (dpmdt/rrhom)**2.*epm**2.+(dpmdt/rrhos)**2.*eps**2.
      sigdpm = sigdpm + (dpmdt/dpsdt)**2.*sigdps
    rrhos = rrhos + dpsdt*dt
      sigps = sigps + dt**2.*sigdps
    rrhol = rrhol + dpldt*dt
      sigpl = sigpl + dt**2.*sigdpl
    rrhom = rrhom + dpmdt*dt
      sigpm = sigpm + dt**2.*sigdpm
c     And because the whole body must sinter at the same relative
c     rate the matrix portion is:
    if(rrhoh.gt.1.) rrhoh = 1.0
    if(rrhom.gt.1.) rrhom = 1.0
       if(rrhos.gt.1.) rrhos = 1.0
       if(rrhol.gt.1.) rrhol = 1.0
    eph = sigph**.5
    epm = sigpm**.5
    eps = sigps**.5
    epl = sigpl**.5
    write(2,200) time, rrhoh, rrhom, rrhos, rrhol
200 format(e12.5,8(f9.4))
    if (rrhom.eq.1.0) go to 550
```

```
      go to 150
  500 continue
  550 continue
      end
c     **********************************************************************
c     **********************************************************************
c     This function calculates the value of x = ratio of cylinder radius
c     to length associated with a given value of the relative density
c     for a unit cell consisting of intersecting right cylinders
c     (Scherer model).
c
      subroutine fx(rrho,ep,x,ex)
         hnumer = 2.**.5*(3.14159**3.-64.*rrho)
         sighn = (64.*2.**.5*ep)**2.
        hdenom = 16.*(rrho*(3.14159**3.-32.*rrho))**.5
               ta = 8.*(rrho*(3.14159**3.-32*rrho))**(-.5)
               tb =  3.14159**3.-64.*rrho
               sighd = (ta*tb)**2.*ep**2.
        term1 = atan(hnumer/hdenom)
               ta = 1./(1.+(hnumer/hdenom)**2.)
               tb = ta/hdenom
               sigtc = tb**2.*sighn
               td = -hnumer/(hnumer**2.+hdenom**2.)
               sigte = (td)**2.*sighd
               sigt1 = sigtc+sigte
        term2 = 3.14159*2.**.5*sin(term1/3.)/8.
               sigt2 = (3.14159*2.**.5/24*cos(term1/3.))**2.*sigt1
        term3 = 3.14159*2.**.5/16.
        x = term3-term2
               sigx = sigt2
               ex = sigx**.5
        return
      end
c     **********************************************************************
c     This function calculates K(t-to) for a given value of x.
c     It essentially calculates the definite integral (so it does not
c     substract the portion for x=0).
      subroutine fkt(x,ex,calint,ecal)
         y = (3.*3.14159/x-8.*2.**.5)**(1./3.)
         sigy = 3.14159/x**2.*(3.*3.14159/x-8*2.**.5)**(-2./3.)
               sigy = sigy**2.*ex**2.
```

```
      beta = (8.*2.**.5)**(1./3.)
      term1 = beta**2.-beta*y+y**2.
            sigt1 = (-beta+2.*y)**2.*sigy
      term2 = (beta+y)**2.
            sigt2 = (2.*(beta+y))**2.*sigy
      term3 = (2.*y-beta)/(beta*3.**.5)
            sigt3 = (2./(beta*3.**.5))**2.*sigy
      term4 = .5*alog(term1/term2)
            sigt4 = (.5/term1)**2.*sigt1+(.5/term2)**2.*sigt2
      term5 = 3.**.5*atan(term3)
            sigt5 = (3.**.5/(1+term3**2.))**2.*sigt3
      calint = -2.*(term4+term5)/beta
            sigcal = 4./beta*(sigt4+sigt5)
            ecal = sigcal**.5
      return
    end
c   ***********************************************************************
c   This subroutine determines the relative density for a given value
c   of K(t-to). It uses Scherer's model at low densities and the MS
c   model at higher densities. The rrho switchover point is 0.942.
    subroutine rdense(rrho,sigp,sumhint,sigint)
    if(sumhint.lt.2.407) then
c     THIS FUNCTION CALCULATES THE VALUE OF X = RATIO OF
CYLINDER RADIUS
C     LENGTH WHICH CORRESPONDS TO INPUTTED VALUE OF K(t-to)
USING THE
C     SCHERER SINTERING MODEL.
c
    ytest = 1.9674
 50 gamma = 2.244924 + ytest
    beta = (11.31371 + ytest**3.)/gamma
    delta = .51436*(gamma - 3.36739)
    hnum = -sumhint + .44545*alog(gamma**2./beta) -
   11.54308*atan(delta)
    hdenom = -(1.33635/beta/gamma**2.)*(beta-(gamma - 2.244924)**2.)+
   1.7937/(1. + delta**2.)
    hn = hnum/hdenom
      sighn = sigint/hdenom**2.
    ytest = ytest + hn
      sigy = sighn
    if(hn.le..0001.and.hn.ge.-.0001) go to 60
```

```
      go to 50
   60 oldy = ytest
      caly = ytest
      subx = 9.42478/(caly**3. + 11.31371)
        sigx = (9.42478/(caly**3.+11.31371)**2.*3.*caly**2.)**2.*sigy
      rrho = 9.42478*subx**2. - 11.31371*subx**3.
        sigp = (6.*3.14159*subx-24.*2.**.5*subx**2.)**2.*sigx
      else
      If(rrho.ge.1.0) go to 62
c     Here the reduced time must be adjusted by a constant determined
c     by the changeover density for the MS and Scherer models.  At rrho
c     of .942, Kt for Scherer is 2.407 and that of MS is 1.0176.  Note
c     we still retain sumhint to keep track of absolute time.
      rdtims = sumhint - 2.407 + 1.0176
        sigp = 100.
      rrho = densms(rdtims)
   62 continue
      endif
      return
      end


c     ***********************************************************************
c     THIS FUNCTION CALCULATES THE RELATIVE DENSITY OF A UNIT CELL WITH
C     K(t-to) VALUE OF PKMS USING THE MACKENZIE-SHUTTLEWORTH MODEL.  IT
C     USES BOTH BISECTION AND NEWTON-RAPHSON TECHNIQUES FOR FINDING THE
C        ROOT.  THE ALGORITHIM IS BASED ON PROGRAM RTSAFE IN "NUMERICAL
C     RECIPES".  NOTE THAT THE PROGRAM FINDS THE ROOT X WHERE

C      X = ((1-RD)/RD)**(1/3).
C
      FUNCTION densms(pkms)
      data MAXIT/100/
      x1 = 2.5
      x2 = 0.0
      xacc = 0.0001
      calL FUNCD(X1,pkms,FL,DF)
```

```
      CALL FUNCD(X2,pkms,FH,DF)
      IF(FL*FH.GE.0.) PAUSE 'root must be bracketed'
      IF(FL.LT.0.)THEN
        XL=X1
        XH=X2
      ELSE
        XH=X1
        XL=X2
        SWAP=FL
        FL=FH
        FH=SWAP
      ENDIF
      yden=.5*(X1+X2)
      DXOLD=ABS(X2-X1)
      DX=DXOLD
      CALL FUNCD(yden,pkms,F,DF)
      DO 11 J=1,MAXIT
        IF(((yden-XH)*DF-F)*((yden-XL)*DF-F).GE.0.
     *      .OR. ABS(2.*F).GT.ABS(DXOLD*DF) ) THEN
          DXOLD=DX
          DX=0.5*(XH-XL)
          yden=XL+DX
          IF(XL.EQ.yden)goto 50
        ELSE
          DXOLD=DX
          DX=F/DF
          TEMP=yden
          yden=yden-DX
          IF(TEMP.EQ.yden)goto 50
        ENDIF
        IF(ABS(DX).LT.XACC) goto 50
        CALL FUNCD(yden,pkms,F,DF)
        IF(F.LT.0.) THEN
          XL=yden
          FL=F
        ELSE
          XH=yden
          FH=F
        ENDIF
   11 CONTINUE
      PAUSE 'yden exceeding maximum iterations'
```

```
 50  continue
     densms = 1/(1+yden**3)
     RETURN
     END
c
     subroutine funcd(y,pkms,fn,df)
     alpha = 1 + y**3
     beta = (1 + y)**3
     delta = (2*y-1)/1.73205
     fn=0.413567*(0.5*alog(alpha/beta)-1.73205*atan(delta)+2.720699)
     fn = fn - pkms
     df=0.413567*(1.5*(y-1)/alpha - 2/(1+delta**2))
     return
     end
C    ******************************************************************
```

APPENDIX D

PREDICTING VISCOSITIES

USING BOTTINGA AND WEILL'S METHOD

Bottinga and Weill[43] devised an expression for predicting the viscosity for a variety of silicate melt glasses. By using the expression

$$\ln\eta = \sum X_i D_i \qquad \text{(D.1)}$$

the viscosity of a homogeneous glass can be computed in terms of the mole fractions of several of its components, X_i, and the associated parameters, D_i. The values for D_i depend on the type of oxide being added to silica, how much, and at what temperature. These values have been fitted to experimental data for a variety of compositions and temperatures.

In this appendix, the viscosities will be computed for the three homogeneous compositions analyzed in this study and listed in Table 4.1 and Table D.1.

Table D.1 - Composition and Viscosity Coefficients

Composition	mol% SiO_2	mol% $MgAl_2O_4$	D (SiO_2)	D ($MgAl_2O_4$)
Si	81.43	18.57	13.62	1.5
St	71.43	28.57	13.22	3.6
Sp	61.43	38.57	12.32	-0.4

The values given by Bottinga and Weill are for melt glasses. The values listed in Table D.1 are for 1200°C because that is the lowest temperature listed. If the activation constants for these glasses are approximately the same, then using the ratio of the viscosities at sintering temperatures should be acceptable.

The viscosities for the compositions listed in Table D.1 were computed using Bottinga and Weill's model, Equation D.1, and are listed in Table D.2.

Table D.2 - Predicted Viscosities

Composition	log η	η (Poise)
Si	11.37	86623
St	10.47	35297
Sp	7.41	1659

The ratio of the computed viscosities of the Silica-Rich and Spinel-Rich compositions is 52. The ratio of the Silica-Rich to Stoichiometric composition is only 2.4.

One of the limitations of this technique is that the coefficients for the viscosities are computed according to within what range the glass composition lies with respect to the amount of SiO_2. The Si composition lies just outside the highest range listed (0.81), so it may at least partially be in error. The other problem is whether or not these relationships can be extrapolated down to sintering temperatures.

APPENDIX E

PROGRAM FOR COMPUTING

THE FITTED CURVE USING LEAST SQUARES

```
c     ************************************************************************
c                    Least Squares
c
c     This program will calculate all of the coefficients for a set of
c     data which fits the sum of two exponentials and a line.  The
c     input is a file containing time (in minutes) and relative density
c     from the experimental curve.  This program will then calculate
c     the six coefficients needed to reproduce that curve.  It will
c     also ask for an initial set of coefficients which fit the
c     equation:  y=-exp(At+B)-exp(Ct+D)+Et+F.
c
c     ************************************************************************
c
      character foutput*14,finput*14
      real f,fn
      exp=2.7182818
c
      read(*,*) finput
      read(*,*) foutput
      open(1,file=finput,status = 'old')
      open(2,file=foutput,status = 'new')
c
      read(*,*) a
c     a = 0.0
      read(*,*) b
c     b = 0.0
      read(*,*) c
c     c = 0.0
      read(*,*) d
```

```
c     d = 0.0
      read(*,*) e
c     e = 0.01
      read(*,*) f
c     f = 3.0
c
c      write(*,'(a/)') ' Enter an initial value for lambda'
c      read(*,*) y
      y = 0.001
c
      m=1
c     ***********************************************************************
c           Calculating values for chi2, beta, and alpha
c     ***********************************************************************
 100  read(1,*) time, rrho
      if(time.lt.0.) go to 210
      rrhoc = -exp**(a*time+b)-exp**(c*time+d)+e*time+f
      diff = rrho-rrhoc
      chi2 = diff**2
      b1 = diff*(-time*exp**(a*time+b))
      b2 = diff*(-exp**(a*time+b))
      b3 = diff*(-time*exp**(c*time+d))
      b4 = diff*(-exp**(c*time+d))
      b5 = diff*time
      b6 = diff
      a11 = (-time*exp**(a*time+b))*(-time*exp**(a*time+b))
      a12 = (-time*exp**(a*time+b))*(-exp**(a*time+b))
      a13 = (-time*exp**(a*time+b))*(-time*exp**(c*time+d))
      a14 = (-time*exp**(a*time+b))*(-exp**(c*time+d))
      a15 = (-time*exp**(a*time+b))*(time)
      a16 = (-time*exp**(a*time+b))*1
      a21 = a12
      a22 = (-exp**(a*time+b))*(-exp**(a*time+b))
      a23 = (-exp**(a*time+b))*(-time*exp**(c*time+d))
      a24 = (-exp**(a*time+b))*(-exp**(c*time+d))
      a25 = (-exp**(a*time+b))*(time)
      a26 = (-exp**(a*time+b))*1
      a31 = a13
      a32 = a23
      a33 = (-time*exp**(c*time+d))*(-time*exp**(c*time+d))
      a34 = (-time*exp**(c*time+d))*(-exp**(c*time+d))
```

```
      a35 = (-time*exp**(c*time+d))*(time)
      a36 = (-time*exp**(c*time+d))*1
      a41 = a14
      a42 = a24
      a43 = a34
      a44 = (-exp**(c*time+d))*(-exp**(c*time+d))
      a45 = (-exp**(c*time+d))*(time)
      a46 = (-exp**(c*time+d))*1
      a51 = a15
      a52 = a25
      a53 = a35
      a54 = a45
      a55 = time*time
      a56 = time*1
      a61 = a16
      a62 = a26
      a63 = a36
      a64 = a46
      a65 = a56
      a66 = 1*1
c     Now to sum all of them to get a running total
      schi2 = schi2 + chi2
      sb1 = sb1 + b1
      sb2 = sb2 + b2
      sb3 = sb3 + b3
      sb4 = sb4 + b4
      sb5 = sb5 + b5
      sb6 = sb6 + b6
      sa11 = sa11 + a11
      sa12 = sa12 + a12
      sa13 = sa13 + a13
      sa14 = sa14 + a14
      sa15 = sa15 + a15
      sa16 = sa16 + a16
      sa21 = sa12
      sa22 = sa22 + a22
      sa23 = sa23 + a23
      sa24 = sa24 + a24
      sa25 = sa25 + a25
      sa26 = sa26 + a26
      sa31 = sa13
```

```
      sa32 = sa23
      sa33 = sa33 + a33
      sa34 = sa34 + a34
      sa35 = sa35 + a35
      sa36 = sa36 + a36
      sa41 = sa14
      sa42 = sa24
      sa43 = sa34
      sa44 = sa44 + a44
      sa45 = sa45 + a45
      sa46 = sa46 + a46
      sa51 = sa15
      sa52 = sa25
      sa53 = sa35
      sa54 = sa45
      sa55 = sa55 + a55
      sa56 = sa56 + a56
      sa61 = sa16
      sa62 = sa26
      sa63 = sa36
      sa64 = sa46
      sa65 = sa56
      sa66 = sa66 + a66
      sl = sl + 1
      go to 100
  200 continue
  210 continue
c
c     Modifying sums of alpha with lambda (y)
c
  300 sam11 = sa11*(1+y)
      sam22 = sa22*(1+y)
      sam33 = sa33*(1+y)
      sam44 = sa44*(1+y)
      sam55 = sa55*(1+y)
      sam66 = sa66*(1+y)
c
```

```
c     ***********************************************************************
c           Solving a system of six linear equations
c     ***********************************************************************
c
c     Here are all the replacement coefficients
      c1 = (sam33*sam11-sa13*sa31)/(sa32*sam11-sa12*sa31)-
     1 (sa23*sam11-sa13*sa21)/(sam22*sam11-sa12*sa21)
      c2 = (sa34*sam11-sa14*sa31)/(sa32*sam11-sa12*sa31)-
     1 (sa24*sam11-sa14*sa21)/(sam22*sam11-sa12*sa21)
      c3 = (sa35*sam11-sa15*sa31)/(sa32*sam11-sa12*sa31)-
     1 (sa25*sam11-sa15*sa21)/(sam22*sam11-sa12*sa21)
      c4 = (sa36*sam11-sa16*sa31)/(sa32*sam11-sa12*sa31)-
     1 (sa26*sam11-sa16*sa21)/(sam22*sam11-sa12*sa21)
      c5 = (sa43*sam11-sa13*sa41)/(sa42*sam11-sa12*sa41)-
     1 (sa23*sam11-sa13*sa21)/(sam22*sam11-sa12*sa21)
      c6 = (sam44*sam11-sa14*sa41)/(sa42*sam11-sa12*sa41)-
     1 (sa24*sam11-sa14*sa21)/(sam22*sam11-sa12*sa21)
      c7 = (sa45*sam11-sa15*sa41)/(sa42*sam11-sa12*sa41)-
     1 (sa25*sam11-sa15*sa21)/(sam22*sam11-sa12*sa21)
      c8 = (sa46*sam11-sa16*sa41)/(sa42*sam11-sa12*sa41)-
     1 (sa26*sam11-sa16*sa21)/(sam22*sam11-sa12*sa21)
      c9 = (sa53*sam11-sa13*sa51)/(sa52*sam11-sa12*sa51)-
     1 (sa23*sam11-sa13*sa21)/(sam22*sam11-sa12*sa21)
      c10 = (sa54*sam11-sa14*sa51)/(sa52*sam11-sa12*sa51)-
     1 (sa24*sam11-sa14*sa21)/(sam22*sam11-sa12*sa21)
      c11 = (sam55*sam11-sa15*sa51)/(sa52*sam11-sa12*sa51)-
     1 (sa25*sam11-sa15*sa21)/(sam22*sam11-sa12*sa21)
      c12 = (sa56*sam11-sa16*sa51)/(sa52*sam11-sa12*sa51)-
     1 (sa26*sam11-sa16*sa21)/(sam22*sam11-sa12*sa21)
      c13 = (sa63*sam11-sa13*sa61)/(sa62*sam11-sa12*sa61)-
     1 (sa23*sam11-sa13*sa21)/(sam22*sam11-sa12*sa21)
      c14 = (sa64*sam11-sa14*sa61)/(sa62*sam11-sa12*sa61)-
     1 (sa24*sam11-sa14*sa21)/(sam22*sam11-sa12*sa21)
      c15 = (sa65*sam11-sa15*sa61)/(sa62*sam11-sa12*sa61)-
     1 (sa25*sam11-sa15*sa21)/(sam22*sam11-sa12*sa21)
      c16 = (sam66*sam11-sa16*sa61)/(sa62*sam11-sa12*sa61)-
     1 (sa26*sam11-sa16*sa21)/(sam22*sam11-sa12*sa21)
c
      c17 = (c11*c1-c3*c9)/(c10*c1-c2*c9)-(c7*c1-c3*c5)/(c6*c1-c2*c5)
      c18 = (c12*c1-c4*c9)/(c10*c1-c2*c9)-(c8*c1-c4*c5)/(c6*c1-c2*c5)
      c19 = (c15*c1-c3*c13)/(c14*c1-c2*c13)-(c7*c1-c3*c5)/(c6*c1-c2*c5)
```

```
      c20 = (c16*c1-c4*c13)/(c14*c1-c2*c13)-(c8*c1-c4*c5)/(c6*c1-c2*c5)
c
c     Including the error calculation (finding the inverse matrix)
c
c
      d1 = -sa31/(sa32*sam11-sa12*sa31)+sa21/(sam22*sam11-sa12*sa21)
      d2 = -sam11/(sam22*sam11-sa12*sa21)
      d3 = sam11/(sa32*sam11-sa12*sa31)
      d4 = -sa41/(sa42*sam11-sa12*sa41)+sa21/(sam22*sam11-sa12*sa21)
      d5 = sam11/(sa42*sam11-sa12*sa41)
      d6 = -sa51/(sa52*sam11-sa12*sa51)+sa21/(sam22*sam11-sa12*sa21)
      d7 = sam11/(sa52*sam11-sa12*sa51)
      d8 = -sa61/(sa62*sam11-sa12*sa61)+sa21/(sam22*sam11-sa12*sa21)
      d9 = sam11/(sa62*sam11-sa12*sa61)
c
      d10 = (d6*c1-d1*c9)/(c10*c1-c2*c9)-(d4*c1-d1*c5)/(c6*c1-c2*c5)
      d11 = (d2*c1-d2*c9)/(c10*c1-c2*c9)-(d2*c1-d2*c5)/(c6*c1-c2*c5)
      d12 = -d3*c9/(c10*c1-c2*c9)+d3*c5/(c6*c1-c2*c5)
      d13 = -d5*c1/(c6*c1-c2*c5)
      d14 = d7*c1/(c10*c1-c2*c9)
      d15 = (d8*c1-d1*c13)/(c14*c1-c2*c13)-(d4*c1-d1*c5)/(c6*c1-c2*c5)
      d16 = (d2*c1-d2*c13)/(c14*c1-c2*c13)-(d2*c1-d2*c5)/(c6*c1-c2*c5)
      d17 = -d3*c13/(c14*c1-c2*c13)+d3*c5/(c6*c1-c2*c5)
      d18 = d9*c1/(c14*c1-c2*c13)
c
c     Now to solve for the matrix components
c
c     In Gaussian form
c     The "x" components refer to the left portion of the matrix
c     while the "y" components are the right portion.
      x12 = sa12/sam11
      x13 = sa13/sam11
      x14 = sa14/sam11
      x15 = sa15/sam11
      x16 = sa16/sam11
      x23 = (sa23*sam11-sa13*sa21)/(sam22*sam11-sa12*sa21)
      x24 = (sa24*sam11-sa14*sa21)/(sam22*sam11-sa12*sa21)
      x25 = (sa25*sam11-sa15*sa21)/(sam22*sam11-sa12*sa21)
      x26 = (sa26*sam11-sa16*sa21)/(sam22*sam11-sa12*sa21)
      x34 = c2/c1
      x35 = c3/c1
```

```
      x36 = c4/c1
      x45 = (c7*c1-c3*c5)/(c6*c1-c2*c5)
      x46 = (c8*c1-c4*c5)/(c6*c1-c2*c5)
      x56 = c18/c17
c
      y11 = 1/sam11
      y21 = -sa21/(sam22*sam11-sa12*sa21)
      y22 = sam11/(sam22*sam11-sa12*sa21)
      y31 = d1/c1
      y32 = d2/c1
      y33 = d3/c1
      y41 = (d4*c1-d1*c5)/(c6*c1-c2*c5)
      y42 = (d2*c1-d2*c5)/(c6*c1-c2*c5)
      y43 = -d3*c5/(c6*c1-c2*c5)
      y44 = d5*c1/(c6*c1-c2*c5)
      y51 = d10/c17
      y52 = d11/c17
      y53 = d12/c17
      y54 = d13/c17
      y55 = d14/c17
      y61 = (d15*c17-d10*c19)/(c20*c17-c18*c19)
      y62 = (d16*c17-d11*c19)/(c20*c17-c18*c19)
      y63 = (d17*c17-d12*c19)/(c20*c17-c18*c19)
      y64 = (d13*c17-d13*c19)/(c20*c17-c18*c19)
      y65 = -d14*c19/(c20*c17-c18*c19)
      y66 = d18*c17/(c20*c17-c18*c19)
c
c
      z61 = y61
      z62 = y62
      z63 = y63
      z64 = y64
      z65 = y65
      z66 = y66
      z51 = y51-x56*z61
      z52 = y52-x56*z62
      z53 = y53-x56*z63
      z54 = y54-x56*z64
      z55 = y55-x56*z65
      z56 =    -x56*z66
      z41 = y41-x46*z61-x45*z51
```

```
      z42 = y42-x46*z62-x45*z52
      z43 = y43-x46*z63-x45*z53
      z44 = y44-x46*z64-x45*z54
      z45 =    -x46*z65-x45*z55
      z46 =    -x46*z66-x45*z56
      z31 = y31-x36*z61-x35*z51-x34*z41
      z32 = y32-x36*z62-x35*z52-x34*z42
      z33 = y33-x36*z63-x35*z53-x34*z43
      z34 =    -x36*z64-x35*z54-x34*z44
      z35 =    -x36*z65-x35*z55-x34*z45
      z36 =    -x36*z66-x35*z56-x34*z46
      z21 = y21-x26*z61-x25*z51-x24*z41-x23*z31
      z22 = y31-x26*z62-x25*z52-x24*z42-x23*z32
      z23 =    -x26*z63-x25*z53-x24*z43-x23*z33
      z24 =    -x26*z64-x25*z54-x24*z44-x23*z34
      z25 =    -x26*z65-x25*z55-x24*z45-x23*z35
      z26 =    -x26*z66-x25*z56-x24*z46-x23*z36
      z11 = y11-x16*z61-x15*z51-x14*z41-x13*z31-x12*z21
      z12 =    -x16*z62-x15*z52-x14*z42-x13*z32-x12*z22
      z13 =    -x16*z63-x15*z53-x14*z43-x13*z33-x12*z23
      z14 =    -x16*z64-x15*z54-x14*z44-x13*z34-x12*z24
      z15 =    -x16*z65-x15*z55-x14*z45-x13*z35-x12*z25
      z16 =    -x16*z66-x15*z56-x14*z46-x13*z36-x12*z26
c
c     Calculating the change in the coefficients (delta)
c
      del1 = sb1*z11+sb2*z12+sb3*z13+sb4*z14+sb5*z15+sb6*z16
      del2 = sb1*z21+sb2*z22+sb3*z23+sb4*z24+sb5*z25+sb6*z26
      del3 = sb1*z31+sb2*z32+sb3*z33+sb4*z34+sb5*z35+sb6*z36
      del4 = sb1*z41+sb2*z42+sb3*z43+sb4*z44+sb5*z45+sb6*z46
      del5 = sb1*z51+sb2*z52+sb3*z53+sb4*z54+sb5*z55+sb6*z56
      del6 = sb1*z61+sb2*z62+sb3*z63+sb4*z64+sb5*z65+sb6*z66
c
      if(y.eq.0.0) go to 910
c
c
c     ********************************************************************
c        Calculating the new coefficients and chi2
c     ********************************************************************
c
      an = a + del1
```

```
      bn = b + del2
      cn = c + del3
      dn = d + del4
      en = e + del5
      fn = f + del6
      close (1)
      open(1,file=finput,status = 'old')
  500 read(1,*) time, rrho
      if(time.lt.0.) go to 600
      t1 = an*time+bn
      t2 = cn*time+dn
      if(t1.gt.100.0) go to 550
      if(t2.gt.100.0) go to 550
      rrhoc = -exp**(an*time+bn)-exp**(cn*time+dn)+en*time+fn
      if(rrhoc.gt.100.0) go to 550
      if(rrhoc.lt.-100.0) go to 550
      diff = rrho-rrhoc
      chi2n = diff**2
      snchi2 = snchi2 + chi2n
      go to 500
  550 snchi2 = schi2*100
  600 close (1)
      open(1,file=finput,status = 'old')
c     ***********************************************************************
c        Comparing chi2 and new chi2
c     ***********************************************************************
c
      stop = (((snchi2-schi2)/schi2)**2)**0.5
      if(stop.lt.0.0001) go to 900
c     if new chi2 larger, increase y, recalc sums, redo system of eq.
      if(snchi2.ge.schi2) then
         y = y*10.
         snchi2 = 0.0
         go to 300
      else
c     if new chi2 smaller, replace coeff, recalc all sums
         y = y/10
         a = an
         b = bn
         c = cn
         d = dn
```

```
        e = en
        f = fn
c       reset all sums
            schi2 = 0.0
            sb1 = 0.0
            sb2 = 0.0
            sb3 = 0.0
            sb4 = 0.0
            sb5 = 0.0
            sb6 = 0.0
            sa11 = 0.0
            sa12 = 0.0
            sa13 = 0.0
            sa14 = 0.0
            sa15 = 0.0
            sa16 = 0.0
            sa22 = 0.0
            sa23 = 0.0
            sa24 = 0.0
            sa25 = 0.0
            sa26 = 0.0
            sa33 = 0.0
            sa34 = 0.0
            sa35 = 0.0
            sa36 = 0.0
            sa44 = 0.0
            sa45 = 0.0
            sa46 = 0.0
            sa55 = 0.0
            sa56 = 0.0
            sa66 = 0.0
            snchi2 = 0.0
            m=m+1
          go to 100
      endif
  900 continue
      y = 0.0
      go to 300
```

```
 910  continue
c     Calculating the error in the coefficients
c
      close (1)
      open(1,file=finput,status = 'old')
 920  read(1,*) time, rrho
      if(time.lt.0.0) go to 930
      if(time.eq.0.0) go to 920
        rrhoc = -exp**(a*time+b)-exp**(c*time+d)+e*time+f
        diff = rrho-rrhoc
        der1a = -time*exp**(a*time+b)
        der2a = -time**2*exp**(a*time+b)
        der1b = -exp**(a*time+b)
        der2b = -exp**(a*time+b)
        der1c = -time*exp**(c*time+d)
        der2c = -time**2*exp**(c*time+d)
        der1d = -exp**(c*time+d)
        der2d = -exp**(c*time+d)
        der1e = time
        der2e = 1
        der1f = 1
        der2f = 0
c
        var = diff**2+var
        vara = (der1a**2-diff*der2a)+vara
        varb = (der1b**2-diff*der2b)+varb
        varc = (der1c**2-diff*der2c)+varc
        vard = (der1d**2-diff*der2d)+vard
        vare = (der1e**2-diff*der2e)+vare
        varf = (der1f**2-diff*der2f)+varf
        sn = sn+1
      go to 920
 930  continue
        stdp = (1/sn*var)**0.5
        stda = stdp/vara**0.5
        stdb = stdp/varb**0.5
        stdc = stdp/varc**0.5
        stdd = stdp/vard**0.5
        stde = stdp/vare**0.5
        stdf = stdp/varf**0.5
```

```
c     **********************************************************************
c           We're done so now we need to output the results
c     **********************************************************************
      write(2,*) schi2, snchi2, stdp, a, b, c, d, e, f, stda, stdb,
     1stdc, stdd, stde, stdf
      end
```

REFERENCES

1. Scherer, G.W., "Thermal Stresses in a Cylinder: Application to Optical Waveguide Blanks," J. Non-Cryst. Sol. **34** 233-238 (1979).

2. Scherer, G.W., "Sintering Inhomogeneous Glasses: Application to Optical Waveguide Blanks," J. Non-Cryst. Sol. **34** 239-256 (1979).

3. Sawhill, H.T., "Ultrastructure Processing of Ceramics in Electronics Packaging," in Ultrastructure Processing of Advanced Materials ed. by D.R. Uhlmann and D.R. Ulrich, John Wiley and Sons, Inc., New York, NY 599-611 (1992).

4. Hsueh, C.H., Evans, A.G., and Cannon, R.M., "Viscoelastic Stresses and Sintering Damage in Heterogeneous Powder Compacts," Acta Metall. **34** [5] 927-36 (1986).

5. Raj, R., and Bordia, R.K., "Sintering Behavior of Bimodal Powder Compacts," Acta Metall. **32** [7] 1003-1019 (1984).

6. Scherer, G.W., "Viscous Sintering of a Bimodal Pore-Size Distribution," J. Am. Ceram. Soc. **67** [11] 709-715 (1984).

7. Scherer, G.W., "Sintering with Rigid Inclusions," J. Am. Ceram. Soc. **70** [10] 719-25 (1987).

8. Aruchamy, A., et al., "Effect of Synthesis Route on Properties of Cordierite Based Glasses - Melt and Wet-Chemical Derived Glass Powders," (To be Published).

9. Scherer, G.W., "Sintering of Low-Density Glasses: I, Theory," J. Am. Ceram. Soc. **60** [5-6] 236-239 (1977).

10. Frenkel, J., "Viscous Flow of Crystalline Bodies Under the Action of Surface Tension," J. Phys. (Moscow) **9** [5] 385-91 (1945).

11. Mackenzie, J.K., and Shuttleworth, R., "Phenomenological Theory of Sintering," Proc. Phys. Soc. London **62** [12-B] 833-52 (1949).

12. Zelinski, B.J.J., "Sintering and Crystallization in Sol-Gel Derived Ternary Silicate Glasses," Ph.D. Dissertation (1988).

13. Scherer, G.W., "Cell Models for Viscous Sintering," J. Am. Ceram. Soc. **74** [7] 1523-1531 (1991).

14. Jagota, A., and Dawson, P.R., "Simulation of the Viscous Sintering of Two Particles," J. Am. Ceram. Soc. **73** [1] 173-177 (1990).

15. Scherer, G.W., and Bachman, D.L., "Sintering of Low-Density Glasses: II, Experimental Study" J. Am. Ceram. Soc. **60** [5-6] 239-243 (1977).

16. Rahaman, M.N., DeJonghe, L.C., Scherer, G.W., and Brook, R.J., "Creep and Densification During Sintering of Glass Powder Compacts," J. Am. Ceram. Soc. **70** [10] 766-74 (1987).

17. Sacks, M.D., and Tseng, T-Y., "Preparation of SiO_2 Glass from Model Powder Compacts: I, Formation and Characterization of Powders, Suspensions, and Green Compacts," **67** [8] 526-532 (1984).

18. Sacks, M.D., and Tseng, T-Y., "Preparation of SiO_2 Glass from Model Powder Compacts: I, Sintering," **67** [8] 532-537 (1984).

19. Exner, H.E., and Petzow, G., "Shrinkage and Rearrangement During Sintering of Glass Spheres," Sintering and Catalysis, Edited by G. C. Kuczynski, Plenum, New York, NY 279-293 (1975).

20. Exner, H.E., and Giess, E.A., "Anisotropic Shrinkage of Cordierite-type Glass Powder Cylindrical Compacts," J. Mater. Res. **3** [1] 122-125 (1988).

21. Cutler, I.B., and Henrichsen, R.E., "Effect of Particle Shape on the Kinetics of Sintering Glass," J. Am. Ceram. Soc. **51** [10] 604-605 (1968).

22. Scherer, G.W., "Sintering of Low-Density Glasses: III, Effect of a Distribution of Pore Sizes," J. Am. Ceram. Soc. **60** [5-6] 243-246 (1977).

23. Evans, A.G., and Hsueh, C.H., "Behavior of Large Pores During Sintering and Hot Isostatic Pressing," J. Am. Ceram. Soc. **69** [6] 444-448 (1986).

24. Selsing, J., "Internal Stresses in Ceramics," J. Am. Ceram. Soc. **44** [8] 419 (1961).

25. Skorokhod, V.V., "On the Phenomenological Theory of Densification in the Sintering of Porous Bodies," Poroshk. Metall. **2** 14-20 (1961).

26. Skorokhod, V.V., "Electrical Conductivity, Modulus of Elasticity, and Viscosity Coefficients of Porous Bodies," Powder Metall. **12** 188-200 (1963).

27. Hashin, Z., and Shtrikman, S., "A Variational Approach to the Theory of the Elastic Behavior of Multiphase Materials," J. Mech. Phys. Solids **11** 127-40 (1963).

28. Rahaman, M.N., DeJonghe, L.C., and Hsueh, C.H., "Creep During Sintering of Porous Compacts," J. Am. Ceram. Soc. **69** [1] 58-60 (1986).

29. Venkatachari, K.R., and Raj, R., "Shear Deformation and Densification of Powder Compacts," J. Am. Ceram. Soc. **69** [6] 499-506 (1986).

30. Bordia, R.K., and Scherer, G.W., "Overview No. 70. On Constrained Sintering - I. Constitutive Model for a Sintering Body," Acta Metall. **36** [9] 2392-2397 (1988).

31. Bordia, R.K., and Scherer, G.W., "Overview No. 70. On Constrained Sintering - II. Comparison of Constitutive Models," Acta Metall. **36** [9] 2399-2409 (1988).

32. Rahaman, M.N., DeJonghe, L.C., and Brook, R.J., "Effect of Shear Stress on Sintering," J. Am. Ceram. Soc. **69** [1] 53-58 (1986).

33. Bordia, R.K., and Raj, R., "Sintering of TiO_2-Al_2O_3 Composites: A Model Experimental Investigation," J. Am. Ceram. Soc. **71** [4] 302-310 (1988).

34. Coble, R.L., and Kingery, W.D., "Effect of Porosity on Physical Properties of Sintered Alumina," **39** [11] 377-385 (1956).

35. Lange, F.F., "Constrained Network Model for Predicting Densification Behavior of Composite Powders," J. Mater. Res. **2** [1] 59-65 (1987).

36. DeJonghe, L.C., Rahaman, M.N., and Hsueh, C.H., "Transient Stresses in Bimodal Compacts During Sintering," Acta Metall. **34** [7] 1467-71 (1986).

37. Bordia, R.K., and Scherer, G.W., "Overview No. 70. On Constrained Sintering - III. Rigid Inclusions," Acta Metall. **36** [9] 2411-2416 (1988).

38. Rahaman, M.N., and DeJonghe, L.C., "Effect of Rigid Inclusions on the Sintering of Glass Powder Compacts," J. Am. Ceram. Soc. **70** [12] C348-C351 (1987).

39. Dutton, R.E., and Rahaman, M.N., "Sintering, Creep, and Electrical Conductivity of Model Glass Matrix Composites," J. Am. Ceram. Soc. **75** [8] 2146-2154 (1992).

40. Hardy, A.B., and Rhine, W.E., "SiC-Reinforced Cordierite Composites Formed by Viscous Sintering of Cordierite Powders," Mat. Res. Soc. Symp. **249** 487-492 (1992).

41. Mazurin, O.V., Streltsina, M.V., and Shavaiko-Shvaikovskaya, T.P., Handbook of Glass Data - Part C: Ternary Silicate Glasses Elsevier, Amsterdam 720-870 (1983).

42. Ermolaeva, E.V. Ogneuproy, **5** 221-228 (1955) from Mazurin, O.V. (1983), Streltsina, M.V., and Shavaiko-Shvaikovskaya, T.P., Handbook of Glass Data - Part C: Ternary Silicate Glasses Elsevier, Amsterdam 807 (1983).

43. Bottinga, Y., and Weill, D.F., "The Viscosity of Magmatic Silicate Liquids: A Model for Calculation," Am. J. of Sci. **272** [May] 438-475 (1972).

44. Scherer, G.W., "Constitutive Models for Viscous Sintering," Mechanics of Granular Materials and Powder Systems **37** 1-18 (1992).

45. Phase Diagram Schraiyer and S???

46. Press, W.H., Flannery, B.P., Teukolsky, S.A., and Vetterling, W.T., Numerical Recipes Cambridge University Press, Cambridge, 521-528 (1986).

47. Scherer, G.W., "Viscous Sintering of Inorganic Gels," Surface and Colloid Science ed. Matijevic Egon, Plenum Press, New York, NY, 14 265-301 (1987).

48. Zelinski, B.J.J., Personal communication (1994).